Remote sensing of European spruce (*Ips typographus*, L.) bark beetle green attack

Haidi Jamal Abdullah

REMOTE SENSING OF EUROPEAN SPRUCE (*IPS TYPOGRAPHUS*, L.) BARK BEETLE GREEN ATTACK

DISSERTATION

to obtain
the degree of doctor at the University of Twente,
on the authority of the rector magnificus,
prof.dr. T.T.M. Palstra,
on account of the decision of the Doctorate Board,
to be publicly defended
on Thursday 27 June 2019 at 16:45 hrs

by

Haidi Jamal Abdullah
born on 05 January 1986
in Sulaymaniyah, Iraq

This thesis has been approved by
Prof.dr. A.K. Skidmore, supervisor
Dr. R. Darvishzadeh, co-supervisor

ITC dissertation number 357
ITC, P.O. Box 217, 7500 AE Enschede, The Netherlands

ISBN 978-90-365-4795-6
DOI 10.3990/1.9789036547956

Cover photo by Lio Khoshnaw
Cover designed by Benno Masselink
Printed by ITC Printing Department

UNIVERSITY OF TWENTE.

FACULTY OF GEO-INFORMATION SCIENCE AND EARTH OBSERVATION

Graduation committee:

Chairman/Secretary

Prof.dr.ir. A. Veldkamp	University of Twente

Supervisor

Prof.dr. A.K. Skidmore	University of Twente

Co-supervisor

Dr. R. Darviszadeh Varchehi	University of Twente

Members

Prof.dr.ing. W. Verhoef	University of Twente
Prof.dr. K. Pfeffer	University of Twente
Prof.dr.ir. P.H. Verburg	Free University Amsterdam
Prof.dr. O. Niemann	University of Victoria, Canada

This thesis is dedicated to my family
for their love, endless support
and encouragement.

Acknowledgements

I would not be able to complete this thesis without the encouragement and support of a number of people and organisations that I would like to sincerely thank and acknowledge:

Firstly, I would like to express my appreciation and sincere gratitude to my promoter, Prof. Andrew K. Skidmore. I feel very fortunate and honoured to have worked with him; he was always there to motivate, support and guide with his wisdom throughout my PhD. He taught me very important research skills and problem-solving techniques, and he kindly guided and supported me during the time of researching and writing this thesis. I will always remember the early days when I have struggled writing my proposal, but you have always supported and helped me, to stay on track. It has been an incredible honour and privilege to do my PhD under your supervision.

I am also greatly indebted to the excellent supervision and advisory of Dr Roshanak Darvishzadeh, who has become my supervisor after four months of my PhD. The proposal development and field data collection phase of this work would have not been possible without the precious support from Dr Roshanak Darvishzadeh. Her guidance and suggestions during the proposal development were pivotal to wipe out the early stage confusions I encountered. Moreover, I am very grateful for the many inspiring scientific discussions we shared. Her comments were always to the point that had the power to sharpen this work. Above all, she is sincere, friendly, and a very easy person to communicate with. Many thanks go to Dr.Thomas A. Groen, who had a great contribution to my knowledge on the subject of this study during writing my proposal, and he continued supporting me during writing my first scientific papers.

Thanks also go to the Bavarian Forest National Park particularly to Dr Marco Heurich and Prof. Joerg Mueller for approving access to the study area, other field and logistical facilities. I would like to thank the NRs department staffs, especially Esther Hondebrink for her enormous assistance and support, ITC student affairs, Geoscience laboratory team, ITC library, ICT help desk, travel unit and finance department staffs who helped me during my stay at ITC. My special thanks go to Loes Colenbrander, Marga Koelen, Carla Gerritsen, Theresa van den Boogaard and Roelof Schoppers for their excellent services.

My deep gratitude goes to the PhD community at ITC. I have been fortunate to come across wonderful colleagues at NRS department. It's hard to mention all the friends and colleagues. However among them, Dr. Elnaz Neinavaz, Dr. Abebe Ali, Dr. Xi Zhu, Dr. Wanderi Festus, Dr. Maria Fenanda, Dr. Jing Liu, Gara Tawanda, Alby Duarte Rocha, Nina Amiri, Yifang Shi, Trini Del Rio, and Sugandh Chauhan, I would like to thank them for their friendship and valuable

support. It has been a great pleasure working with you and discussing different scientific topics during our special PhD tutorial every month. Special thanks also go to my relatives and friends back home and abroad for their relentless support and encouragement.

Most of all I would like to thank all my family in particular my parents who, as always, has given me endless love and support throughout my PhD journey. In particular, I would like to thank my wife Jwan Anwer, for her love, understanding and inspiration. To my sons Hasti and Hema, I am full of apologies for being away from all of you.

Finally, I would like to acknowledge the European Commission's Erasmus Mundus program for awarding me PhD scholarship and Faculty of Geo-information Science and Earth Observation (ITC) for the financial support to pursue this study. Without this financial support, my dream would not have been accomplished. My appreciation and gratitude go to Salahaddin University-Erbil as well for offering me a sabbatical to conduct my PhD study.

Table of contents

List of figures

List of tables

Chapter 1 : General Introduction

1.1 Biology and ecology of European spruce bark beetle (Ips typographus, L.)

The eight-spined spruce bark beetle *Ips typographus* L. is one of the most important and serious insect pests in Central Europe which threaten the Norway spruce tree (*Picea abies*) (Lausch et al., 2011; Wermelinger, 2004). The flight activity of the European spruce bark beetle depends strongly on the air temperature as the beetles start to swarm and attack new host trees during the European springtime (between the end of April and the beginning of May) when the air temperature reaches 16.5 °C and maximum temperature does not exceed 26 °C (Lobinger, 1994a; Wermelinger, 2004). The male initiates gallery construction and then emits aggregation pheromones which attract other beetles to the host tree (Zuber and Benz, 1992). The spruce bark beetle feeds and reproduces within the phloem tissue under the bark of the infested trees.

Moreover, in the process of the infestation, the beetle also carries pathogenic fungi such as blue stain fungi (*Ophiostoma and Cerato-cystis species*) (Krokene and Solheim, 1998). This combination of the beetle larva and the fungi may cut the translocation of water, sugar and other nutrients within the bole of the tree when both began to penetrate through the living phloem and xylem cells (Paine et al., 1997b; Wermelinger, 2004). This feeding behaviour impairs the transport of nutrients from the leaves massively to the roots (Rohde et al., 1996). From the middle of June through to the end of July, the imagoes then leave their host tree and attack new trees during their second stage of development. The development of the European spruce beetle, from laying the eggs to adulthood, lasts 7-11 weeks. During winter time, all the beetles at different development stages (larva, pupa and adult) hibernate in the galleries; the adults can also hibernate in stumps, litter or mineral soil over the winter. In general, the European spruce beetle *Ips typographus*, L. has one to two generations per year, depending on weather conditions, in particular, temperature. The first generation are active from April to May, while the second generation is active from July to August (Nikolov et al., 2014).

Generally, the bark beetle infestation occurs on two levels; (i) on an endemic level (non-outbreak) (small bark beetle population) and (ii) on an epidemic level (outbreak level). During the endemic level (non-outbreak), old trees with big diameter (DBH), weakened by storms and drought, are susceptible to be attacked by bark beetles (Allain et al., 2011; Latifi et al., 2014; Lausch et al., 2011; Lausch et al., 2013b; Wermelinger, 2004). Therefore, the structure and composition of a forest may not be greatly affected on top of the damage already inflicted by storms or drought. This is because healthy trees may erect defences by producing resin or latex which may contain a number of insecticidal and fungicidal compounds that can kill or injure attacking insects,

or the sticky fluid simply immobilises and suffocates them. However, on an epidemic level (outbreak), the large number of beetles can overwhelm a tree's defences, resulting in the death of even healthy trees (Christiansen and Bakke, 1988a; Sambaraju et al., 2012; Skakun et al., 2003).

Historically, in central Europe, outbreaks of bark beetle have often coincided with certain abiotic disturbances such as windthrows trees, heat waves, snow damage (Öhrn, 2012; Seidl et al., 2017b). However, recent outbreaks are different, as climate moderation has acted as their initiating factor. Dry, warm summers have led to the desiccation of host trees, which then become stressed and attractive for the bark beetle. As a result, an increase in temperature may lead to an increase in beetle population size, as their eggs hatching and developing into adults sooner than usual. In addition, an increase in the beetle population size may have an impact on existence healthy trees, because the trees' defence system cannot cope with an attack from a large number of beetles (Wermelinger, 2004). An increase in temperature will also stress healthy trees and increase the probability of an attack by bark beetles. Moreover, there are a number of abiotic factors that have impact on bark beetles and host trees including elevation, slope and aspect. These factors influence the interaction process between trees and bark beetle activity (Jönsson et al., 2009; Simard et al., 2012). Trees at a higher elevation are less susceptible to attack by bark beetles because elevation is a proxy for temperature. Thus the higher the elevation, the lower the temperature and that will limit the bark beetle activities. On the other hand, trees on a steep slope suffer more from water stress and are therefore more susceptible to attacks by the bark beetles (Chinellato et al., 2014). Furthermore, factors such as stand characteristics of the forest affect the process of bark beetle attacks. For example, areas of high stand density, trees with large diameters are more susceptible to the attack by bark beetles (Cudmore et al., 2010; Safranyik, 1974; Skakun et al., 2003). In addition, forests with mixed tree species are less susceptible to attack by the bark beetles compared to pure spruce stands (Faccoli and Bernardinelli, 2014).

1.2 Host tree response and control strategies

Norway Spruce (*Picea abies*) trees possess defence mechanisms on several levels that can prevent a bark beetle attack. The first level of defence (the so-called primary defence) is activated when the beetle attempts to tunnel under the bark of the trees, and the attacked tree attempts to release stored resin. When the first resistance is exhausted by the beetle, the second stage of the tree's defence will start. During this stage, the local metabolism around the entrance hole changes. As such the trees produce procyanidins as a defensive chemical to prevent the entrance of bark beetle and to affect the establishment of a brood by impairing the food quality. (Rohde et al., 1996; Wermelinger,

2004). At the third defence level, a systemic change in the whole tree's metabolism occurs. This leads to the production of fewer carbohydrates but more proteins, which are needed for constitutional resistance. Thus, the successful colonisation of the bark beetle within the tree is considered to occur in three successive steps. Firstly, the tree's defences are exhausted by pioneer beetles that chemically emit aggregation pheromones to attract a large number of conspecifics for a mass attack (Wood, 1982). Secondly, mutualistic relationships with certain fungi play an active part in killing the trees. Thirdly, the ability to tolerate the defensive secretions of the attacked trees allows for the final colonisation of the tree (Lieutier, 2002).

The infested tree exhibits three different stages of damage when it is a host of the bark beetle (Coulson et al., 1985; Raffa et al., 2008; Wermelinger, 2004) (Fig. 1.1). These stages are commonly known as green, red, and grey attacks. In the first stage (the green attack), the beetle starts to lay its eggs under the bark of the tree, and the infested trees have yet to show distinct symptoms observable by the human eye (Niemann and Visintini, 2005a; Wermelinger, 2004). However, the subsequent degradation of the needles can be noted by regular field observations. In addition, one of the earliest signs of bark beetle infestation in trees is a drop in sapwood moisture, as a result of the inoculation of blue fungi by the beetles that bore through the bark. The spores of the fungi penetrate the living cells in the phloem and xylem, resulting in a disruption of water and nutrient flow. A decrease in the transpiration cooling process of the infested tree results, causing an increase in leaf and canopy temperature (Christiansen and Bakke, 1988a; Sprintsin, 2011). In the red attack stage, the needles of the tree turn from green to yellow to red-brown. Finally, the needles fall off, and only the grey bark remains, hence the last stage is referred to as a grey attack. This discolouration of the attacked trees is evident at the canopy level (Coulson et al., 1985).

It is important to note that the length (specification) of these stages varies depending on the type of beetles. For example, visible symptoms of an attacked Norway spruce tree by the European Spruce Bark Beetle (*Ips typographus*, L.) were evident in the crown in late August (red attack). However, for North American and Canadian Mountain Pine Beetles (*Dendroctonus ponderosae*, *Hopkins*) visible symptoms of an attack were evident in the crown from late May to early June following the initial attack (Safranyik and Carroll, 2006; Sprintsin, 2011).

Bark beetle outbreaks are an important factor in the ecological development of the forest landscape affecting forest structure and composition (Pfeifer et al., 2011; Schowalter, 2012; Simard et al., 2012; Zeppenfeld et al., 2015), as well as biodiversity and ecosystem services (Thom and Seidl, 2016). Bark beetles can affect forest ecosystems both directly and indirectly. Direct impacts include

an increase in tree mortality rates and a reduction in forest stand densities (Bright et al., 2013; Eitel et al., 2011; Filchev, 2012a; Schowalter, 2012; Vanderhoof et al., 2013; Verbesselt et al., 2009). Indirect impacts include a reduction in carbon uptake, changes in tree species' distribution, changes in erosion processes, increasing fire frequency, and nutrient cycling (Beudert et al., 2015; Kurz et al., 2008; Lehnert et al., 2013). Recent studies have shown that bark beetle infestation leads to the enhancement of biodiversity by opening the canopy layers and altering the microclimate conditions in the forest. This alteration provides the essential habitats and sources of energy for various organisms, allowing for species to persist in areas disturbed by the bark beetle (Beudert et al., 2015; Lehnert et al., 2013; Müller et al., 2008).

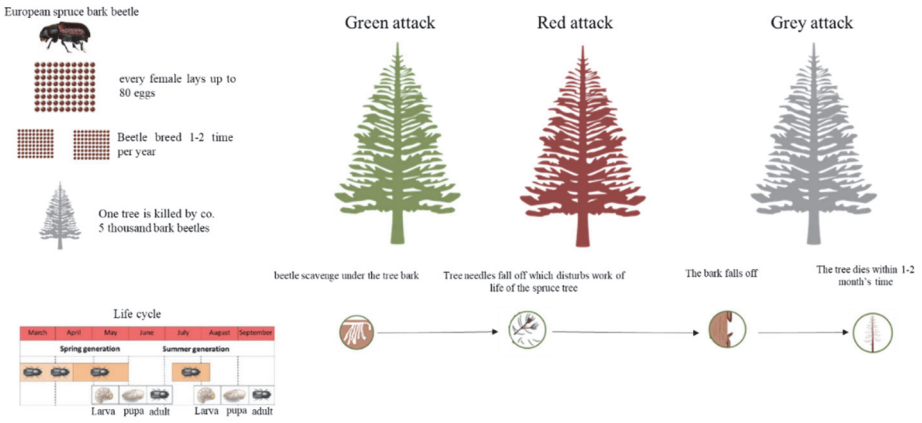

Figure 1.1: The generalised life cycle of the European spruce bark beetle and the process of killing host trees.

When forest management aims to control or preclude a mass outbreak and minimise economic loss, two control approaches are commonly practised: indirect control through long-term forest management and direct control management. Indirect control approaches are essential to forest health, improving the vitality of trees and the stability of stands; therefore, decreasing the possibility of bark beetle infestation and outbreak. The long-term management practices of indirect control include maintaining soil quality, encouraging mixed wood stands, and addressing thinning and harvesting time considering the life cycle of the bark beetle (Wermelinger, 2004). Previous studies have shown that thinning or lowering tree densities reduced tree mortality rate caused by bark beetle infestation (Egan et al., 2010; Negrón et al., 2017). Direct control can take many forms, such as salvage and biological control (trapping). Salvage includes the harvesting of storm-damaged timber and freshly infested trees (green attack) (Göthlin et al., 2000; Stadelmann et al., 2013). Harvesting of infested trees is the most common measure for

controlling *I. typographus* L. However; this action task must be completed before a new brood emerges and migrates (Wulder et al., 2009). Therefore, the removal of fallen and freshly infested trees reduces the emergence of new infestation locations, and it also moderates the beetle population. Biological control strategies, such as pheromone trapping, can be used to lure beetles. The main goal of this approach is to reduce bark beetle infestation in the remaining stands. Thus, the traps are more often used to prevent attacks on the remaining healthy trees than to diminish beetle populations (Lobinger and Skatulla, 1996).

In general, the logistics of the direct (salvage) control of bark beetles require a mechanism for the early detection of infested trees and monitoring known infestation locations in the forest (Wermelinger, 2004). Traditionally, foresters had to look for early signs of infestation by searching for a dry brown powder that was produced by the bark beetles during the colonisation process when the beetles tunnel under the bark of the trees. Such a technique, however, is not practical and is inefficient for application in large areas because it is significantly laborious and costly.

1.3 Remote sensing of Ips typographus, L. green attack

Remote sensing has the potential to monitor and detect forest stress induced by pest infestations over large areas in relatively short periods of time. The premise of employing remotely sensed data to detect insect-infested forests is that distinct symptoms are observable by different portions of the electromagnetic spectrum, which can be acquired from remote sensing platforms (Chen and Meentemeyer, 2016). Depending on the stage of the attack, the symptoms indicate the decline in biochemical and biophysical properties, such as chlorophyll and water content, defoliation, treefall gaps, and changes in leaf area index (LAI) (Wulder et al., 2009). For example, during the advanced stages of bark beetle infestation (i.e. red attack), needles on Norway Spruce trees turn from green to yellow to red-brown, which can be detected by the human eye at both leaf and canopy levels (Coops et al., 2006; Franklin et al., 2003b; Niemann and Visintini, 2005a). As a result, these symptoms can be observed using the visible portion of the electromagnetic spectrum (400 to 700 nm), which appear similar in the human visual system. It is important to note that the stress exhibited by the trees mediated by the bark beetle is brought on gradually, and therefore, it is difficult to detect early-stage symptoms using the visible portion of the electromagnetic spectrum. Instead, sensors with the capacity to detect the near-infrared spectrum (700 to 1300 nm) are more sensitive to such physiological stress. Likewise, the amount of energy reflected in the short-wave infrared range (1300 to 2500 nm) was correlated with vegetation moisture; in particular, leaf water content

(Aldakheel and Danson, 1997; Laurent et al., 2005). In general, the length of time required for a moisture deficit to produce visible symptoms in foliage can vary from weeks to several months. However, these changes are detectable with spectral data, particularly if acquired in the shortwave and thermal infrared spectra, where water absorption features in vegetation are well documented (Berni et al., 2009; Buitrago Acevedo et al., 2017; Jang et al., 2006; Sepulcre-Cantó et al., 2006).

In general, the usefulness of remotely sensed data to provide forest health-relevant information (stress signal) depends on the spectral, spatial, temporal and radiometric resolution of remote sensing instrument (Chen and Meentemeyer, 2016; Wulder et al., 2009). Recent studies have discovered that the subtle changes in spectral discrepancies induced by insect infestation can be better detected by fine-spectral and spatial resolution data (Coops et al., 2006; Hatala et al., 2010; Ortiz et al., 2013). For example, previous studies confirmed the potential of high spatial resolution data for fine-scale forest stress detection (Filchev, 2012a; Immitzer and Atzberger, 2014; Latifi et al., 2014). Moreover, many forest diseases or insect infestations do not cause tree death instantly; therefore, continuous monitoring is essential for investigating and understanding the dynamic characteristics of leaf properties and canopy reflectance during infestation events. Such observation provides detailed information regarding the impact on infested trees, and it also allows for the exploration of diagnostic effects at any stage to detect insect infestation as early as possible.

Many studies have attempted to use remote sensing data and techniques for the detection of bark beetle infestation at an early (green attack) stage. As Table 1 shows, most studies performed on the detection of green attacks were conducted at the canopy level. The literature review revealed that no previous studies focused on both the leaf level and the canopy level. Furthermore, the effect of an *Ips typographus* green attack on host tree biochemical and spectral reflectance properties has not yet been investigated in detail. To date, the successful detection of bark beetle green attack using remote sensing data has not been documented in the literature.

The little attention that has been paid to the changes in biochemical and biophysical properties of Norway Spruce trees under bark beetle *Ips typographus* infestation and the link with variation in spectral reflectance behaviour may be due to several issues. First, there are biological limitation factors, such as the flight activity of the bark beetle, the time lapse for the colonisation process, and the period during which trees are yet to show visual signs of stress. As mentioned in section 1.1, the development of the bark beetle is dependent on temperature, as an increase in temperature may lead to an increase in the beetle population, due to eggs hatching and developing into

adults sooner (Bentz et al., 2010; Wermelinger, 2004). Therefore, the fading of the infested tree is not a consistent or linear process, but it instead depends on the local environment and tree conditions (Safranyik, 1974). Second, there are logistical and technological limitation factors. In remotely sensed and field survey data of bark beetle green attacks, it is evident that time plays a critical role (Wulder et al., 2009). For example, during a field survey, the temporal observation associated with beetle biology and the appearance of the symptoms in the tree foliage should be considered. Likewise, the flight time of the beetle must be considered in the case of remotely sensed surveys. For example, the adult bark beetle starts to attack new host trees during the European springtime (between the end of April and the beginning of May).

This thesis is concerned with the detection of the European Spruce bark beetle green attack at both leaf and canopy levels using various types of remotely sensed data in parallel with field measurements. It also considers the impact of bark beetle green attack on the variation of biochemical and biophysical properties of the infested leaves. The relationship between bark beetle infestation and changes in foliar biochemical properties, such as chlorophyll content, chlorophyll fluorescents, nitrogen content, stomatal conductance, water content, and dry matter content, are examined and interpreted.

Table 1.1: Existing literature that utilised various remote sensing data (including aerial photography) to detect bark beetles at the green attack stage over the last 50 years.

No	Author	Data used	Beetle species	level
1	(Murtha, 1972b)	aerial photography	MPB	canopy
2	(Murtha and Wiart, 1989)	aerial photography	MPB	canopy
3	(Runesson, 1991)	aerial photography + field spectrometer	MPB	leaf and canopy
4	(Gimbarzevsky et al., 1992a)	multi-spectral scanner imagery + aerial photography	MPB	canopy
5	(Schweigler,2007)	aerial photography	NSB	canopy
6	(Ortiz et al., 2013)	TerraSAR-X and RapidEye	NSB	canopy
7	(Ahern, 1988b)	field spectrometer (350 -1100nm)	MPB	leaf
8	(Cheng et al., 2010)	field spectrometer (350-2500nm)	MPB	leaf
9	(Sprintsin, 2011)	Landsat ETM+	MPB	canopy
10	(Heath, 2001a)	Compact Airborne Spectrographic imager (CASI)	NSB	canopy
11	(Lawrence and Labus, 2003)	hyperspectral imagery	DFB	canopy
12	(Marx, 2010; Marx and an der Havel, 2010a)	RapidEye	NSB	canopy
13	(Filchev, 2012a)	worldview-2	NSB	canopy
14	(Lausch et al., 2013b)	HyMAP	NSB	canopy
15	(Latifi et al., 2014)	Landsat MSS + SPOT2&4	NSB	canopy
16	(Fassnacht et al., 2014)	HyMAP	NSB	canopy
17	(Immitzer and Atzberger, 2014)	WorldView-2	NSB	canopy
18	(Näsi et al., 2018)	Hypex UAV	NSB	canopy
19	(Foster et al., 2017)	field spectrometer + Landsat TM	ESB	canopy
20	(Niemann et al., 2015)	VNIR-SWIR and discrete LiDAR	MPB	canopy
21	(Mullen, 2016)	Hypex & WorldView-2	MPB	canopy
22	(Roberts et al., 2005)	aerial photography	MPB	canopy

ESB = Engelmann spruce beetle (*Dendroctonus rufipennis*), MPB = mountain pine beetle (*Dendroctonus ponderosae*), NSB = Norway spruce beetle (*Ips typographus*)

1.4 Research objectives

The main objective of this research is to utilise different remote sensing data and approaches at different scales (leaf and canopy) to detect early stage of bark beetle infestation. This includes four sub-objectives:

First objective: To investigate the impact of an *Ips typographus* L. green attack on the foliar properties (i.e. foliar reflectance and biochemical properties) of Norway Spruce trees. In this objective, the following research questions are addressed

- How does the early stage bark beetle infestation affect foliar spectral and biochemical properties?
- Does bark beetle infestation affect the accuracy of foliar biochemical estimations when using hyperspectral measurements?

Second objective: To study the dynamics of leaf traits and canopy reflectance spectra of Norway Spruce trees from early to advanced stages (green to red) of spruce bark beetle *Ips typographus*, L. infestation. In this objective, the following research question is addressed

- What are the spectral regions and leaf traits that are affected by infestation over time and how would this impact the discrimination between healthy and infested plots in the early stages of an attack?

Third objective: To examine the sensitivity of thermal and visible-short wave infrared data to foliar properties under bark beetle *Ips typographus*, L. infestation. In this objective the following research question is addressed:

- How accurate are thermal and visible-short wave infrared data from Landsat-8 at detecting an early stage *Ips typographus*, L. green attack and estimating foliar properties?

Fourth objective: To evaluate the potential of different spectral vegetation indices from multispectral satellites to detect and map bark beetle infestation at the green-attack stage. In this objective the following research question is addressed:

- To what extent can spectral vegetation indices from multispectral satellite imagery be utilised to map and detect canopy stress induced by a bark beetle green attack?

1.5 Thesis outline

This PhD thesis consists of six chapters, four of which are standalone papers. Three of them have been already published in peer-review ISI journals, and the other one are under review. The structure of the chapters is as follows:

Chapter 2 is about the impact of the early stage of bark beetle infestation on foliar properties (chlorophyll and nitrogen concentration) and reflectance spectra.

Chapter 3 focuses on the temporal dynamics of foliar properties and canopy reflectance using temporally dense time series of six RapidEye senses and five SPOT-5 senses in parallel with field data collection.

Chapter 4 examined the sensitivity of optical and thermal infrared data to foliar properties (chlorophyll fluorescence, stomatal conductance and water content) at early stage bark beetle (*Ips typographus*, L.) infestation.

Chapter 5 deals with using a set of spectral vegetation indices calculated from Sentinal-2 and Landsat-8 images to map bark beetle infestation at the green attack stage. Moreover, in this chapter, foliar properties such as reflectance spectra, chlorophyll content, water content, leaf dry matter content and nitrogen content were studied.

Chapter 6 provides a synthesis of the results of this research, including the answers to the research questions.

Chapter 2 : European spruce bark beetle (*Ips typographus*, L.) green attack affects foliar reflectance and biochemical properties*

* This chapter is based on:

Abdullah, H., Darvishzadeh, R., Skidmore, A.K., Groen, T.A. and Heurich, M., 2018. European spruce bark beetle (*Ips typographus*, L.) green attack affects foliar reflectance and biochemical properties. *International Journal of Applied Earth Observation and Geoinformation*, 64: 199-209.

Abdullah, H., Darvishzadeh, R., Skidmore, A.K., Groen, T.A. and Heurich, M. Detecting the effect of (*Ips typographus*, L.) green attack on leaf reflectance. The Netherlands Annual Ecology Meeting, 14-15 February 2017, Lunteren, Netherlands.

Abdullah, H., Darvishzadeh, R., Skidmore, A.K., Groen, T.A. and Heurich, M. Effects of (*Ips typographus*, L.) green attack on leaf properties. 10th EARSel SIG Imaging Spectroscopy Workshop, 19-21 April 2017, Zurich, Switzerland.

Abstract

The European spruce bark beetle *Ips typographus*, L. (hereafter bark beetle), causes major economic loss to the forest industry in Europe, especially in Norway Spruce (*Picea abies*). To minimise economic loss and preclude a mass outbreak, early detection of bark beetle infestation (so-called "green attack" stage – a period at which trees are yet to show visual signs of infestation stress) is, therefore, a crucial step in the management of Norway spruce stands. It is expected that a bark beetle infestation at the green attack stage affects a tree's physiological and chemical status. However, the concurrent effect on key foliar biochemical such as foliar nitrogen and chlorophyll as well as spectral responses are not well documented in the literature. Therefore, in this study, the early detection of bark beetle green attacks is investigated by examining foliar biochemical and spectral properties (400 – 2000 nm). We also assessed whether bark beetle infestation affects the estimation accuracy of foliar biochemicals. An extensive field survey was conducted in the Bavarian Forest National Park (BFNP), Germany, in the early summer of 2015 to collect leaf samples from 120 healthy and green attacked trees. The spectra of the leaf samples were measured using an ASD FieldSpec3 equipped with an integrating sphere. Significant differences ($p < 0.05$) between healthy and infested needle samples were found in the mean reflectance spectra, with the most pronounced differences being observed in the NIR and SWIR regions between 730 and 1370 nm. Furthermore, significant differences ($p < 0.05$) were found in the biochemical compositions (chlorophyll and nitrogen concentration) of healthy versus green attacked samples. Our results further demonstrate that the estimation accuracy of foliar chlorophyll and nitrogen concentrations, utilising partial least square regression model, was lower for the infested compared to the healthy trees. We show that early stage of infestation reduces not only foliar biochemical content but also their retrieval accuracy. Our results further indicate that remote sensing measurements can be successfully used for the early detection of the bark beetle infestation. We demonstrated that bark beetle infestation at the green attack stage effects leaf spectral response as well as leaf biochemical properties and their retrievals from hyperspectral measurements.

2.1 Introduction

Bark beetles (*Ips typographus*, L., and *Dendroctonus* spp.) are important biotic disturbance agents in the coniferous forests of Europe and North America, respectively (Christiansen and Bakke, 1988b; Fahse and Heurich, 2011; Raffa et al., 2008; Seidl et al., 2011; Seidl et al., 2014). In the past decades, an increasing number of severe bark beetle outbreaks has led to an extensive economic loss in the forest industry (Goheen and Hansen, 1993; Waring et al., 2009). The economic impacts include a reduction in the commercial value of the infested trees and increased management costs (Schowalter, 2012). Besides causing economic losses, outbreaks of the bark beetle form an important factor in the ecological development of the forest landscape, in terms of forest structure and composition (Pfeifer et al., 2011; Schowalter, 2012; Simard et al., 2012; Zeppenfeld et al., 2015), as well as biodiversity and ecosystem services (Thom and Seidl, 2015). Bark beetles can affect forest ecosystems both directly and indirectly. Direct impacts include an increase in tree mortality rates and a reduction in forest stand densities (Bright et al., 2013; Eitel et al., 2011; Filchev, 2012b; Hais and Kučera, 2008; Schowalter, 2012; Vanderhoof et al., 2013; Verbesselt et al., 2009). Other indirect impacts are; reduction in carbon uptake, changes in tree species' distribution, as well as changes in erosion processes, fire frequency, and nutrient cycling (Beudert et al., 2015; Kurz et al., 2008; Lehnert et al., 2013; Lindenmayer and Franklin, 2002; Mikkelson et al., 2013). Additionally, recent studies showed that the infestation of bark beetle leads to biodiversity enhancement by opening the canopy layers and altering microclimate condition in the forest. This alteration will provide the essential habitats and sources of energy for various organisms, and allow them to persist in the disturbed areas by bark beetle (Beudert et al., 2015; Lehnert et al., 2013; Müller et al., 2008).

The phenology of bark beetle and the associated host responses are well described in Wermelinger, (2004). The infested tree goes through three stages of attack (Coulson et al., 1985; Sprintsin et al., 2011; Wermelinger, 2004). These stages are termed green, red and grey attacks, respectively. During the green attack stage, the foliage remains green (hence the name green attack), and therefore, it is difficult to detect this stage by the human eye at leaf and canopy levels (Niemann and Visintini, 2005b; Wulder et al., 2006b). However, the subsequent degradation of the needles can be noted by regular field observations, as, during the red attack stage, the needles of the tree turn from green to yellow and red-brown. Finally, the needles fall off, and only the grey bark will remain, hence the last stage being called a grey attack. This discolouration of the attacked trees is evident at canopy level (Coulson et al., 1985). It is expected that bark beetle infestation induces changes in the spectral response of the infested trees (Filchev, 2012b; Meddens et al., 2013), as the biophysical characteristics of the entire tree, and very likely the

biochemical features of the needles, change. Therefore, during the infestation period, the trees are subjected to increasing stress and face physiological change (Heath, 2001b). This is due to the interruption of the water flow and the deterioration of chloroplasts as the beetle drills into the tree's cambium tissue (Yamaoka et al., 1990). The fungi carried by the beetles penetrate the living phloem and xylem cells, hampering the translocation of water, sugar and other nutrients within the bole of the tree (Paine et al., 1997a; Rohde et al., 1996; Safranyik et al., 2007; Wermelinger, 2004). This leads to a gradual change in biochemical and water content in the attacked tree, thus inducing alterations to its spectral characteristics over the course of the infestation (Deshayes et al., 2006; Lawrence and Labus, 2003; Marx and an der Havel, 2010b; Reid, 1961; Sprintsin et al., 2011; Yamaoka et al., 1990).

A considerable increase in unplanned harvesting of European forests following bark beetle infestation has led to increased research interest in understanding the dynamics and improving the management of *Ips typographus*, L. outbreaks (Seidl et al., 2011). Furthermore, an increase in the frequency and severity of bark beetle outbreaks is expected due to global climate change (Bentz et al., 2010). Consequently, more attention is devoted to this topic. It has also been evoked to increase discussion regarding salvage logging in protected areas in Europe (Lehnert et al., 2013). Early detection of *Ips typographus*, L. outbreaks at the green attack stage may prove an important step, as management aims to control this species and preclude a mass outbreak. At the green attack stage, the trees hold the next generation of beetles. Management intervention to prevent further outbreaks may, therefore, involve the removal of infested trees before the new brood emerges and migrates (Wermelinger, 2004; Wulder et al., 2009). Traditionally, foresters have performed field surveys to identify infested trees; such surveys are very laborious, costly, and therefore it is inefficient and hard to apply for management purposes in large areas. Remote sensing has the potential to detect pest infestations over large areas in relatively short periods of time. Employing remotely sensed data allows monitoring of the changes in leaf and canopy properties before and after insect infestation (Bentz and Endreson, 2003; Deshayes et al., 2006; Dye et al., 2008; Jensen, 2009). To date, the utilisation of remote sensing for the monitoring and detection of bark beetles by forest managers has mainly focused on the last two attack stages (i.e., the red and grey stage) and has achieved high degrees of accuracy. During the last two stages of the attack, the changes in canopy colour effect the spectral reflectance signature which are mainly been used as an indicator to detect infestations (Carter et al., 1998; Franklin et al., 2003a; Heurich et al., 2010b; Latifi et al., 2014; Meddens, 2012; Nikolov et al., 2014; Skakun et al., 2003; Wulder et al., 2006b). However, detecting the infestation in the last two stages is not sufficient for appropriate management, as phenological research proved that during the red attack stage the newly developed beetles have already left

their host trees and started to attack new trees. Therefore, the continuing of an outbreak cannot be prevented by salvage logging during this stage. Consequently, the detection of the bark beetle at the green attack stage by means of remote sensing is necessary to have a meaningful effect on the spreading of the beetle, but is challenging due to the lack of apparent visual symptoms in needles.

Early detection of infestations by *Dendroctonus* spp in lodgepole pine trees has been investigated at canopy level (Gimbarzevsky et al., 1992b; Heath, 2001b; Klein, 1973; Murtha and Wiart, 1989; Murtha, 1972a). Similarly, detection of a bark beetle green attack (*Ips typographus*, L.) at canopy level in Norway spruce trees has been investigated by (Immitzer and Atzberger, 2014; Lausch et al., 2013a; Marx and an der Havel, 2010b; Ortiz et al., 2013). However, these studies did not succeed in discriminating healthy from green attacked trees. More recently, Niemann et al. (2015) used LIDAR and hyperspectral data to examine the spectral properties of healthy trees and those under mountain pine beetle green attack and demonstrated that the most promising wavelengths, for the detection of mountain pine beetle at green attack stage, is located in the shortwave infrared region. Furthermore, Näsi et al. (2015) used a hyperspectral sensor (500-900 nm) mounted on an unmanned aerial vehicle (UAV) to map bark beetle damage at the tree level, by dividing tree stands into three different classes (healthy including trees with potential early infestation stage, red attack; and dead). They found that the healthy and dead trees can be classified with 90% over-all accuracy, however, when all classes were considered (healthy, red and dead), the overall accuracy dropped to 76%. At the leaf level, there are very few studies, although with different beetle and tree species, that have examined the differences in spectral reflectance between healthy needles and those that have been under bark beetle green attack (Ahern, 1988a; Cheng et al., 2010; Foster et al., 2017). In addition to a change in spectral reflectance properties, Cheng et al. (2010) observed that there were differences in the water content of healthy and infested needles, particularly, between 1318 – 1322 nm.

These results show that remote sensing has the potential to detect early stages of bark beetle attacks. However, these studies have mostly considered the effect of early infestation on reflectance spectra and not on the biochemical properties of the needles. Therefore, it is highly important to understand whether, in addition to the spectral reflectance, the biochemical properties are also affected at the bark beetle early infestation stage. Consequently, the topic warrants further investigation.

As mentioned earlier, it is expected that the infested tree will exhibit a change in terms of its biochemical and spectral properties, due to the beetle larva and blue stain fungi such as (*Ophiostoma* and *Cerato-cystis* species) carried by the

beetles starts to penetrate the living phloem and xylem cells, hampering the translocation of water, sugar and other nutrients within the bole of the tree (Paine et al., 1997a; Rohde et al., 1996; Safranyik et al., 2007; Wermelinger, 2004).Therefore, in this study, we aim to investigate the possible early detection of a bark beetle green attack by examining and comparing the foliar biochemical (chlorophyll and nitrogen) and spectral properties (400 – 2000 nm) of both healthy and green attacked trees. Chlorophyll and nitrogen are two important elements that have a key role to play in plant life and status and can be considered as indicators that reflect the status of plant growth and health (Heinze and Fiedler, 1976; van Maarschalkerweerd and Husted, 2015; Wang et al., 2015a; Wang et al., 2015b). As such changes, initiated by bark beetle attack cause stress during the infestation time, we hypothesise that chlorophyll and nitrogen concentrations are reduced during such an attack. These can thus provide suitable proxies for detecting the presence of Ips *typographus* L. during a green attack stage. Specifically, there are three main objectives: (a) to investigate the impact of an *Ips typographus* L. green attack on folair spectral reflectance; (b) to examine the changes in folair biochemical properties due to the *Ips typographus* L. green attack ; (c) to explore the impact of the *Ips typographus* L. green attack on the estimation accuracy of folair biochemical properties utilizing hyperspectral measurements.

2.2 Material and Methods

2.2.1 Study area

The study area is the Bavarian Forest National Park (BFNP) in south-east Germany, which covers an area of 240 km^2 between 13°12'9" E (longitude) and 49°3'19" N (latitude) (Fig. 2.1). The elevation in the BFNP ranges from 600 m to 1453 m. This region is characterised as having a temperate climate with a total annual precipitation along the gradient between 900 and 1800mm as well as a mean annual temperature that varies between 3.5 and 7.2°C (Bässler et al., 2008b; Lehnert et al., 2013). The area is divided into three ecological zones: high elevations, hillsides, and valley bottoms. Around 90% of the tree stands in high elevations are Norway spruce (*Picea abies* (L.) Karst), 2% are beech (*Fagus sylvatica* L.), and the remaining 8% are covered by other broad-leaves trees, mainly Common Rowan (*Sorbus aucuparia*). While on the hillsides, around 58% is occupied by Norway spruce, and the rest is a mixture of European silver fir (*Abies alba*) and beech. In the valley bottoms, 83% of the trees are Norway spruce, and the rest is a mix of species (Cailleret et al., 2014b; Heurich et al., 2010a). Multiple storm events in the 1980s and a series of hot summers in the 1990s have led to an extensive mortality of canopy trees by bark beetles on about 8 000 ha (Lausch et al., 2013a).

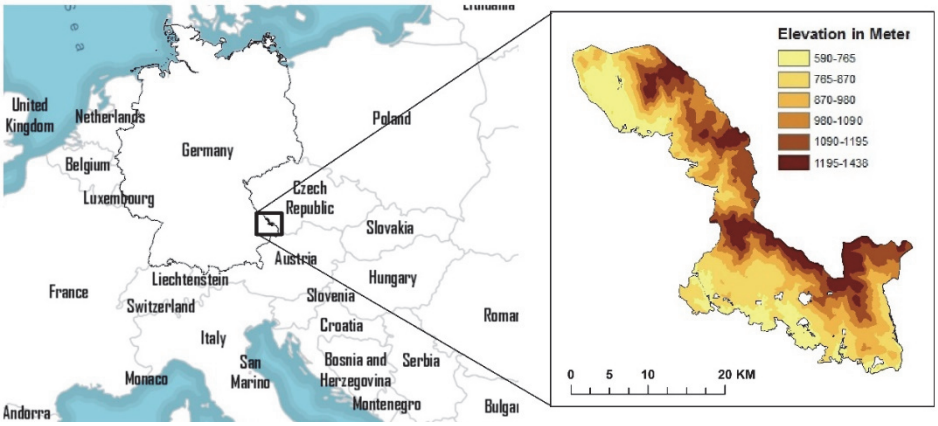

Figure 2.1: The location of Bavarian Forest National park in Central Europe.

2.2.2 Data acquisition

The adult bark beetle starts to attack new host trees during the European springtime (between the end of April and the beginning of May). This process strongly depends on the air temperature as the beetles start their swarming when the air temperature reaches 16.5°C (Lobinger, 1994a; Wermelinger, 2004). Therefore, the field data were collected in the early summer of 2015 within 15 to 30 days from the early stages of infestation. In total 120 trees were measured, of which 66 were healthy, and 54 were freshly infested trees. An extensive field survey was conducted to identify the trees under bark beetle green attack by spotting piles of dry, boring dust, which had been pushed out onto the bark surface (Fig. 2.2). An Average of 2 – 3 branches were taken from each tree. Needle samples from each branch were collected separately. All the branches were taken from the upper part of the trees, which was exposed to the sunlight. The heights of the trees varied between approximately 25 and 30 meters. A crossbow was used to shoot an arrow with a fishing line attached to a branch with sunlit leaves (Ali et al., 2016). The fishing line was used to feed a rope over the targeted branch. Once the rope was in place, the branch was pulled down gently until it broke off. Needles were immediately removed from the fallen branches and placed in a labelled plastic zip-locked bag, which was then covered with wet pulp paper and subsequently transported to the laboratory in a portable cooling box filled with frozen ice packs to keep the sample cool. The aim was to retard, as much as possible, any changes in the needles' reflectance spectra and biochemical characteristics (Malenovský et al., 2006). Once the spectral measurements were completed, the same sample branch was transported to the laboratory to measure the fresh weight, leaf area and the biochemical properties of the foliar samples.

Figure 2.2: Dry dust produced through boring by the bark beetle *Ips typographus*, L.; used to identify freshly infested trees in the field.

2.2.3 Chemical analyses

The concentration of Chlorophyll *a* and *b* in the collected fresh leaf samples was determined destructively by a spectrophotometer following the Lichtenthaler (1987) method using acetone (v 100%). In addition, to determine foliar nitrogen, the needles were dried for 72 hours using an oven dryer at 60º C. The dried needles were properly grounded using mortar and pestle until the ground leaves became a soft powder and were passed through a 0.25 mm mesh screen. Subsequently, 2 mg of powdered leaves was transferred to a small aluminium capsule to measure the nitrogen content, using an organic elemental analyser (FLASH 2000).

2.2.4 Reflectance measurements

The leaf directional hemispherical reflectance from 350 to 2500 nm was measured for collected samples, using an ASD FieldSepc-3 Pro FR spectrometer equipped with an ASD RT3-3ZC integrating sphere (Analytical Spectral Devices, Inc., Boulder, Co, USA). The integrating sphere had a port diameter of 15 mm for a reflectance measurement. The Norway spruce needles did, however, not cover the entire sample port of the integrating sphere. Therefore, the method proposed by Daughtry et al. (1989) was applied, where a universal sample holder, designed by Malenovský et al. (2006), was used to accommodate all sizes and lengths of Norway spruce needles. For every measurement five to six needles were secured on the sample holder with cellophane tape, leaving a gap of one needle's width between needles to avoid multiple reflectances of the adjusted needles (Ali et al., 2016; Daughtry et al.,

1989). To minimise the effect of spectral signal noise, for every needle sample two hundred scans were averaged to present a single spectrum. The integrating sphere has an internal light source, and therefore, the sun angle and cloudiness does not affect the spectral measurement (Foster et al., 2017). However, to prevent possible light entering into the integrating sphere ports, covering the integrating sphere with a black piece of cloth is recommended by Mesarch et al. (1999).

The measured spectral reflectance from the sample holder contained the effects of the gap between the attached needles to the sample holder; therefore, the spectral measurements were corrected by calculation of the gap fraction. To do so, a black painted paper mask with a 15-mm diameter circular aperture was precisely superimposed onto the samples and photographs were taken using a 16.1 megapixel Panasonic LUMIX camera (Ali et al., 2016). Then, the images were imported into ImageJ software (Schneider et al., 2012), to compute the gap fraction, based on the illuminated area of the sample port. The following equation was adapted from Mesarch et al. (1999) for the Field ASD spectrometer and to compute the hemispherical reflectance of the sample needles:

$$\text{Reflectance} = [((\rho - \text{Rd}) / (1 - \text{Rd})) \times \text{Rr}] / (1 - \text{GF}); \quad (2.1)$$

where: ρ is the measured reflectance from the sample holder; Rd is stray light (ambient light) inside the integrating sphere, measured as a radiation flux of the empty illuminated sample port in reflectance mode; Rr, is the reference of sample reflectance; and GF is the gap fraction of the sample.

2.2.5 Data pre-processing and statistical analysis

A series of pre-processing steps were performed on the measured reflectance data. First, the spectral reflectance was examined, and "noisy" bands (in the spectral ranges 350 – 399 nm and 2000 – 2500 nm) were excluded from the analysis. Secondly, to eliminate and reduce the sensor noise, a Savitzky – Golay smoothing filter with a frame size of 15 (2nd-degree polynomial) was applied to the reflectance spectra (Savitzky and Golay, 1964).

The significance of differences ($p \leq 0.05$) in foliar reflectance as well as chlorophyll and nitrogen concentration between leaf samples from green attacked and healthy trees, was examined using Student *t*-tests, in order to determine whether there is spectral variation at any spectral band. Because the considered adjacent wavelengths are highly correlated, we corrected the p-value using Holm (1979) procedure, next the significant wavebands with mean reflectance spectra of both healthy and infested samples were plotted following the technique used by Schmidt and Skidmore (2003).

To investigate the relationship between the spectral reflectance of the healthy and infested samples and their biochemical parameters, the *Pearson's* correlation coefficients were calculated between spectral reflectance (400 - 2000 nm) and chlorophyll as well as nitrogen concentration for both healthy and infested samples to identify the most sensitive wavebands in healthy and infested samples.

2.2.5.1 Partial least square regression model (PLSR)

Partial least squares regression (PLSR) was used to investigate the impact of the bark beetle green attack stage on the retrieval accuracy of the chlorophyll and nitrogen concentrations in needles. PLSR is a regression method that takes into account both the variance of the explanatory and the dependent variables. It specifies a linear relationship between a set of dependent (Y) variables and a set of predictor (X) variables (Wold et al., 2001). PLSR performs particularly well when the various X-variables have strong correlations, as is normally the case with hyperspectral data. (Carrascal et al., 2009; Nicolaï et al., 2007). Further details on PLSR can be found in Geladi and Kowalski (1986).

PLSR was used to predict the foliar chlorophyll and nitrogen concentrations (dependent variables) of the healthy and infested needles from spectral reflectance (predictor variables). PLSR models were built independently for the healthy and infested samples. For the chlorophyll concentration, PLSR was fitted to the VNIR range (400 - 790 nm), as this spectral region mainly contributes to chlorophyll estimation in plants (Curran, 1989; Yoder and Pettigrew-Crosby, 1995). However, as nitrogen is associated with many other leaf chemical compounds, the spectral wavebands corresponding to nitrogen are distributed over the whole spectrum (VIR, NIR, SWIR) (Curran, 1989; Peterson et al., 1988) and consequently, for the nitrogen concentration, PLSR was fitted to the entire spectrum (400 - 2000nm). To determine the number of components needed to build the PLSR model, Monte Carlo cross-validation (MCCV) was applied (Xu and Liang, 2001). The procedure involves adding an extra component to the model when the value of the root mean square error of cross-validation ($RMSE_{cv}$) is reduced by ≥ 2 % (Darvishzadeh et al., 2008; Geladi and Kowalski, 1986). The performance of the PLSR models were assessed by computing the coefficient of determinations (R^2), the normalised root mean square error of predictions ($nRMSE_P$) (Kvalheim,1987), and normalised root mean square error of cross-validations ($nRMSE_{cv}$) of predicted versus measured values.

We further examined whether the most informative wavelengths for the estimation of chlorophyll and nitrogen concentrations in both healthy and infested samples correspond. To achieve this, the variable importance in the projection (VIP) was calculated for all wavebands from the PLSR models. VIP scores summarise the influence of individual X variables (reflectance) in the

PLSR model. A variable with a VIP score close to, or greater than 1, can be considered significant in a given model (Chong and Jun, 2005; Tenenhaus, 1998; Wold et al., 1993). A detailed description of the calculation of VIP scores can be found in Farrés et al. (2015); Wold et al. (1993). TOMCAT and libPLS toolbox was used within MATLAB to establish PLSR analysis and calculate VIP score, respectively (Daszykowski et al., 2007; Li et al., 2014).

2.3 Results

2.3.1 Spectral reflectance variation due to bark beetle green attack

The results demonstrated that the mean reflectance spectra of healthy and green attacked foliage were statistically different ($p \leq 0.05$) for 917 wavebands out of the 1600 wavebands used in this study (Fig. 2.3). As can be seen from Figure 2.3, a clear distinction was observed in the mean reflectance between healthy and infested foliage in the visible and near-infrared regions. In the visible region, the mean reflectance of the infested foliage was higher than of the healthy leaves, in conjunction with chlorophyll degradation (Fig. 2.4). However, there was a larger difference ($p \leq 0.05$) between infested and healthy needles in the wavelength range 730 – 1370 nm, as the healthy needles had higher reflectance compared to mean infested spectra.

2.3.2 Impact of bark beetle green attacks on foliar biochemical properties

A Student *t*-test demonstrated a significant difference between total chlorophyll and foliar nitrogen concentrations of healthy and infested leaves ($p < 0.05$). In healthy foliage, the mean and ± of the total chlorophyll concentration were 0.766 ± 0.140 mg/g, respectively, whereas for the green attacked leaves they were 0.657 ± 1.62 mg/g, respectively. Furthermore, the concentration of nitrogen was 1.25 ± 0.21 % within healthy leaves, while for the infested leaves they were 1.13 ± 0.18 %, respectively (Fig. 2.4). The correlation between total chlorophyll and nitrogen concentration was higher in needles from healthy trees ($r = 0.68$, $p < 0.05$) than in needles from green attacked trees ($r = 0.57$, $p < 0.05$) .

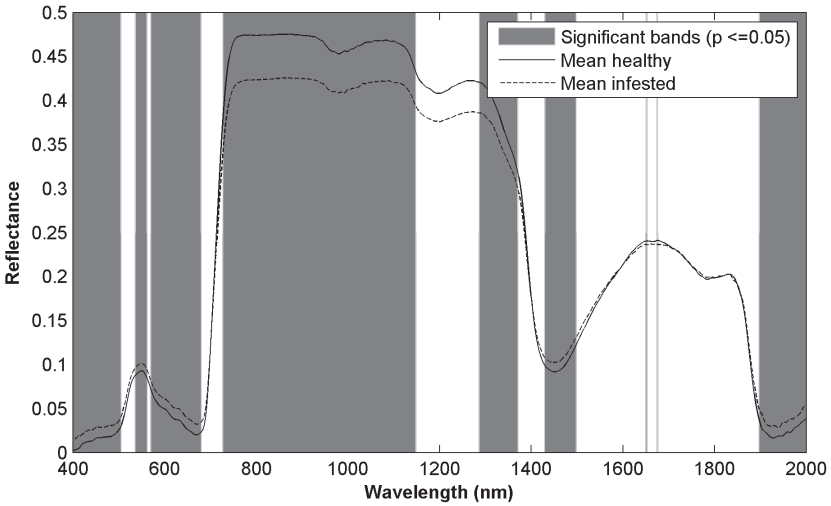

Figure 2.3: Mean reflectance spectra of healthy and infested leaves at the green attack stage. Gray areas depict the location of wavebands displaying is a significant difference between healthy and infested spectra.

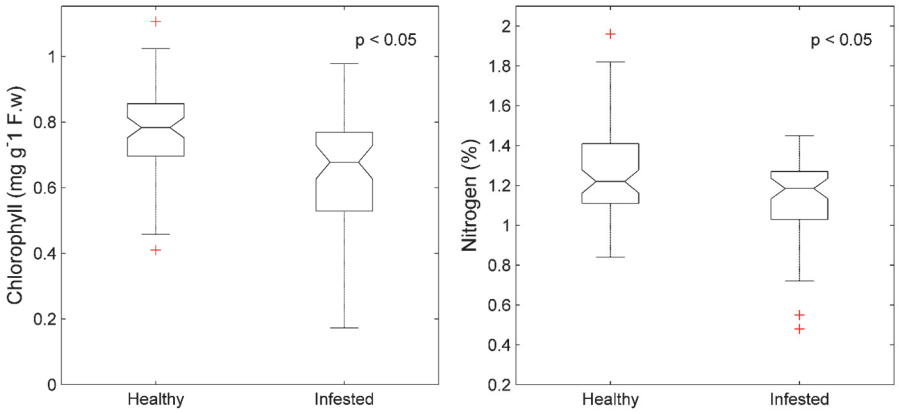

Figure 2. 4: Distribution of measured chlorophyll and nitrogen concentration for healthy and infested needles. There is a significant difference ($p < 0.05$) in chlorophyll and foliar nitrogen concentration between healthy and infested sample.

2.3.3 Effects of bark beetle green attack on the retrieval accuracy of leaf biochemical properties.

The impact of bark beetle green attack on the retrieval accuracy of foliar chlorophyll and nitrogen concentrations was assessed using PLSR. In general, higher accuracies were observed when healthy samples were assessed (Table 2.1). For healthy foliage, the coefficients of determination for chlorophyll and nitrogen concentrations were $R^2 = 0.64$ and $R^2 = 0.76$, respectively. However,

these coefficients decreased for models fitted to data from infested foliage, both for chlorophyll (R^2 = 0.55) and for nitrogen (R^2 = 0.68) (Table 2.1). Similar results were discerned with the Pearson correlation coefficient between chlorophyll and the reflectance data, as well as between nitrogen and the reflectance data. As can be observed from Figure 6, significantly higher correlations were observed for healthy leaves than for infested leaves. In addition, the prediction error for chlorophyll in healthy leaves ($nRSMSE_p$ = 0.20) was much lower than for chlorophyll in infested leaves (nRMSEp = 0.62) (Fig. 2.5). However, this variation in $nRMSE_p$ for nitrogen content was much lower (0.12 and 0.22) in both healthy and infested samples respectively.

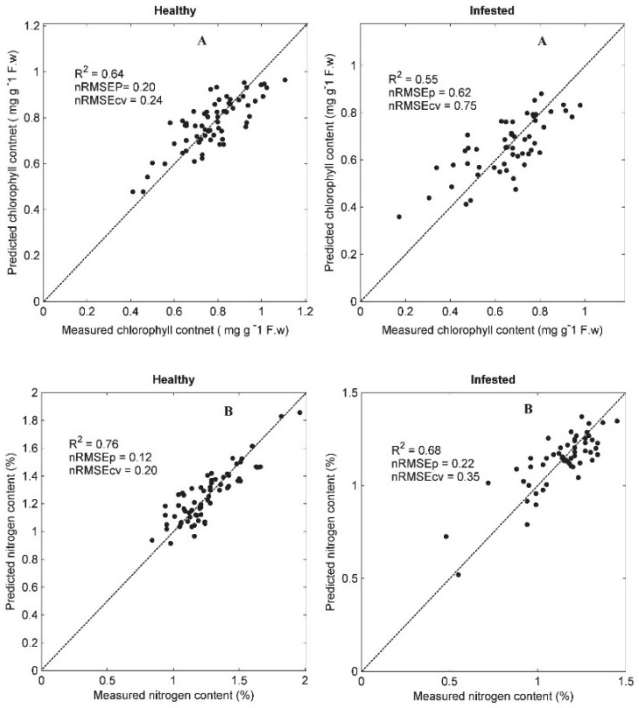

Figure 2.5: Measured versus predicted foliar chlorophyll (a) and nitrogen (b) concentration for healthy and infested samples derived from the PLSR analysis.

Table 2. 1: Number of latent variables, R2 and nRMSEp between measured and predicted chlorophyll and nitrogen in healthy and green attacked needles.

Sample Condition	**Variables**	**Nr. Of latent variables**	**$nRMSE_p$**	**$nRMSE_{CV}$**	**R^2**
Healthy	Chl	9	0.20	0.24	0.64
	N	10	0.12	0.20	0.76
Infested	Chl	10	0.62	0.75	0.55
	N	8	0.22	0.35	0.68

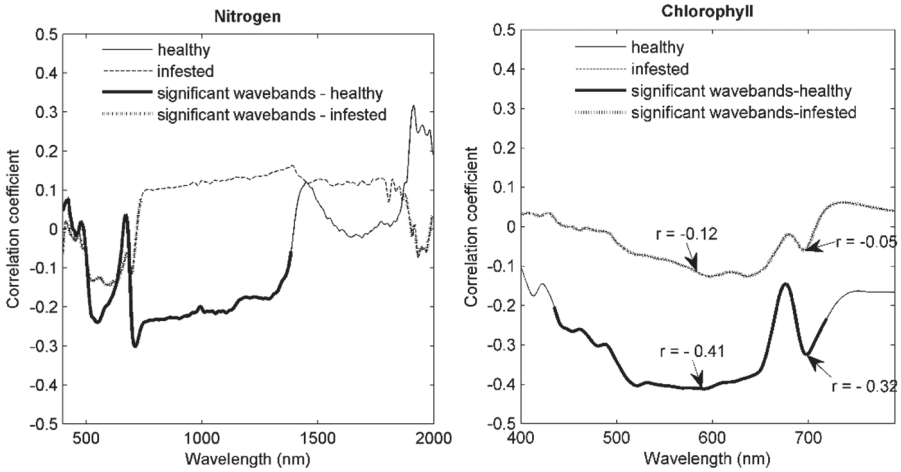

Figure 2. 6: Correlation between chlorophyll and nitrogen and the reflectance of individual wavebands. The bold lines represent the wavebands at which the reflectance spectra correlated significantly with the chlorophyll and nitrogen concentrations. The arrows show the wavebands in which recorded the highest correlation with chlorophyll content in both healthy and infested samples.

As shown in Fig. 2.6 and 2.7, the spectral regions, in particular, the green and the red edge (536 - 559nm and 732 - 790nm, respectively), demonstrated the highest VIP (VIP > 1) and a moderately negative correlation ($r = -0.41$ and -0.32, for the green and red edge, respectively; $P < 0.05$) between chlorophyll and the reflectance spectra of healthy foliage. The high VIP value indicated that the spectral feature was of major importance in estimating the chlorophyll concentration. A weaker negative correlation with a lower VIP score was observed for the infested samples ($r = -0.12$, $P < 0.05$).

The spectral regions that were most sensitive to changes in nitrogen content were in the range of 980 - 1000 nm and 1448 - 1469 nm, where the infested leaves had a lower VIP score (Fig. 2.7). Furthermore, the correlation coefficients between foliar nitrogen concentration and the reflectance spectra show a distinct variation between healthy and infested foliage, especially in the spectral region between 720 - 1400 nm. The healthy foliage showed a moderately negative correlation ($r = -0.30$, $P < 0.05$), while for the infested foliage a positive correlation was found (Fig. 2.6).

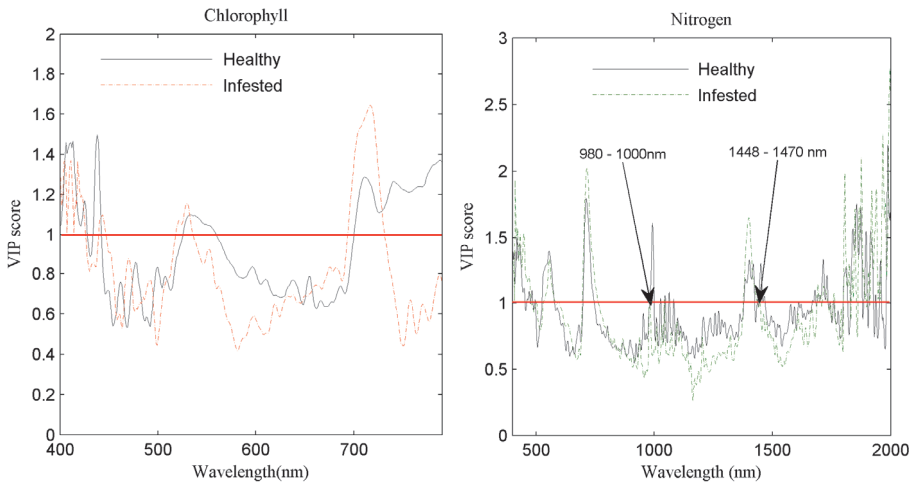

Figure 2. 7: Importance of wavelengths corresponding to the highest value of variable importance in the projection scores of partial least squares regression in healthy and infested samples, used for chlorophyll and nitrogen estimation

2.4 Discussion

It has long been believed that the detection of bark beetle green attack using remote sensing data is a challenging task (Wulder et al., 2009; Niemann and Visintini, 2005). However, recent studies have shown that remote sensing data obtained across a number of wavelengths have the potential for the detection of bark beetle green attack (Cheng et al., 2010; Foster et al., 2017; Niemann et al., 2015). In this study, we investigated whether bark beetle green attack has a concurrent effect on key foliar biochemical properties (i.e. chlorophyll and nitrogen concentration) as well as spectral responses (400–2000 nm). The results demonstrate that the foliar reflectance of needles from green attacked trees differs significantly from healthy needles ($p \leq 0.05$), in particular between wavelengths of 730 and 1370nm. Furthermore, the infestation significantly ($p \leq 0.05$) affected the biochemical concentrations of total chlorophyll and foliar nitrogen and reduced their retrieval accuracy using PLSR (Fig. 2.3 and 2.4).

The measured reflectance spectra of healthy needles matched those of similar studies which measured needle reflectance of Norway Spruce (Ali et al., 2016; Atzberger and Werner, 1998; Kováč et al., 2012). However, there were significant differences observed between the reflectance spectra of the healthy and the green attacked samples. This can be attributed to differences in their foliar biochemical properties, especially to their chlorophyll concentration which is known to be effected by vegetation stress. In our study, the reflectance increased in the visible region, and decreased in the NIR, for the green attack leaves. This is in line with the findings of Ahern (1988a), who

studied the spectral range of 400- 1100 nm and showed that the spectral band at the green peak increased for the lodgepole pine needles infested by similar beetle species (Mountain pine beetle) at the green attack stage. In the visible region, the concentration of pigments such as total chlorophyll is the main factor for determining leaf spectral variation and absorption peaks (Carter and Knapp, 2001; Demetriades-Shah et al., 1990; Feret et al., 2008; Zhang et al., 2008). The infested trees had significantly ($p < 0.05$) lower chlorophyll and foliar nitrogen concentrations than the healthy ones, resulting in lower absorption and higher scattering (Fig. 2.3 and 2.4). The observed behaviour of the reflectance spectra in the visible region in this study is a clear indication of stress caused by early infestation and is in agreement with the results of earlier studies focused on plant stress (Carter, 1993; Carter and Knapp, 2001; Zarco-Tejada and Sepulcre-Cantó, 2007). Furthermore, wavelength ranges between 730-790 nm that contained the most informative spectral region regarding variations in chlorophyll concentration, demonstrated the greatest amount of dissimilarity (58 wavebands) between the healthy and infested leaf samples (Fig. 2.7). This spectral region is often referred as red-edge, and it responds quickly to changes in foliar chlorophyll (Carter, 1993; Carter and Knapp, 2001; Smith et al., 2004). This is in good agreement with finding by Lottering et al. (2016), as they studied the utility of spectral vegetation indices derived from WorldView-2 data in detecting and mapping G. scutellatus induced vegetation defoliation. Their result showed that the combination between red-edge and NIR region has the potential to detect stress induced by G. scutellatus insect.

Moreover, as noted in Figure 2.3, the more pronounced changes in the reflectance spectra were observed at the wavelength region between the NIR and SWIR regions (730-1370 nm), where the reflectance of the infested leaves was distinctively lower than that of the healthy ones. This can probably be explained by the changes in water content that occur due to the infestation, which leads to a degeneration of the internal leaf structure at the cellular level (Miller et al., 1991; Murtha, 1978; Paine et al., 1997a; Slaton et al., 2001a; Zhang et al., 2012b). This result partially agrees with the findings of Niemann et al. (2015), who demonstrated that at the wavelength of 970 nm there was no separation between healthy trees and samples infested by mountain pine beetle, while at the wavelength of 1200 nm a significant difference existed between them. Additionally, Ismail and Mutanga (2010) showed the importance of the wavelength between 900 – 1110nm and identified both Ratio975 and water index has the ability to assess water stress induced by *S. noctilio* in *P. patula* trees from an early stage of infestation when there is no sign of infestation at the canopy level.

In addition to the variations in VIS and NIR, the reflectance spectra of healthy and green attacked samples were also significantly different ($p < 0.05$) in two short-wave infrared regions (1430-1500 nm and 1897-2000 nm) (Fig. 2.3).

The most likely cause for this variation is the low water and nitrogen content in the infested samples (Curran et al., 1992; Mirzaie et al., 2014; Peñuelas and Filella, 1998). Physiological research has shown that the fungi carried by the beetles penetrate the living phloem, hampering the translocation of water, sugar and other nutrients within the bole of the tree (Paine et al., 1997a; Rohde et al., 1996; Safranyik et al., 2007; Wermelinger, 2004). Not only are the fungi instrumental in the decline of trees, but they also provide a necessary food source for insects during the infestation period (Runesson, 1991). This leads to a gradual decrease in needle biochemical content and water content. Foster et al. (2017) and Cheng et al. (2010) showed that a number of wavebands in the shortwave infrared region have the potential for the detection of bark beetle infestation at the green attack stage which is in line with our observation. Furthermore, in our study, we have verified that the infested trees had a significantly ($p < 0.05$) lower nitrogen concentration than that found in the healthy trees.

It should also be noted that we found that infestation at the green attack stage weakened the correlation between chlorophyll and foliar nitrogen concentrations. The correlation dropped from $r = 0.68$ to $r = 0.57$, which may be partially explained by the reduction in the range of the two parameters (Fig. 2.4). Furthermore, the correlation between reflectance and both total chlorophyll and foliar nitrogen deteriorated as leaves were stressed by a bark beetle green attack (Fig. 2.6). The significant correlation (negative) between foliar nitrogen and spectral reflectance at the 700 and 1200nm (Fig. 2.6) is due to high concentrations of foliar nitrogen in healthy needles as they also contain high chlorophyll (and possibly other pigment) concentrations, lowering the reflectance. Under stress, trees tend to break down their pigments (Carter and Knapp, 2001), which probably effects the relationship between nitrogen and reflectance for the infested needles. Therefore, the infestation affects the selection of wavelengths that were most sensitive to the biochemical properties, in particular, the chlorophyll concentration, and their retrieval from spectral reflectance. This is demonstrated in Figure 2.7, where distinctively lower VIP scores were observed for the infested samples in the 730-790 nm spectral region. Consequently, the accuracy of estimation of the two parameters in the infested samples decreased (Table 2.1). To investigate the effects of bark beetle green attack on the prediction bias for total chlorophyll and foliar nitrogen we have used standardized residuals. In general, as can be seen from figure 2.8, the infestation at the green attack stage caused under-estimation of these two biochemical parameters from hyperspectral measurements.

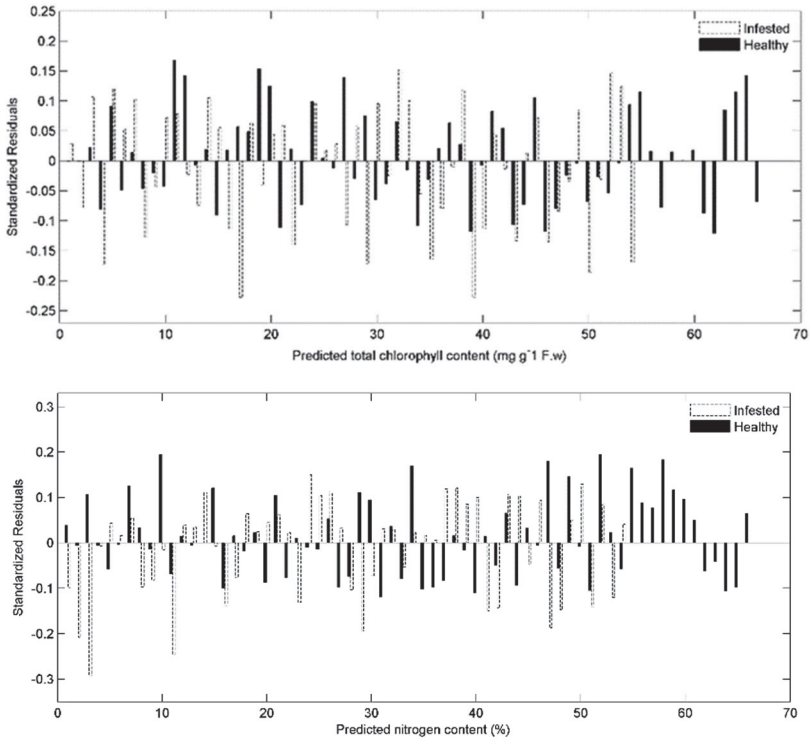

Figure 2. 8: Standardized residuals of predicted total chlorophyll and nitrogen concentration for healthy and infested samples.

2.5 Implications for remote sensing applications

Our study confirms the importance of hyperspectral measurement as well as foliar biochemical properties (i.e. chlorophyll and nitrogen) for the detection of Ips typographus, L. green attack. An extension of this finding would be to investigate the up-scaling of our findings to the canopy level. However, this forms a challenge as many factors such as logistical and technological aspects may limit the scaling up to the canopy level (Foster et al., 2017; Wulder et al., 2009). One of the critical logistical factors that affect a remotely sensed survey for green attacked trees is the timing of the optimal conditions for image acquisition. In addition, spatial and spectral resolutions play an important role in the studies of bark beetle green attack. However, this limitation may be overcome by utilising a UAV-based application and newly available multispectral satellite data, such as provided by Sentinel-2. In our study, the estimation accuracy of foliar chlorophyll and nitrogen concentration using hyperspectral measurements decreased when the tree was infested by bark beetle green attack. This might be used as an indicator for the efficient landscape-wide detection of bark beetle green attack. It is, however, important to note that retrieval accuracies for the total chlorophyll and foliar nitrogen

concentrations at the leaf level would probably be different from those at the canopy level, because structural and external factors such as illumination and atmospheric conditions may affect the reflectance spectra at the canopy level. Additionally, we found that the wavelength region between 730 and 790 nm (red-edge) is the most informative spectral region regarding variations in chlorophyll concentration due to bark beetle green attack (Fig. 2.6 and 2.7). This portion of the spectrum can be found in new multispectral satellites such as Sentinel-2, World View-2&3 RapidEye and therefore it might be possible to scaling up our findings to the canopy level, particularly considering the high spectral and spatial resolution data. Further investigation will show how accurate green attack stages can be detected with different air and spaceborne sensors.

2.6 Conclusion

This study demonstrates that reflectance properties of healthy and green attached Norway spruce trees are significantly different in 917 wavebands between 400-2000 nm. We also observed differences in the biochemical properties chlorophyll and nitrogen between healthy and green attacked needles by the bark beetle (*Ips typographus*, L.). Furthermore, the results demonstrated that the relationship between reflectance and both chlorophyll and nitrogen deteriorated as the leaves became stressed by a bark beetle green attack. Such an infestation affected the estimation accuracy of chlorophyll and nitrogen concentrations, examined using PLSR and hyperspectral reflectance data. The research findings indicate that hyperspectral measurements are promising, and present a powerful tool to determine the damage caused by bark beetle green attack at the leaf level. Further research is required to assess whether or not, the findings of the current study can be verified at the canopy level using different remote sensing data.

Chapter 3: Timing of red-edge and shortwave infrared reflectance critical for early stress detection induced by bark beetle (*Ips typographus*, L.) attack*

* This chapter is based on:

Abdullah, H., Darvishzadeh, R., Skidmore, A.K., and Heurich, M. (Under review). Timing of red-edge and shortwave infrared reflectance critical for early stress detection induced by bark beetle (*Ips typographus*,L.) attack. *International Journal of Applied Earth Observation and Geoinformation.* Accepted.

Abdullah, H., Darvishzadeh, R., Skidmore, A.K and Heurich, M. Understanding dynamics of leaf spectral properties under bark beetle (*Ips typographus*,L.) infestation. 11th EARSel SIG Imaging Spectroscopy Workshop, 6-8 February 2019, Brno, Czech republic.

Abstract

Forest disturbance in Europe, induced by European spruce bark beetle *Ips typographus*, L., results in regional-scale dieback. Early stress detection in Norway spruce stands caused by bark beetle infestation at the green attack stage (when trees are yet to show distinct symptoms observable by the human eye) is crucial and can lead to effective forest management and reduce economic losses. This study aims to investigate and understand the dynamics of leaf traits and reflectance of Norway spruce (*Picea abies*) trees during bark beetle green attack. Using temporal high-resolution images from RapidEye and SPOT-5 in parallel with the collection of field data, we examined which spectral regions and leaf traits are affected by infestation over time and how they affect discrimination between healthy and infested plots at the early stage of attack. To achieve this aim, we used a novel approach by targeting both leaf and canopy level. We measured leaf reflectance spectra and six leaf traits (water content, nitrogen, chlorophyll fluorescence, chlorophyll, and stomatal conductance) from 66 healthy and 54 infested trees at three consecutive repeated time measurements in the summer of 2015 in the Bavarian Forest National Park. Concurrently, canopy reflectance and spectral vegetation indices (SVIs) were extracted from seven RapidEye images and six SPOT-5 images. Results showed significant differences ($p \leq 0.05$) in the studied leaf traits between healthy and infested samples, and this difference increased with the progression of infestation. We found that leaf and canopy reflectance were significantly higher ($p \leq 0.05$) for the infested trees by bark beetle than the healthy ones in the 'red edge' (680–790 nm) and 'shortwave infrared' (1110–1490 nm) spectrum throughout the infestation event. Our results further demonstrated that the spectral vegetation indices calculated from the red-edge and SWIR spectral bands, such as NDRE, DSWI, LWCI and NDWI, were able to differentiate between healthy and infested trees earlier than the other SVIs. The new insight offered by these results is that the red-edge and SWIR spectral information from multispectral satellites has the potential to considerably improve monitoring and detection of forest stress and has important implications for European field bark beetle management and future studies.

3.1 Introduction

Insect outbreaks are one of the key natural disturbances in conifer forests that trigger large-scale tree mortality, with noticeable effects on ecosystem services (Aakala et al., 2011; Raffa et al., 2008; Thom and Seidl, 2016). One of the insects that can create large-scale disturbances in short periods of time is the European spruce bark beetle (*Ips typographus*, L.) (hereafter, referred to as the bark beetle) (Fahse and Heurich, 2011). During recent decades, bark beetle frequency and intensity have dramatically increased (Bentz et al., 2010). For example, in the Norway spruce forests in Central Europe, spruce bark beetles have killed a large number of Norway spruce trees in the order of tens of millions of hectares (Lausch et al., 2013a; Meddens et al., 2012; Raffa et al., 2008). Similarly, in British Columbia, Mountain pine beetles (*Dendroctonus ponderosae*) have killed several million hectares of pine trees since 1999 (Aukema et al., 2008; Westfall and Ebata, 2009). Bark beetles and their host trees are susceptible to climatic change, in particular, decreasing precipitation and increasing temperature (Netherer and Schopf, 2010). Because the global average temperature is predicted to increase by 1.4–5.8°C by 2100, enhancements of the intensity and incidence of bark beetle outbreaks are expected (Morris et al., 2018; Netherer and Schopf, 2010; Overbeck and Schmidt, 2012; Seidl et al., 2011). The bark beetle population has rapidly changed from one to three generations per year, as regional and global temperatures have increased (Bentz et al., 2010). Beetle survival rates have also increased during the winter at northern latitudes, particularly in the old spruce forests of northern and central Europe that have thus far been spared from major outbreaks (Morris et al., 2018; Öhrn, 2012). Furthermore, simulation studies on the bark beetle population have shown an increase in temperature at higher latitudes and have identified high-risk areas for bark beetle outbreaks and related tree mortality in the future (Bentz et al., 2010; Cailleret et al., 2014).

The extensive increment in harvesting of European conifer forests, due to bark beetle infestation, has resulted in further research that focuses on various underlying forces to reduce further bark beetle outbreaks (Seidl et al., 2011). One of the common techniques used to combat this threat is to cut and remove the infested trees at an early stage to protect neighbouring unaffected trees (Fahse and Heurich, 2011). This step should be performed during the early phase of the infestation —the so-called 'green attack'—and before beetle larvae are fully developed and able to infest other nearby trees (Wermelinger, 2004). At this stage, the beetles carry pathogenic blue stain fungus (*Ophiostoma* and *Ceratocystis* species) and will transfer it to the host trees. This fungus affects the translocation of nutrients and water within the trunk of an infested tree (Paine et al., 1997; Rohde et al., 1996). As a result, the initial response of the hosted trees by bark beetles is to close their stomata, a process which

decreases the water content due to the shutting down of the stem (Edburg et al., 2012). This behaviour (closing stomata) of the infested trees leads to a decrease in photosynthesis as a result of CO2 limitation (Flexas et al., 2004) and eventual death through water stress.

Traditionally, foresters had to look for early signs of infestation by searching for a dry brown powder that was produced by the bark beetles during the colonisation process when the beetles tunnel under the bark of the trees (Abdullah et al., 2018a). Such a technique, however, is not practical and is inefficient for application in large areas because it is significantly laborious and costly. Remote sensing data and techniques are a useful alternative for effective forest management. The premise of employing remotely sensed data to monitor and identify stressed or insect-infested forests is that the infested trees show symptoms detectable by remote sensing sensors (Chen and Meentemeyer, 2016).

Previous studies have shown the significant potential of remote sensing data for detecting the advanced stages of bark beetle infestation (so-called 'red-attack' and 'grey-attack') (Coops et al., 2006; Filchev, 2012; Franklin et al., 2003; Hais et al., 2009; Havašová et al., 2015; Meddens et al., 2013; Skakun et al., 2003; White et al., 2007; White et al., 2006; Wulder et al., 2006). A red-attack is the advanced stage of bark beetle infestation, in which the attacked trees develop stress symptoms by turning their needles' colour from green to yellow to red-brown. Subsequently, the needles fall from the infested trees, and only the grey bark remains; hence, this stage is termed 'grey attack' (Coulson et al., 1985). It is important to note that the early detection (green attack) of a bark beetle attack is crucial for preventing an outbreak, and salvage logging which is performed for loss recovery and appropriate bark beetle management (Fahse and Heurich, 2011).

Timing plays a critical role in remote sensing and field surveys of bark beetle green attack (Wulder et al., 2009). An operational survey has to be performed when the infestation is in its early phase and should consider the temporal field observation associated with beetle biology and the appearance of the symptoms in the tree foliage. In other words, in remote sensing-based surveys of green attack, the swarming event of the beetles must be considered. For example, the European spruce bark beetle (*Ips typographus*, L.) starts to swarm when the air temperature reaches 16.5°C (Lobinger, 1994; Wermelinger, 2004). To date, the identification of green attack has been less satisfactory due to many biological, technical and logistical constraints/limitations. These issues include the flight activity of the bark beetle, the time duration required for the colonisation process and the period when the infested trees have yet to show distinct symptoms capable of being observed by human eye. Hence, it is important to consider biological as well

as logistical factors when using remotely sensed data to detect bark beetle green attack (Wulder et al., 2009).

Numerous studies have focused on using single-date remote sensing data or have compared the utility of different remotely sensed data from different sensors, to detect early infestation stages; hence, very little attention has been paid to investigating the temporal response of trees under bark beetle attack. For example, early detection of a different beetle (*Dendroctonus* southern pine beetle (spp) in lodgepole pine trees) has been investigated by Gimbarzevsky et al. (1992), Murtha (1972) and Murtha and Wiart (1989) using multispectral aerial photographs. However, it has been challenging in these studies to differentiate between green attacked trees and the healthy ones. Similarly, Heath (2001) encountered similar challenges when using airborne hyperspectral data from CASI (Compact Airborne Spectrographic Imager). On the other hand, a number of studies have attempted to detect the early stage of *Ips typographus*, L. green attack using different remote sensing data and techniques. Ortiz et al. (2013) used TerraSAR-X and single-date high-resolution data from the RapidEye satellite. Lausch et al. (2013b) used a single date airborne hyperspectral HyMAP image data for detecting bark beetle green attack. More recently, Immitzer and Atzberger (2014) and Näsi et al. (2018) have used WorldView-2, and hyperspectral data obtained from an unmanned aerial vehicle (UAV) to detect bark beetle green attack.

As mentioned previously, during the colonisation process, the beetles inoculate the host trees with pathogenic fungi, such as *Ophiostoma* and *Cerato-cystis*. Therefore, the infested trees will develop stress symptoms, due to changes in biochemical and spectral properties. As a result, the biochemical properties such as leaf water content, chlorophyll, nitrogen, and stomatal conductance are expected to decline within trees colonised by bark beetles (Abdullah et al., 2018a).

Given the above biological and logistical factors, continuous monitoring is essential for investigating and understanding the dynamic characteristics of leaf properties and canopy reflectance under bark beetle infestation, which may help to detect and monitor changes at an early stage. Such observation provides detailed information regarding the impact of bark beetle on infested trees and it also allows us to explore the diagnostic effects at any stage and to achieve and detect the possible effects of bark beetle infestation as early as possible. Therefore, in this study for the first time, we sought to investigate the temporal effect of bark beetle attack on infested trees in the early development phase (green until the red attack stage). To do this, we targeted both the foliar and canopy levels by continuously monitoring the changes using temporal field data measurements and temporal remote sensing satellite data from RapidEye and SPOT-5. The main goals of this study are (i) to analyse the

temporal dynamics for a number of leaf traits influenced by bark beetle attack from the beginning of infestation until the advanced stage of attack (red attack) and (ii) to identify and explore remote sensing time-series indices effective for explaining changes in leaf traits, as well as for detecting early stages of bark beetle infestation.

3.2 Material and methods

3.2.1 Study area

The study site is the southern part of Bavarian Forest National Park (BFNP), which is located in south-eastern Germany along the border of the Czech Republic, and it lies between 13°12'9" E (longitude) and 49°3'19" N (latitude). The BFNP established in 1970 and extended in 1977, covering an area of 240 km2. Depending on the elevation in the BFNP, which ranges from 600 m to 1450 m, the mean annual temperature fluctuates between 3.5° and 9°C, and the total annual precipitation varies from 900 to 1800 mm (Bässler et al., 2008; Heurich et al., 2010).

In the BFNP three major forest types can be recognised; these are, highlands, hillsides, and valleys. The highlands above 1100 m are dominated by Norway spruce (*Picea abies*), and some Mountain ash (*Sorbus aucuparia*); in the hillsides, with elevation between 600 – 1100 m, is mixed forest including Norway spruce (*Picea abies*), European beech (*Fagus sylvatica*), White fir (*Abies alba*), and Sycamore maple (*Acer pseudoplatanus*); in the valleys, spruce forests exist, including Mountain ash, Norway spruce, and birches (Betula pendula, Betula pubescens) (Cailleret et al., 2014; Heurich et al., 2009; Latifi et al., 2018). Since 1984, the forests of BFNP have been affected by the spruce bark beetle (*Ips typographus*, L.), which have caused extensive disturbance and economic losses to timber production in this region (Cailleret et al., 2014).

3.2.2 Field data collection

From mid-May to mid-July 2015, an extensive field survey was conducted to collect field measurements, in which the selected sample trees were visited on three separate occasions (Table 3.1). We divided the study site into healthy Norway spruce trees stands as well as stands with trees freshly infested by bark beetles. Considering the nature of the forest heterogeneity in tree species, tree age and density, 30 healthy plots were randomly selected. To select the green attacked trees, we conducted an extensive field survey to search for dry brown powder around the trees. Altogether, we selected 120 trees (66 healthy and 54 green attacked) to measure foliar properties. The collected tree samples were divided between 30 healthy and eight infested plots. Bark beetle outbreaks generally occur over the course of several years, and to avoid mixed

reflectance from previous years' attacked trees and green attacked trees, only those plots that showed freshly infested or green-attacked trees were considered. A Leica GPS 1200 differential global positioning system (DGPS) (Leica Geosystems AG, Heerbrugg, Switzerland) was used to locate the centre of each plot (Abdullah et al., 2018b).

From each tree, an average of two to three branches were taken from the upper canopy exposed to sunlight. Because the height of Norway spruce trees reaches 25 to 30 m, we used a crossbow to shoot an arrow with a fishing line into a branch with sunlit leaves. Full details regarding the use of the crossbow can be found in Ali et al. (2016). Next, to measure leaf traits, needle samples were removed from collected branches. In the field, total chlorophyll, chlorophyll fluorescence and stomatal conductance were measured. A handheld chlorophyll content meter (CCM) was used to measure both chlorophyll and chlorophyll fluorescence. From the fallen branches, an average of ten readings were immediately taken using the CCM. To measure the needle stomatal conductance, a steady-state instrument (SC-1 Leaf Porometer) was used. This instrument computes stomatal conductance utilising a leaf clip chamber that can monitor the relative humidity (RH %) released from the leaf stomata.

The needle samples were covered by wet paper and placed in a labelled plastic zip-locked bag in order to transport to the laboratory in a portable cooling box. In the laboratory, an ASD FieldSepc-3 Pro FR spectrometer equipped with an ASD RT3-3ZC integrating sphere (Analytical Spectral Devices, Inc., Boulder, Co, USA) was used to measure the directional hemispherical reflectance from 350 to 2500 nm for the collected samples. The details concerning the measurements of hemispherical needle reflectance can be found in Abdullah et al. (2018) and Malenovský et al. (2006). To calculate leaf water content, fresh weight (Fw/g) and leaf surface area (LA cm^2) were determined for the collected samples using a digital scale and an AMH 350 leaf area meter. The needle samples were then oven-dried for 72 hours at 60°C until a constant weight was obtained. Finally, to measure the nitrogen concentration of the dried needles, an organic elemental analyser (FLASH 2000) was used.
Leaf water content (Cw) was determined using the following equations:

$$Cw\ (g/cm^2) = (Fw - Dw) / LA \quad (3.1)$$

where Fw, Dw, and A represent fresh leaf weight (g), dry leaf weight (g). The studied leaf traits (total chlorophyll, chlorophyll fluorescence, nitrogen concentration, water content, and stomatal conductance) were continuously measured at three different times for the representative trees (Table 3.1).

Table 3. 1: The leaf traits measured and overview of satellite data acquisition in the Bavarian Forest National Park, 2015. The (✓) are the SPOT-5 data and (•) are the RapidEye data. T1, 2, and 3 represent first, second, and third field measurements, respectively.

Field measurements time				Leaf traits								
Time-1 (T1) (15/May To 1/Jun)				Total chlorophyll (Ch mg/m^2)								
Time-2 (T2) (2/Jun To 18/Jun)				Chlorophyll fluorescence								
				Nitrogen concentration (g/ cm^2)								
Time-3 (T3) (20/Jun To 10/July)				Leaf water content (C_w g/cm^2)								
				Stomatal conductance (mmol/(m^2·s)								
				Leaf reflectance spectra (nm)								
Satellite data												
RapidEye		•		•	•		•		•	•		•
SPOT-5	✓		✓			✓		✓			✓	✓
	11-May	13-May	05-Jun	14-Jun	02-July	10-July	17-July	04-Aug	06-Aug	26-Aug	29-Aug	13-Sep

3.2.3 Satellite imagery

We identified two series of high-resolution multispectral satellite data, namely RapidEye and SPOT-5 (Table 3.1). The RapidEye orbit system consists of five satellites, each of them collecting radiation in the five spectral bands blue, green, red, red edge and near-infrared (NIR). In this study, seven RapidEye images were captured within the time period May 2015 to September 2015. They were systematically geo-corrected radiance and orthorectified at 5 m spatial resolution and matched each other with sub-pixel accuracy (RapidEye, 2011; Tyc et al., 2005).

For the SPOT-5, we used six images from L2A reflectance product, that provides data with atmospheric and topographic corrections as well as with corresponding masks, clouds, and shadows. It captures data in 4 spectral bands (green, red, near infrared and shortwave infrared). The SPOT-5 L2A has 10 m spatial resolution when acquired within the Take-5 initiative (Meygret, 2007).

3.2.3.1 Ancillary data (reference disturbance data)

Vector-based reference data of the green attacked areas in 2015 were obtained from the Bavarian Forest National Park (BFNP) administration (Abdullah et al., 2018b). The reference data is produced from aerial colour-infrared (VIS and NIR) images with 0.1 m spatial resolution. The aerial images were obtained during the flight campaign that were carried out in September 2016, and for which the new deadwood (grey attack stage) from the 2015 infestation was documented by stereo photogrammetry. For more detailed information about

the processing and interpretation of aerial images in the BFNP see Heurich et al. (2009) and Lausch et al. (2013a).

The data were rasterised into 5 m × 5m grid cells to match with a spatial resolution of RapidEye, and 10 m × 10 m grid cells to match with a spatial resolution of SPOT-5 data. From the rasterised data 299 infested plots were selected to extract the reflectance value (Fig. 3.1).

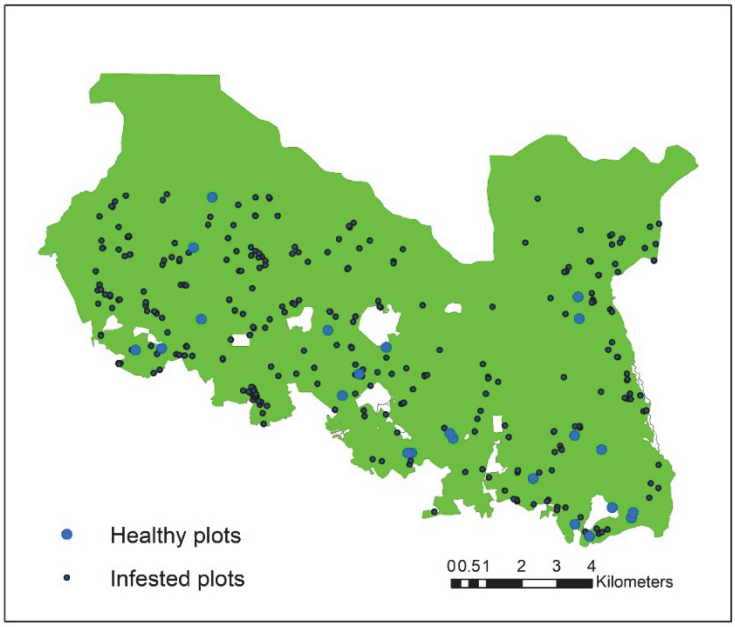

Figure 3. 1: Distribution of sample plots in the southern part of Bavarian Forest National Park, Germany.

3.2.3.2 Spectral vegetation indices

Several spectral vegetation indices exist in the literature that are used for the estimation of vegetation biochemical properties (Collins and Woodcock, 1996; Eitel et al., 2006). In this study, spectral vegetation indices linked to measured leaf traits were calculated from the spectral reflectance data collected from the SPOT-5 and RapidEye images (Table 3.2). The spectral reflectance and SVIs value were extracted from satellite images for the selected 30 healthy and 299 infested sample plots. The value extraction was done using ENVI-IDL5.5 spectral analysis toolbox. From the calculated vegetation indices, time series data stacks were then generated from each sample plot. The time series data were then subjected to further analysis.

Table 3. 2: List of spectral vegetation indices calculated from SPOT-5 and RapidEye data for both healthy and infested sample plots.

Index	Satellite		Equation	Reference
	SPOT-5	RapidEye		
NDVI Normalize difference vegetation indices	✓	✓	$\frac{(NIR-Red)}{(NIR+Red)}$	(Tucker, 1979)
NDRE Normalize difference red-edge indices	×	✓	$\frac{(NIR-Rededge)}{(NIR+Rededge)}$	(Haboudane, 2004)
GLI Green leaf index	×	✓	$\frac{2\times(Green-Red-Blue)}{2\times(Green+Red-Blue)}$	(Gobron et al., 2000)
CIG Chlorophyll index green	✓	✓	$\left(\frac{NIR}{Green}\right)-1$	(Gitelson et al., 2003)
CVI Chlorophyll vegetation index	✓	✓	$NIR\left(\frac{Red}{Green\hat{}2}\right)$	(Vincini et al., 2008)
NGRDI Normalize difference Green/red	✓	✓	$\frac{(Green-Red)}{(Green+Red)}$	(Hunt et al., 2011)
PBI Plant biochemical index	✓	✓	$\frac{(NIR)}{(Green)}$	This study
RDI Ratio drought index	✓	×	$\frac{(SWIR)}{(NIR)}$	(Pinder and McLeod, 1999)
NDWI Normalize difference water index	✓	×	$\frac{(NIR-SWIR)}{(NIR+SWIR)}$	(Hardisky et al., 1983)
DSWI Disease stress water index	✓	×	$\frac{(NIR+Green)}{(SWIR+Red)}$	(Galvao et al., 2005)
LWCI Leaf water content index	✓	×	$\frac{log(1-(NIR-SWIR))}{-log(1-(NIR-SWIR))}$	(COHEN, 1991)

3.2.4 Data analysis

To understand the temporal variations in all the measurements (leaf traits and extracted canopy reflectance data), we first explored the temporal variation from the time-series data (T1–T3). At the leaf level, mean and standard error values were calculated for both the healthy and infested sample trees to determine the temporal variation in the biochemical components. In addition, we conducted a Student t-test to investigate whether the variations in the measured leaf traits were significantly different ($p < 0.05$) between healthy and green attacked samples. Similarly, an unpaired Student t-test was used to examine whether the temporal variation in leaf reflectance spectra correlated with the bark beetle infestation and to identify the wavelength regions which were significantly different between the healthy and infested samples.

At the canopy level, box plots and Student t-tests were applied. Firstly, a box plot was used to explore temporal variations in the extracted spectral reflectance data in the given years. Secondly, a t-test was used to examine

whether there were significant differences ($p < 0.05$) in reflectance data between these two sample plots (healthy and infested). Moreover, from the calculated spectral vegetation indices, the mean and standard errors were extracted for each sample plot, and a temporal comparison was made.

3.3 Results

3.3.1 Temporal response of measured leaf traits under bark beetle

The results of the temporal variation demonstrated that there was a clear distinction between healthy and infested sample trees from the Time-1 (T1) to Time-3 (T3) measurements (Fig. 3.2). In the healthy leaves, the mean of the total chlorophyll concentrations were 337, 403, and 399 mg/m2 at T1 and T3 respectively. However, for the infested samples, the mean of the total chlorophyll concentrations were lower, viz. 317, 301, and 275 mg/m2, respectively. Similar trends were observed for the other leaf traits, where all measured leaf traits values decreased within the infested samples from T1 to T3. For example, the stomatal conductance which was measured at the beginning of the infestation at T1 for the infested leaf was higher when compared to the ones at T3, whereas, for the healthy leaves, the opposite result was observed.

This was further confirmed by the results of the Student *t*-test, which showed a significant difference ($p < 0.05$) between healthy and infested samples in all measured leaf traits (chlorophyll fluorescence, chlorophyll, nitrogen concentration, stomatal conductance, and leaf water content). At the beginning of the infestation (T1), the differences were smaller between the two sample groups (healthy and infested) for all studied leaf traits. However, there was a larger difference between the infested and healthy needles at T2 and T3, as the infested trees developed signs of stress (Fig. 3.2).

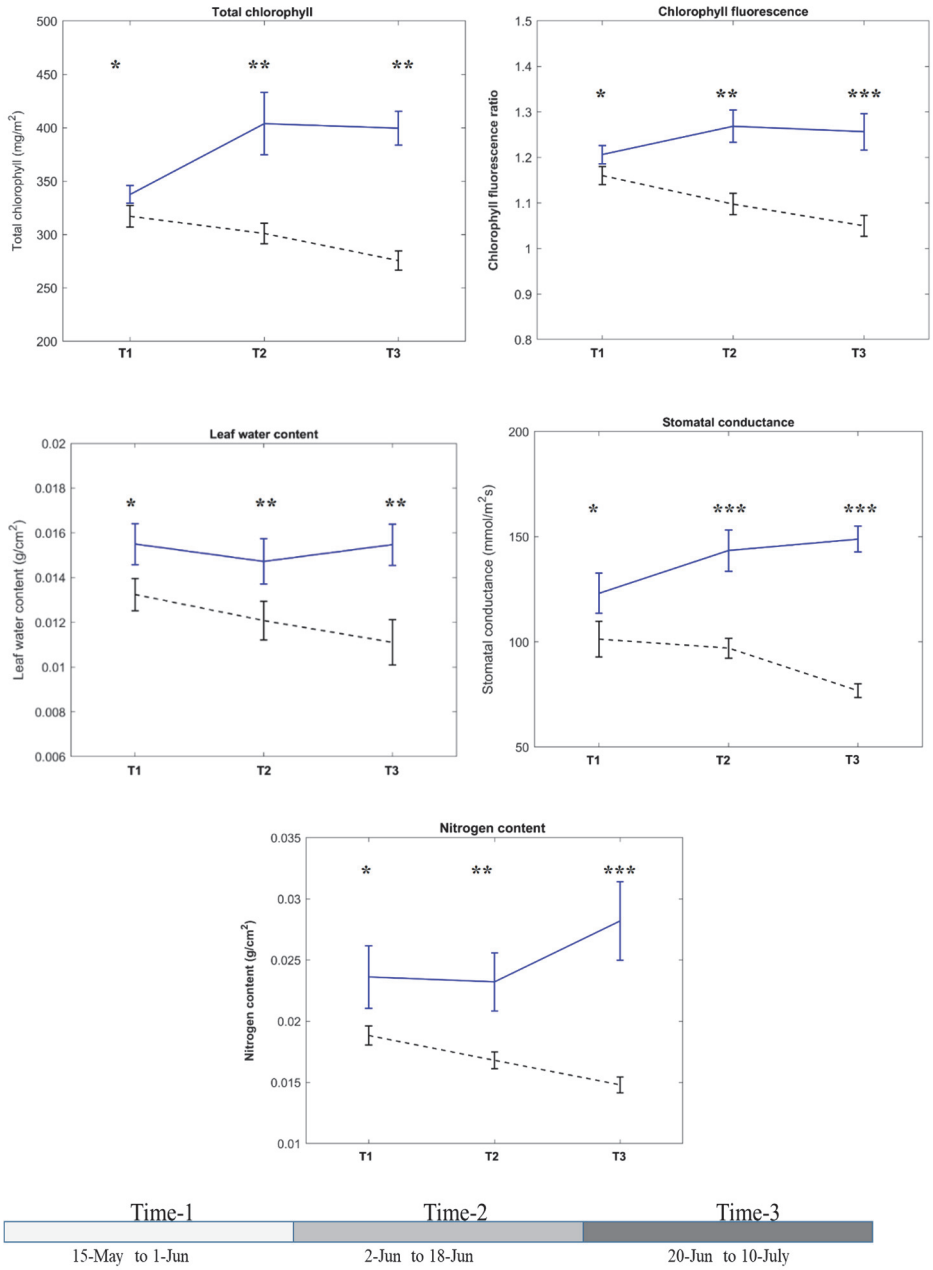

Figure 3.2: Temporal variation of the measured leaf traits for healthy and infested samples. Blue and black lines represent healthy and infested plots, respectively. T1, T,2 and T3 represent first, second, and third measurements, respectively. (*) Hardly significant, (**) significant, (***) Strongly significant.

Further analysis of the leaf spectral reflectance spectra values showed that the mean reflectance spectra of green attacked samples was higher than for the healthy ones in the visible and shortwave infrared region (Fig.3.3). The difference ($p < 0.05$) was stronger during T2 and T3, as the infested trees showed increased stress symptoms.

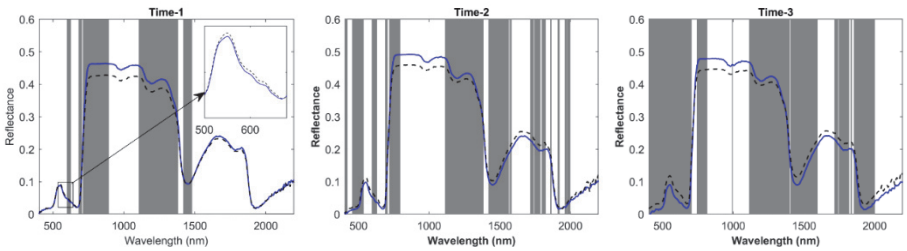

Figure 3. 3: Mean reflectance spectra of healthy and green attacked leaves at three consecutive repeated time measurements in the summer of 2015. Blue and black lines represent healthy and infested leaves, respectively. Wavebands in which there is a significant difference between healthy and green attacked leaves are presents in Gray.

3.3.2 Temporal response of canopy spectral data to bark beetle infestation

We assessed the response of canopy reflectance to bark beetle attack employing a time series of remotely sensed images from RapidEye and SPOT-5. The reflectance data were extracted from each image and for both sets of satellite data (RapidEye and SPOT-5). We found a symmetrical change of reflectance data for both sets of satellite data (Figs. 3.4 and 3.5). For example, for the RapidEye imagery, the reflectance of red-edge and NIR bands were higher for the infested plots than the healthy ones on May 13. The variation of these two spectral bands increased with the progression of infestation on July 2 and the later images. Moreover, a Student t-test of spectral bands revealed similar findings, as the red-edge was significantly different ($p < 0.05$) between healthy and infested plots for all RapidEye imagery considered in this study, while the variation in NIR between healthy and infested plots showed a significant difference ($p < 0.05$) from July 2 and later (Fig. 3.4). For the SPOT-5 imagery, the reflectance of SWIR appears to be the most sensitive to the bark beetle stressor, as it was significantly different ($p < 0.05$) from May 11 onwards (Fig. 3.5).

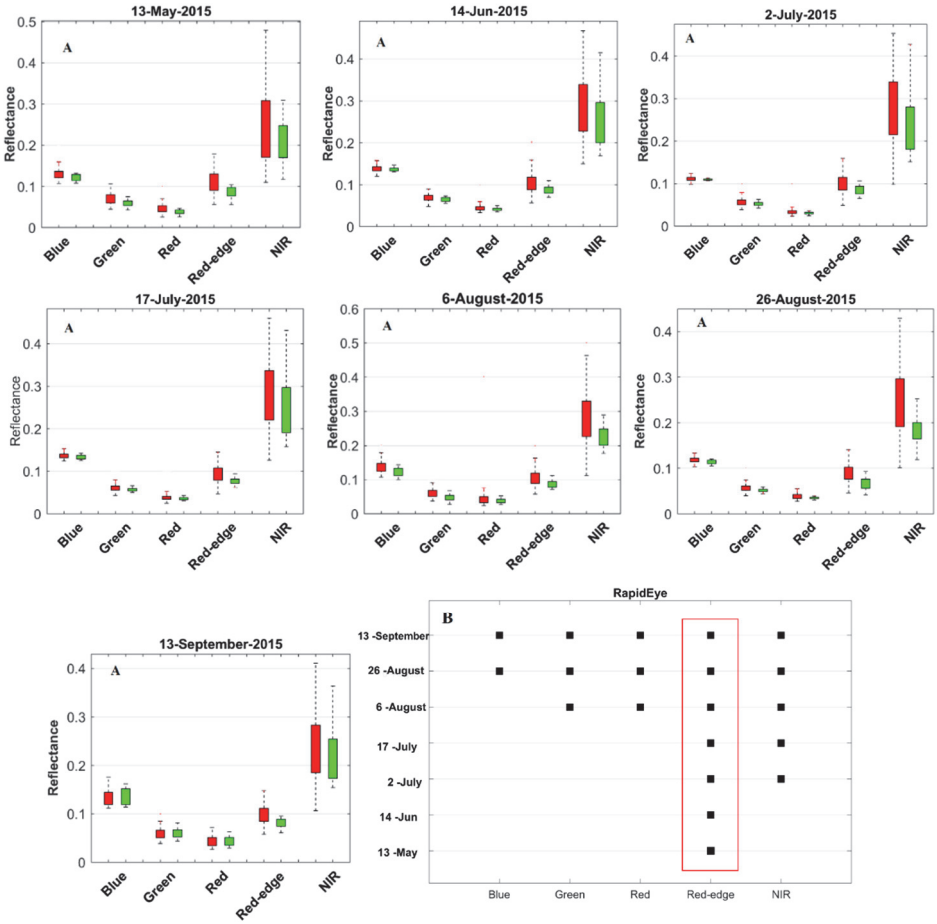

Figure 3. 4: (A) Temporal variation of canopy reflectance for healthy and infested plots in the Bavarian Forest National Park using RapidEye satellite data. Red and Green boxes represent infested and healthy plots, respectively (B) Unpaired t-test canopy reflectance between healthy and infested samples. Dark squares indicate spectral wavebands that were significantly different ($P \leq 0.05$). The red box shows the spectral region that was significantly different overall temporal data considered in this study

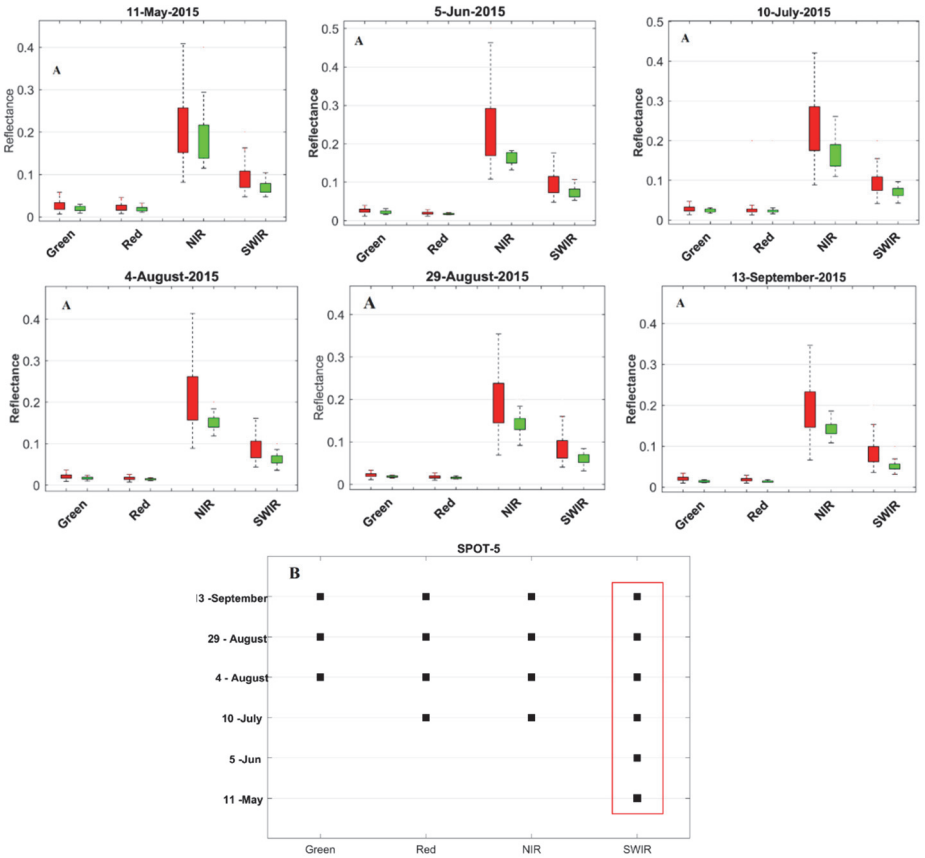

Figure 3. 5: (A) Temporal variation of reflectance spectra for healthy and infested plots in the Bavarian Forest National Park using SPOT-5 satellite data. Red and Green boxes represent infested and healthy plots, respectively (B) Unpaired t-test of canopy reflectance between healthy and infested samples. Dark squares indicate spectral wavebands that were significantly different ($P \leq 0.05$). The red box shows the spectral region that was significantly different overall temporal data considered in this study

Further analysis regarding the SVIs shows that there were a big overlap between healthy and infested plots in May for both RapidEye and SPOT-5. However, as infestation progresses, this variation becomes larger and more distinct (Figs. 3.6 and 3.7). For the RapidEye data, the difference between the healthy and infested plots by means of spectral vegetation indices values started to change from July 2nd using NDRE and NGRDI, while the other indices started to enlarge the variation at the later dates considered in this study (Fig. 3.6). A similar result was found using a reflectance difference index, as the red-edge and NIR bands became statistically different from May, becoming progressively more pronounced at later dates.

Using SPOT-5, the spectral vegetation indices calculated from the combination of SWIR and other spectral bands, such as DSWI, LWCI and NDWI, exhibited a larger difference between the healthy and infested plots at the earlier stage of infestation (Fig. 3.7). This is also confirmed in the result of the Student t-test analysis, where the SWIR was significantly different ($P < 0.05$) for all dates considered in this study.

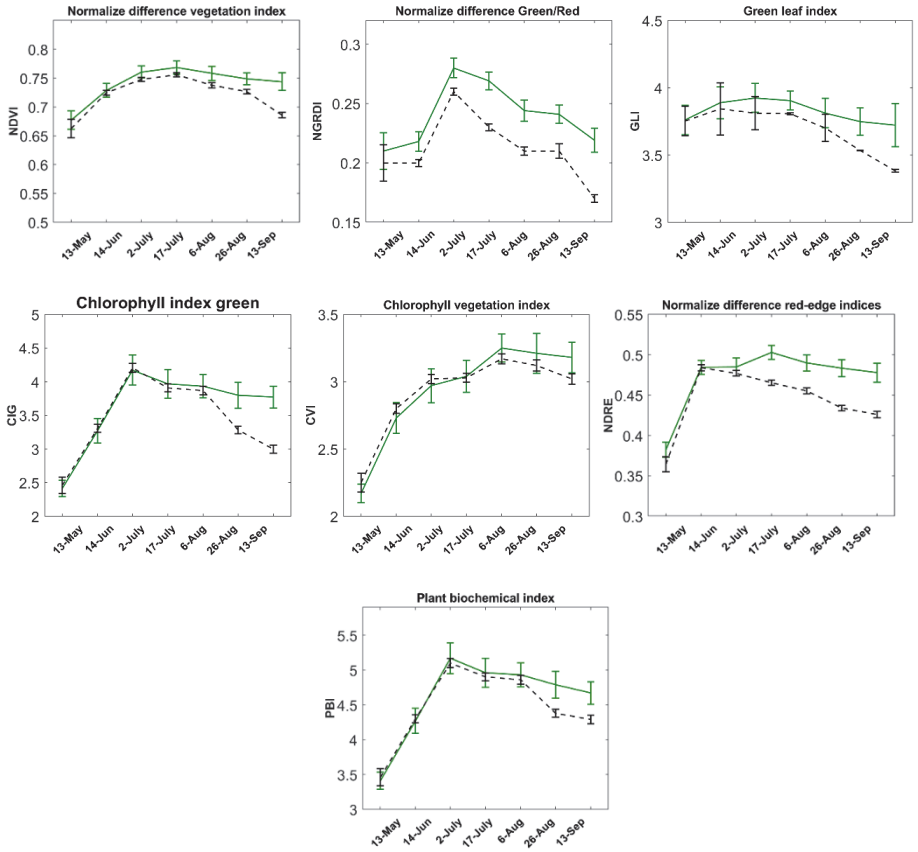

Figure 3. 6: Temporal variation of studied spectral vegetation indices for healthy and infested plots in the Bavarian Forest National Park using RapidEye satellite data. Green and black lines represent healthy and infested plots, respectively.

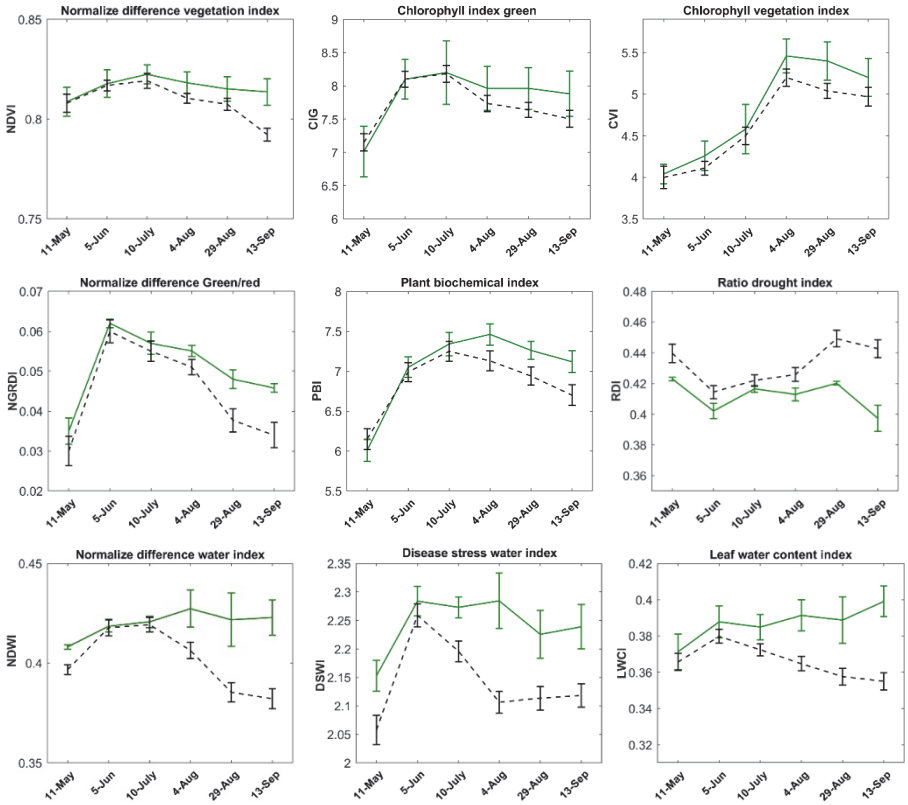

Figure 3. 7: Temporal variation of studied spectral vegetation indices for healthy and infested plots in the Bavarian Forest National Park using SPOT-5 satellite data. Green and black lines represent healthy and infested plots, respectively.

3.4 Discussion

In this study, we demonstrated that the measured leaf traits and leaf reflectance spectra from infested trees differed significantly ($p \leq 0.05$) from healthy ones during T1, T2, and T3 measurements (Figs. 3.2 and 3.3). Furthermore, the red-edge and SWIR spectral bands from RapidEye and SPOT-5 were influential in the separating between healthy and infested plots. Moreover, we found that red-edge and SWIR bands maintained their sensitivity for monitoring and detecting bark beetle infestation from the early to the advanced stages of infestation (Figs. 3.4 and 3.5).

The absolute difference in measured leaf traits between the healthy and infested trees increased from T1 to T3. In particular, stomatal conductance and chlorophyll fluorescence exhibited significant differences between the healthy and infested trees (Fig. 3.2). A possible explanation for this result might be that the initial impact of bark beetles on the infested trees shuts down the translocation of water in the tree due to the blue stain fungi introduced to the

trees during the infestation process. Because the hydraulic systems of plant and stomatal conductance are closely correlated with each other (Ewers et al., 2007), infested trees tend to close their stomata to preserve water. Therefore, the stomatal closure is the first sign of stress that induces the physiological response of infested trees to preserve water. It is well-known that physiological factors, such as plant water content, can control the temperature of plants through the stomatal transpiration process (Oerke et al., 2006). Moreover, the stomatal closure leads to a drop in photosynthesis activity due to the CO2 limitation, and, therefore, the chlorophyll fluorescence decreases (Flexas et al., 2004; Zweifel et al., 2009). Hence, the distinct variation observed in stomatal conductance between healthy and infested trees is attributed to differences in the measured leaf traits—in particular, leaf water content and chlorophyll fluorescence (Fig. 3.2). These findings match those observed in earlier studies that the initial impact of mountain pine beetles on infested trees causes a drop in the sapwood moisture and, hence, stomatal closure (Yamaoka et al., 1990). Likewise, our findings are in agreement with those of (Cheng et al., 2010), who studied the impact of a similar species, the mountain pine beetle (Dendroctonus spp) on the leaf water content of lodgepole pine using hyperspectral data.

Another important finding at the leaf level was that the difference in reflectance spectra between healthy and infested samples increased with the progression of infestation from T1 to T3 (Fig. 3.3). Noticeable changes were perceived at the visible wavelengths, in particular, from 680–790 nm and in the shortwave infrared wavelengths 1110 –1490 nm. The reflectance of the infested leaves in the visible spectrum from T1 was distinctly higher than that of the healthy ones. This result was likely due to having significantly ($p \leq 0.05$) lower chlorophyll in infested leaves than the healthy leaves from T1 to T3, causing lower absorption and higher scattering in the visible wavelengths (Fig. 3.2) (Carter and Knapp, 2001; Zhang et al., 2008). Furthermore, we reported that the reflectance of the healthy leaves was higher in the NIR region and lower in SWIR than that observed in the green attacked ones. Physically, the reflectance at the leaf level is a function of dry matter, water content, chlorophyll and internal leaf structure (leaf thickness) (Ali et al., 2016; Pu and Gong, 2011; Slaton et al., 2001). Hence, the observed reflectance pattern of the infested samples may have been due to the decrease in water content (Fig. 3.2) which is caused by bark beetle infestation.

Similarly, at the canopy level, both red-edge and SWIR bands from RapidEye and SPOT-5, respectively, showed a significant difference between the healthy and infested sites for all the dates considered in this study (Figs. 3.4 and 3.5). When implemented as a time series, they showed distinct temporal variation in reflectance and indices values between the healthy and infested sites, especially during the later stages of infestation. For example, the NDRE

calculated based on the combination of the red-edge and NIR bands is shown to be more sensitive than the other SVIs due to the stress induced by bark beetle infestation. The NDRE is known to detect stress or any forest health decrease earlier than NDVI (Eitel et al., 2011). In our study, the NDRE started to differentiate between the healthy and infested plots from 2nd July, while the other SVIs showed a difference almost one month later (Fig. 3.6). This result is in agreement with our earlier findings (Abdullah et al., 2018b) in which the NDRE calculated from the Sentinel-2 imagery possessed the most sensitive indices to differentiate between the healthy and green attacked sample plots. All the indices, such as DSWI, NDWI and LWCI, which employed the SWIR bands, were mostly sensitive to stress caused by variations in water content and were able to discriminate healthy from infested sites. For example, the DSWI and NDWI showed significant differences between the two groups on June 5th and July 10th, respectively. This is due to the significantly lower water content ($P < 0.05$) of the infested samples, and, therefore, their spectral reflectance in the SWIR region were highly affected (Figs. 3.2 and 3.5). This also accords with our earlier observation (Abdullah et al., 2018b), which showed the SWIR bands from Sentinel-2 and Landsat-8 were sensitive to detecting bark beetle infestation at the early phase of the attack. Likewise, Foster et al. (2017) identified the shortwave infrared region as key for detecting the early stages of beetle infestation in Engelmann spruce trees.

Based on the temporal variations in the canopy reflectance values and measured SVIs, here we identified for the first time in the European situation (and in contrast to earlier works in the US) that mid-June to the beginning of July is an appropriate time frame for the early stress detection induced by bark beetle infestation (Fig. 3.3, 3.4 and 3.5). This is the most initial period when the spectral difference between infested and healthy plots peaks. Although this time period may be slightly late for appropriate bark beetle management, our study has however shown the impending role of multispectral satellite (RapidEye and SPOT-5) data for monitoring and detecting forest stress induced by bark beetle attacks, and thus, has important implications for European field bark beetle management and future studies. However, further research is essential to explore the potential of other spaceborne sensors in detecting canopy reflectance changes due to bark beetle infestation during the early stage of an attack.

3.5 Conclusion

This study presents an innovative approach to investigate the temporal response of leaf properties and canopy reflectance spectra to European bark beetle infestation using a temporally dense time series of seven RapidEye senses and six SPOT-5 senses in parallel with the collection of field data at three consecutive repeated time measurements. Remote-sensing-based SVIs

complemented the ground data collected, providing additional information to help characterise the temporal response of infested trees through time and across the landscape. In conclusion, our key concept is that we show for the first time that:

- All measured leaf traits from infested trees differed significantly from healthy trees during Time-1, -2, and -3 measurements.
- The red-edge and SWIR were important spectral regions at both leaf and canopy levels for detecting subtle changes in Norway spruce trees due to bark beetle infestation.
- The earliest period at which the spectral difference between infested and healthy plots peaks is mid-June to the beginning of July.

We recommend that further studies should investigate different remote sensing datasets and monitor over a longer period to show the relationship between bark beetle infestation and the changes in biochemical variables and spectral reflectance more clearly.

Chapter 4: Sensitivity of Landsat-8 OLI and TIRS Data to Foliar Properties of Early Stage Bark Beetle (*Ips typographus*, L.) Infestation*

* This chapter is based on:

Abdullah, H., Darvishzadeh, R., Skidmore, A.K., and Heurich, M. ,2019. Sensitivity of Landsat-8 optical and thermal infrared data to foliar properties at early stage bark beetle (*Ips typographus*, L.) infestation. *Remote sensing*, 4, 398.

Abstract

In this study, the early stage of European spruce bark beetle (*Ips typographus, L.*) infestation (so-called green attack) is investigated using Landsat-8 optical and thermal data. We conducted an extensive field survey in June and the beginning of July 2016, to collect field data measurements from several infested and healthy trees in the Bavarian Forest National Park (BFNP), Germany. In total, 157 trees were selected, and leaf traits (i.e. stomatal conductance, chlorophyll fluorescence, and water content) were measured. Three Landsat-8 images from May, July, and August 2016 were studied, representing an early stage, advanced stage, and post-infestation, respectively. Spectral vegetation indices (SVIs) sensitive to the measured traits were calculated from the optical domain (VIS, NIR, and SWIR), and canopy surface temperature (CST) was calculated from the thermal infrared band using the mono-window algorithm. The leaf traits were used to examine the impact of bark beetle infestation on the infested trees and to explore the link between these traits and remote sensing data (CST and SVIs). The differences between healthy and infested samples regarding measured leaf traits were assessed using Student's t test. The relative importance of the CST and SVIs for estimating measured leaf traits was evaluated based on the variable importance in projection (VIP) obtained from the partial least squares regression (PLSR) analysis. A temporal comparison was then made for SVIs with a VIP > 1, including CST, using statistical significance tests. The clustering method using a principal components analysis (PCA) was used to examine visually how well the two groups of sample plots (healthy and infested) are separated in 2-D space based on principal component scores. Finally, linear regression (LR) was used to generate the leaf traits maps using the SVI that have highest VIP score and then used to produce a stress map for the study area. The results revealed that all measured leaf traits were significantly different ($p < 0.05$) between healthy versus infested samples. Moreover, the study showed that CST was superior to the SVIs in detecting subtle canopy changes due to bark beetle infestation for the three months considered in this study. The results showed that CST is an essential variable for estimating measured leaf traits with VIP > 1, improving the results of clustering when used with other SVIs. Likewise, the stress map produced by CST and leaf traits well presented the infestation areas at the green attacked stage. The new insight offered by this study is that the stress induced by the early stage of bark beetle infestation is more pronounced by Landsat-8 thermal bands than the SVIs calculated from its optical bands. The potential of CST in detecting the green attack stage would have positive implications for forest practice.

4.1 Introduction

Forests are important ecosystem with economical, social, and ecological values. The economic value of timber in a forest is typically threatened by natural disturbances such as fire, drought, wind, snow, and insect or disease outbreaks (Morris et al., 2017; Tchakerian and Coulson, 2011). In Europe, the European spruce bark beetle (*Ips typographus*, L.) is a common disturbance agent in forests dominated by Norway spruce (Picea abies) (Schelhaas et al., 2003). Bark beetle infestation extends across ten million hectares of trees in Europe. Much public money has been invested to compensate forest owners for their economic loss and for the cost of reforestation (Eidmann, 1992; Pasztor et al., 2014; Seidl et al., 2008). Besides the negative impact on timber production, bark beetles can also have a positive impact on the ecosystem by providing a suitable habitat in the form of opening forest canopy, increasing habitat heterogeneity and biodiversity, all of which enhance the survival of other species (Lehnert et al., 2013; Müller and Bütler, 2010).

The principle of bark beetles killing host trees has been well described in Wermelinger (2004). After a successful attack, the trees change colour in three stages; referred to as green, red, and grey attack, respectively (Raffa et al., 2015; Wermelinger, 2004). The green attack is the early stage of bark beetle infestation in which the colonised trees are yet to show distinct symptoms observable by the human eye (Niemann and Visintini, 2005a; Wulder et al., 2006c). A red-attack is evidence of the advanced stage of bark beetle infestation, in which the attacked trees develop stress symptoms involving turning the colour of their needles from green to yellow to red-brown. Subsequently, the needles fall from the infested trees, and only the grey bark remains; hence, this stage is termed 'grey attack' (Coulson et al., 1985).

Detection of bark beetle infestation at the green attack stage means locating infested trees at the stage where the beetle larvae are still within the tree. Effective measures to manage the beetles can then be undertaken. This will ultimately help reduce the number of infested trees, lessening the economic loss. Visual inspections during field surveys and pheromone traps have traditionally been used to detect bark beetle infestations in Norway's spruce forests. However, these methods are subjective, very laborious, costly, and only able to cover relatively small areas. Remote sensing presents an alternative to existing methods for monitoring and detecting infestations on large spatial scales (Wulder et al., 2006a). To date, remote sensing data have been successfully used to detect the advanced stages (red and grey attacks) of bark beetle infestation.

For example, many studies have employed spectral vegetation indices (SVIs) from low-to-medium resolution satellite data to detect the advanced stages of

bark beetle infestation (red and grey attack) (Filchev, 2012a; Franklin et al., 2003b; Hais et al., 2009; Havašová et al., 2015; Meddens et al., 2013; Wulder et al., 2006c); however, to date, the identification of European spruce bark beetle (*Ips typographus*, L.) green attack has been less satisfactory due to many biological, technical and logistical constraints/limitations. These issues include the flight activity of the bark beetle, the time duration required for the colonisation process and the period when the infested trees have yet to show distinct symptoms capable of being observed by human eye. Hence, it is important to consider biological as well as logistical factors when using remotely sensed data to detect bark beetle green attack (Wulder et al., 2009)

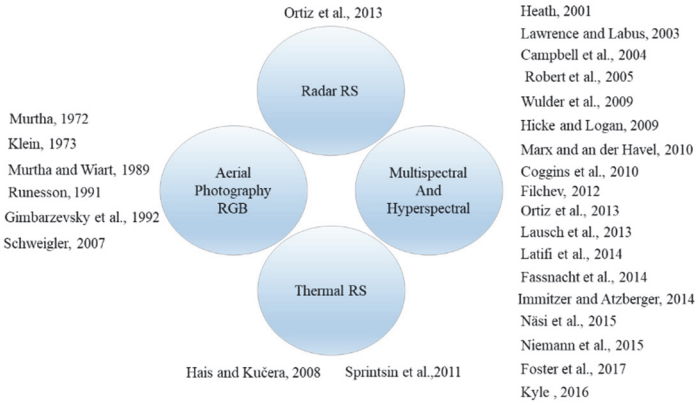

Figure 4. 1: Studies that have used remote sensing data to attempt detecting bark beetle infestation at the green attack stage.

There are very few studies that have paid particular attention to investigating the impact of bark beetle green attack on biochemical properties and physiological status of infested trees. However, they studied different beetle (mountain pine beetle) and tree (lodgepole pine) species. For example, Yamaoka et al. (1990) documented a decline in sapwood moisture content resulting from mountain pine beetle attack. Likewise, Cheng et al. (2010) revealed water deficit and changes in chlorophyll content of artificially stressed pine trees by mountain pine beetle. They also identified the wavelength range between 950 nm and 1390 nm as a good spectral region able to separate healthy from green attacked trees. In general, moisture stress in vegetation may result in non-visual symptoms that are detectable with remote sensing data, particularly in the shortwave and thermal infrared regions, where water absorption features exist (Berni et al., 2009; Buitrago Acevedo et al., 2017; Jang et al., 2006; Sepulcre-Cantó et al., 2006). However, the majority of the studies on bark beetle (either mountain pine beetle or spruce bark beetle) green attack detection with remotely sensed data have mainly utilised optical remote sensing data (Fig. 4.1). There are few published examples of studies which investigate the use of temperature, and none which focus on the impact

of European spruce bark beetle infestation on biochemical properties and physiological status of infested trees in the TIR domain. To our knowledge, only one study, by Hais and Kučera (2008), has investigated the impact of bark beetle (*Ips typographus*, L.) infestation at the advanced stages (Gray attack) on surface temperature using thermal infrared (TIR) data. Their study examined the effect of spruce bark beetle infestation and clear-cutting on surface temperature between 1987 and 2002 in the central part of Sumava National Park in the Czech Republic. Further, Sprintsin et al. (2011) used surface temperature calculated from the Landsat 7 ETM+ to detect an early stage of mountain pine beetle infestation in British Columbia. Although Sprintsin et al. (2011) suggested that temperature condition indices (TCI) used in their study have the potential to differentiate between healthy and green attacked pine they could not validate their results due to lack of ground reference data for their green attacked study areas.

Numerous studies have shown the significant potential of TIR data to elucidate plant biophysical and biochemical properties (Buitrago et al., 2016; Neinavaz et al., 2016; Ullah et al., 2014). For example, the primary absorption feature that is associated with leaf water content can be observed in both shortwave and thermal infrared regions (Table 4.1) (Fabre et al., 2011; Kümmerlen et al., 1999). As such, several studies have shown that TIR data have great potential to detect plant diseases and pathogens before the plants develop visual stress symptoms (Aldea et al., 2005; Moller et al., 2007; Ni et al., 2015; Oerke et al., 2006; Xu et al., 2006). Moreover, retrieving the canopy surface temperature (CST) from TIR data is widely used to track vegetation water status (Hunt and Rock, 1989). The surface temperature is interrelated with plant functions, such as evapotranspiration which is controlled by stomatal conductance. (Kim et al., 2016; Xu et al., 2006). Therefore, alterations in these processes will lead to changes in the air and the surface temperature of leaves (Doughty et al., 2011; Gersony et al., 2016; Stoner and Miller, 1975; Vanderhoof et al., 2013). Furthermore, physiological studies have shown that the reduction of leaf water content disturbs stomatal conductance and leads to an increase in leaf surface temperature (Pierce and Congalton, 1988; Pierce et al., 1990; Schulze and Hall, 1982).

In addition to water content and stomatal conductance, recent studies have shown that there is a strong relationship between canopy surface temperature and photosynthetic activity, which can be measured by chlorophyll fluorescence (Ni et al., 2015). Chlorophyll fluorescence has been found to be a reliable indicator for examining the impact of different stressors (drought, insect infestation, and pathogens) on plant photosynthesis and the physiological state of vegetation (Méthy et al., 1994; Porcar-Castell et al., 2014). When leaf transpiration rate decreases (i.e., by closing stomata) both chlorophyll fluorescence and photosynthetic activity will decrease, while heat

dissipation will increase (McFarlane et al., 1980). Hence, chlorophyll fluorescence has been used as a reliable indicator for monitoring plant water stress (Campbell et al., 2007; Yamaoka et al., 1990).

In this study, for the first time, we sought to explore and compare the potential of both optical and thermal infrared (TIR) data from Landsat-8 for detection of pre-visual symptoms induced by European spruce bark beetle green attack. We studied the impact of spruce bark beetle green attack on leaf properties (foliar stomatal conductance, chlorophyll fluorescence, and water content). To do this, canopy surface temperature (CST) and spectral vegetation indices (SVIs) were calculated using three Landsat-8 images for May, July, and August 2016, as these months, represent the time of early, advanced, and after spruce bark beetle green infestation, respectively. Our study benefits from valuable in situ measurements of leaf traits at the time of infestation that have been used to explain the impact of bark beetle attacks on Landsat 8 optical and TIR data. Our objectives were as follow: (i) to assess the potential of CST and SVIs calculated from Landsat 8 data to differentiate between healthy and infested sample groups; (ii) to study the temporal variation of CST and SVIs under spruce bark beetle infestation; and (iii) to evaluate the utility of CST and a number of SVIs to estimate measured leaf traits within infested and healthy samples.

4.2 Material and Methods

4.2.1 Study site and in situ data collection

The field campaign was conducted during June and July 2016 in the Bavarian Forest National Park (BFNP), which is a 24.222 ha forest located in south-eastern Germany along the border with the Czech Republic, between 13°12'9" E (longitude) and 49°3'19" N (latitude) (Fig. 4.2). The BFNP was established in 1970, and significantly extended in 1997. Depending on the elevation within the BFNP, which ranges from 600 m to 1453 m, the mean annual temperature fluctuates between 3.5°C and 9°C, and the total annual precipitation varies from 900 mm to 1800 mm (Bässler et al., 2008a; Heurich et al., 2010a). The first bark beetle infestations began in 1984 and, to date, more than 7000 ha have been affected. The strict non-intervention policy of the National Park offers the possibility of studying bark beetle dynamics without human interference (Cailleret et al., 2014b; Heurich et al., 2010a).

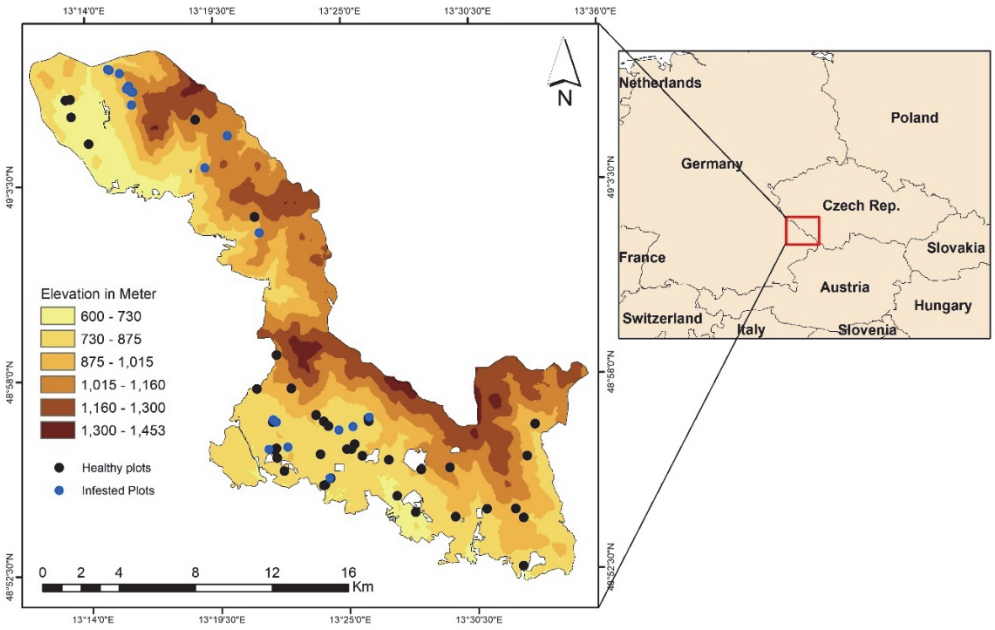

Figure 4. 2: The location of Bavarian Forest National Park in Central Europe.

We sampled trees from healthy stands and stands with trees freshly infested by the bark beetle. For the healthy stands, we randomly selected plots (30 m × 30 m) from all over the national park. To select the green attacked trees, we conducted an extensive field survey to search for dry brown powder around the trees. Care was taken to only consider those plots with all trees freshly infested or which were dominated (80%) by freshly green-attack trees. In this way, we were assured that the extracted remote sensing signature from these plots would not have mixed effects from the attacked trees of previous years. In total, 40 healthy and 21 infested plots were sampled. The centre of each plot was measured using Differential Global Positioning System (DGPS) Leica GPS 1200 (Leica Geosystems AG, Heerbrugg, Switzerland) with an accuracy of better than 1 m after post-processing (Abdullah et al., 2018b). Each of 61 selected plots measured 30 × 30 m to encapsulate the spatial resolution of a Landsat-8 data, which allows for a 30 m radius buffer zone around the 'central pixel' location for uncertainty in spatial registration of image pixels. By doing this we minimized the potentially confounding influence (mixed pixels) of green attacked Norway spruce trees.

From each plot, three to five trees were selected as representative for the plot. Because the height of Norway spruce trees reaches 25 to 30 m, we used a crossbow to shoot an arrow with a fishing line attached to a branch with sunlit leaves. The fishing line was used to feed a rope over the targeted branch from the upper canopy. Once the rope was in place, the branch was pulled down

gently until it broke off. Full details regarding the use of the crossbow can be found in Ali et al. (2016) .n. On average two to three branches, exposed to sunlight, were taken from the upper part of each tree. Next, needle samples were taken from the collected branches to measures leaf traits.

4.2.2 Measurement of leaf properties

In this study, a steady-state instrument (SC-1 Leaf Porometer) was used to measure the needle stomatal conductance. This instrument computes stomatal conductance using a leaf clip chamber that can monitor the relative humidity (RH%) released from the leaf stomata. To measure the stomata, a number of needles were gently attached to cover the chamber port. Since stomata are sensitive to environmental conditions and physical stress, all the measurements were taken under similar environmental conditions (clear sky, between 11 am to 3 pm local time). An average of three to four measurements was taken for each sampled tree within each plot (SC-1 Operator's Manual, 2016).

Immediately after the stomata measurement, a chlorophyll content meter CCM-330 was used to measure the chlorophyll fluorescence ratio (CFR). This instrument uses the emission ratio of fluorescence at both the red (700 nm) and the far red (735 nm) part of the electromagnetic spectrum, as proposed by Gitelson et al. (1999). On average ten readings were taken per sample from each branch. Then, the leaf water content (CW, mg/cm^2) was computed using fresh and dry weight. To do this, three grams of the freshly harvested needles were weighed from each sample. A portable leaf area meter (AM-350) was used to measure the total needles' surface area for each of the three grams considered. Norway spruce needles are cylindrical and, therefore, this surface area was multiplied by a universal conversion factor of 2.57 (Waring, 1983). Then, to acquire the hemispherical-surface projection of the sample surface needles, the total area obtained was divided by 2. Finally, the needle samples were oven dried for 72 hours at 75 ºC, and the dried weight of each sample was measured. The leaf water content (Cw) was computed using the following equation (Colombo et al., 2008):

$$Cw = \frac{Wf - Wd}{A}$$

Where Wf and Wd are the fresh and dry weight, respectively, and A is the sample leaf area.

4.2.3 Landsat-8 imagery and pre-processing

Cloud-free Landsat-8 images were obtained from the USGS Global Visualization Viewer (http://glovis.usgs.gov/) for the months May, July and August 2016. According to the Bavarian Forest National Park authorities, the bark beetles of

the infestation in 2016 had started to swarm on May 10, 2016. Therefore, the May image was designated as the early stage of bark beetle infestation.

Landsat-8 has two sensors called OLI and TIRS. The OLI sensor collects data from nine spectral bands ranging from 0.43 – 2.29 nm with a 30 m spatial resolution, while the TIRS sensor collects data from two thermal bands ranging from 10.6 – 12.5 nm with a 100 m spatial resolution resampled to 30 m in the delivered data product (Table 4.1).

For both the OLI and the TIRS sensor, radiance values were calculated, using the coefficient supplied by USGS. Secondly, for OLI data, a radiometric calibration was applied to convert the radiance value to Top-of-Atmosphere (TOA) reflectance. Then, MODTRAN4-based atmospheric correction software (FLAASH) was used to convert the TOA Reflectance to surface reflectance (Adler-Golden et al., 1999). Full details regarding the use of FLAASH can be found in (Module). Finally, the reflectance values of the infested and healthy plots were extracted from the Landsat-8 scenes and were used for further analysis.

4.2.3.1 Spectral vegetation indices

Several spectral vegetation indices exist in the literature that are used for estimation of vegetation biochemical properties (Collins and Woodcock, 1996; Eitel et al., 2006). In this study, spectral vegetation indices linked to measured leaf traits were calculated from the spectral reflectance data collected from the Landsat OLI sensor. In previous work, the selected SVIs have shown sensitivity to stress-induced variations in chlorophyll and also water content, which are all important indicators of tree health. This sensitivity could potentially be used to assess stomatal closure and tree water stress due to insect infestation. The mathematical transformation for computing these vegetation indices is given in (Table 4.2).

Table 4.1: The Landsat-8 sensors, the operational land imager (OLI), and the thermal infrared sensor (TIRS) spectral bands and their spatial resolution.

Bands	Wavelength (micrometers)	Resoultion (meters)
Band-1 (Coastal aerosol)	0.43–0.45	30
Band-2 (Blue)	0.45–0.51	30
Band-3 (Green)	0.53–0.59	30
Band-4 (Red)	0.64–0.67	30
Band-5 (Near Infrared –NIR)	0.85–0.88	30
Band-6 (SWIR-1)	1.57–1.65	30
Band-7 (SWIR-2)	2.11–2.29	30
Band-9 (Panchromatic)	0.50–0.68	15
Band-10 (Cirrus)	1.36–1.38	30
Band-11 (Thermal infrared-TIRS1)	10.60–11.19	100 (resampled to 30)
Band-12 (Thermal infrared-TIRS2)	11.50–12.51	100 (resampled to 30)

Table 4.2: List of spectral vegetation indices calculated from Landsat-8 optical bands.

Index	Formula	Full name	Reference
Cigreen	(NIR/Green)-1	Chlorophyll index green	(Hunt et al., 2011)
CVI	NIR × (Red / Green2)	Chlorophyll vegetation index	(Hunt et al., 2011)
CI	(Red – Blue) / Red	Coloration index	(Escadafal et al., 1994b)
GVI	NIR - Green	Green difference vegetation index	(Tucker et al., 1979)
DVI	2.4 × (NIR – Red)	Difference vegetation index	(Bannari et al., 1995)
GVMI	[(NIR+0.1)-(SWIR+0.02)]/[(NIR+0.1)+(SWIR+0.02)]	Global vegetation moisture index	(Ceccato et al., 2002)
GARI	[NIR-(Green-(Blue-Red))]/[NIR-(Green+(Blue-Red))]	Green atmospherically resistant vegetation index	(Gitelson et al., 1996)
GLI	[2×(Green-Red-Blue)]/[2×(Green+Red+Blue)]	Green leaf index	(Gobron et al., 2000)
LWCI	[log(1-(NIR-SWIR))]/[log(1-(NIR+SWIR))]	Leaf water content index	(Cohen, 1991)
NLI	(NIR2 – Red) /(NIR2 + Red)	Nonlinear vegetation index	(Goel and Qin, 1994)
PVR	(Green – Red) / (Green + Red)	Normalized Difference Photosynthetic vigour ratio	(Metternicht, 2003)
SIWSI	(NIR-SWIR1) / (NIR+SWIR1)	Normalized Difference 860/1640	(Fensholt and Sandholt, 2003)
BGI	Costal / Green	Blue-green pigment index	This study
RDI	SWIR2 / NIR	Ratio Drought Index	(Pinder and McLeod, 1999)
NDVI	(NIR – Red) /(NIR + Red)	Normalized difference vegetation index	(Tucker, 1979)
TNDVI	Log [(NIR-Red)/NIR+Red) × 0.5]	Transformed NDVI	(Bannari et al., 2002)

4.2.3.2 Canopy surface temperature (CST)

The Landsat-8 TIR sensor provides data from two bands (band 10 and band 11) in the thermal domain. However, band 11 is no longer operational for quantitative analysis, as reported by USGS (https://landsat.usgs.gov/using-usgs-landsat-8-product). Therefore, in our study, band 10 with wavelengths ranging from 10.60 to 11.19 nm was utilised to retrieve canopy surface temperature CST.

To minimise and reduce the effects of different climatic conditions on CST retrieval, the mono-window algorithm, proposed by Qin et al. (2001), was applied. The core of this method is the equation transferring thermal radiance, which converts digital satellite values to a radiometric value (Markham and Barker, 1986). To apply this algorithm, a number of parameters such as emissivity, air transmittance, and effective mean atmospheric temperature are required. The air transmittance and mean atmospheric temperature are estimated using another two additional parameters, namely: air surface temperature and water vapour content. Water vapour was calculated using relative humidity ratio and air surface temperature (Liu and Zhang, 2011). The following equations summarise the steps required when using the Mono-Window algorithm for retrieving CST.

First, digital values (DVs) of band 10 are converted to TOA spectral radiance using the equation:

$$Ly = ML \times Qcal + AL \quad (4.1)$$

where Ly is TOA spectral radiance received by the sensor measured in mW cm-2 sr-1 μm-1; ML is the band specific multiplicative rescaling factor for band 10 equal to 0.0003342; Qcal is the actual band 10 digital number (DN), and AL is a band-specific additive rescaling factor equaling 0.1. This information was obtained from the metadata file and USGS Landsat-8 product use documentation (https://landsat.usgs.gov/using-usgs-landsat-8-product).
The next step was to convert spectral radiance to satellite brightness temperature (blackbody temperatures) by expressing Planck´s function. The equation used was proposed by Markham and Barker (1986) :

$$Bt = [K2 / \log(1+K1 /Ly)] - 273.15 \quad (4.2)$$

where Bt is the satellite brightness temperature in Celsius, K1 and K2 are calibration constants (774.89 and 1321.07, respectively) of Landsat-8 representing at-sensor spectral radiances of Landsat TM Band 10, and Ly is the satellite spectral radiance retrieved from Equation 1. The brightness temperature calculated with this second equation is called the top of the

atmospheric temperature (Zhang et al., 2006). The following additional parameters were measured: :

1.Land surface emissivity

The brightness temperature derived from Equation 2 refers to a black body target. Since the target bodies on land surfaces are not perfect black bodies, the thermal emissivity of the land surface must be retrieved from the area being studied (Gartland, 2012). Several factors such as plant chemical composition and surface roughness affect the estimation of canopy surface emissivity from remote sensing data (Snyder et al., 1998). Several methods have been proposed to retrieve emissivity from remote sensing data, such as image classification and the NDVI-based threshold approach. Image classification based on Landsat imagery is not an appropriate method for the estimation of land surface emissivity due to the spatial resolution, with one pixel possibly comprising different land cover classes (Dozier and Warren, 1982). As a result, the NDVI-based threshold is a more appropriate approach for the calculation of ground emissivity using Landsat imagery (Vlassova et al., 2014). The NDVI-based approach was first proposed by Van de Griend and Owe (1993) and was later modified by Valor and Caselles (1996). In this study, we followed the approach by Valor and Caselles (1996) using NDVITHM to calculate emissivity for the study area as follows:

$$\varepsilon = \varepsilon v \times Pv + (1 - Pv) + 4 < d\varepsilon > Pv \times (1 - Pv) \quad (4.3)$$

where ε is ground emissivity; εv is emissivity for pure vegetation covered area; dε is the constant value of topography factor (0.01), and Pv is the proportion of vegetation, obtained from NDVI, based on the following equation proposed by Carlson and Ripley (1997):

$$Pv = (NDVI - NDVIg) / (NDVIv - NDVIg) \quad (4.4)$$

where Pv is the proportion of vegetation for each pixel; NDVIg is the NDVI value in bare soil (NDVI < 0.2); and NDVIv is the NDVI value for purely vegetation-covered areas (NDVI > 0.5). Further details regarding emissivity based NDVI estimation can be found in (Sobrino et al., 2008).

2. *Estimation of atmospheric transmittance*

The atmospheric transmittance was estimated using water vapour content based on the formula by Qin et al. (2001):

$$Wc = 0.0981 \times [10 \times 0.6108 \times \exp((17.27 \times (T0)) \times RH] + 0.1697 \quad (4.5)$$

where Wc is the water vapour content in g/cm2, T0 is the near-surface or air temperature in degrees Celsius and RH it is the relative humidity.
Both near-surface temperature and relative humidity (RH) data were obtained from climate-station Waldhäuser located in the BFNP at 950 m above sea-level on a south-west slope.
Based on the air surface temperature and humidity ratio data from the Waldhäuser station, the water vapour content ranged between 1.6 and 3.0 g/cm^2 with our data being captured in the summertime. Thus, the following formula was used to estimate atmospheric transmittance:

$$\tau = 1.031412 - 0.11536 \times Wc \quad (4.6)$$

where τ is the atmospheric transmittance, and Wc is the estimated water vapour content obtained from the previous equation.

3. Mean atmospheric temperature

The final parameter required for the calculation of CST using the mono-window algorithm is mean atmospheric temperature. The Landsat data were captured in May, July and August, 2016., which meant summer conditions. Therefore, the following formula was used to estimate the mean atmospheric temperature (Qin et al., 2001; Sun et al., 2010) :

$$\tau a = [16.0110 + 0.92621 \times (T0)]\text{-}273.15 \quad (4.7)$$

where Ta is the mean atmospheric temperature in degrees Celsius, and T0 is the surface air temperature in Kelvin. Data on air temperature were obtained from the Waldhäuser weather station.
Finally, the mono-window algorithm was employed to retrieve canopy surface temperature over the study area, as follows:

$$CST = (A \times (1 - C - D) + [B \times (1 - C - D) + C+D] \times Bt - D \times Ta) / C \quad (4.8)$$

where CST is the canopy surface temperature in degrees Celsius, Bt which is the effective temperature viewed by the satellite under an assumption of unity emissivity in degrees Celsius, and Ta is the mean atmospheric temperature in degrees Celsius. In addition, the parameters A and B have standard values proposed by Qin et al. (2001) which are -67.355351 and 0.458606, respectively, while the parameters C and D are obtained using the following formulae:

$$C = \varepsilon \times \tau \quad (4.9)$$

and

$$D = (1 - \tau) \times [1 + (1 - \varepsilon) \times \tau] \quad (4.10)$$

where ε is emissivity estimated from Eq.3, and τ is atmospheric transmittance.

4.2.4 Statistical Analysis

To fulfil the objective of this research, three statistical analyses were employed, namely, statistical significance test (Student *t*-tests), partial least squares regression (PLSR), and principal components analysis (PCA).The Student *t*-tests were used to assess the impact of bark beetle infestation at the green attack stage on the measured leaf traits (foliar stomatal conductance, chlorophyll fluorescence, and water content) and remote sensing data (SVIs and CST). Next, to identify the key SVIs for estimating the studied leaf traits (foliar stomatal conductance, chlorophyll fluorescence, and water content) Variable Importance in Projection (VIP) was calculated from the PLSR analysis. The VIP scores are useful in understanding X space predictor variables (SVIs & CST) that best explain dependent (Y) variables (leaf traits). The 'VIP method selects those X variables that contribute most to the underlying variation in the X variables. This includes the variation not related to y, but describing interferences, that is so-called orthogonal variation' (Farrés et al., 2015). To achieve this, PLSR analysis was employed. The PLSR 'is a regression method that takes into account both the variance of the dependent and the predictor variables. It specifies a linear relationship between a set of dependent (Y) variables (leaf traits) and a set of predictor (X) variables' (CST and SVIs) (Wold et al., 2001). The PLSR was used for the Landsat-8 image captured in July 2016, as it matched the time of field data collection. Three independent PLSR models were built for each leaf trait separately as well as for each sample group (green attacked and healthy samples). In general, a VIP score > 1 unit indicates that the contribution of the variable (CST or SVI) was significant, and the greater the VIP value, the larger is the contribution of the variable to the model (Chong and Jun, 2005).

Moreover, to investigate the potential of separating healthy plots from infested ones in a 2-D space, the clustering method using PCA was employed. In other words, PCA was used to determine the importance of each SVI for discriminating between healthy and infested plots during all three months considered in this study. PCA is an unsupervised technique and has been successfully used in many remote sensing studies as a data reduction approach (Maitra and Yan, 2008). The mean centring and unit variance producer were used to preprocess the data. The SVIs (those having a VIP score higher than one for both healthy and infested sample plots) were treated as independent variables, and for each image date considered in this study, two PCA models were built as follows: (a) a PCA model including all selected SVIs and CST (VIP > 1); (b) a PCA model including only SVIs. This step is essential because it

allows us to understand and identify the most effective SVIs in terms of making a significant contribution to discriminating healthy from freshly infested spruce plots (Figure 4.3).

From the selected SVIs, those that have VIP > 1, a box plot technique was used to explore the temporal variation between healthy and infested plots for all three months considered in this study. The values of SVIs and CST were normalized between 0 and 1 using the MinMax normalisation method.

4.3 Mapping bark beetle green attack infestation

To generate the map of bark infestation, we considered the SVI with the highest VIP score as the most important variable to estimate studied leaf traits. Linear regression was used to generate maps of the measured leaf traits (foliar stomatal conductance, chlorophyll fluorescence, and water content), and the generated maps of leaf traits were used as a proxy to produce a map of bark beetle green attack. To do this, we classified the produced maps using the range of the leaf traits from the field (Table 4.3). The final map contains three classes corresponding to the stress intensity in each trait. Following this, to validate the generated map of infestation, ancillary vector-based reference data of the green attacked areas in 2016 were obtained from the Bavarian Forest National Park (BFNP) administration (Abdullah et al., 2018b). The flight on 11 Jun 2017 documented new dead wood (grey attack stage) from the previous year 2016, with reference data collected from airborne colour-infrared (VIS and NIR) aerial images (CIR) with 0.1 m spatial resolution. Full details about the processing and interpretation of aerial photography in the BFNP can be found (Heurich et al., 2009; Lausch et al., 2013a). The reference data (ground truth) were in the form of polygons and were rasterised into 30 m $\times$ 30 m grid cells to match with the produced maps from Landsat-8 SVI. In total, 417 pixels were used as the ground truth data. Furthermore, land cover data obtained from the national park administration were used to mask out non-spruce stands and young stands. This is because bark beetles only infest old and mature Norway spruce (*Picea abies* (L.) Karst). The masked land cover was overlaid on the classified leaf traits maps in this study (Fig. 4.3). Finally, the total number of pixels (ground truth) located within each (stress class) were extracted and calculated.

Table 4. 3: Stress level categories classified using the range of the leaf traits (leaf water content, stomatal conductance, and chlorophyll fluorescence) from the field, in the Bavarian Forest National Park, July 2016.

	Severely stressed	**Moderately stressed**	**Healthy**
Leaf water content (g/cm^2)	< 0.0135	0.135 – 0.0145	> 0.0145
Stomatal conductance (mmol/m^{2}s)	< 103	103 - 120	> 120
Chlorophyll fluorescence ratio	< 1.17	1.17 – 1.25	> 1.25

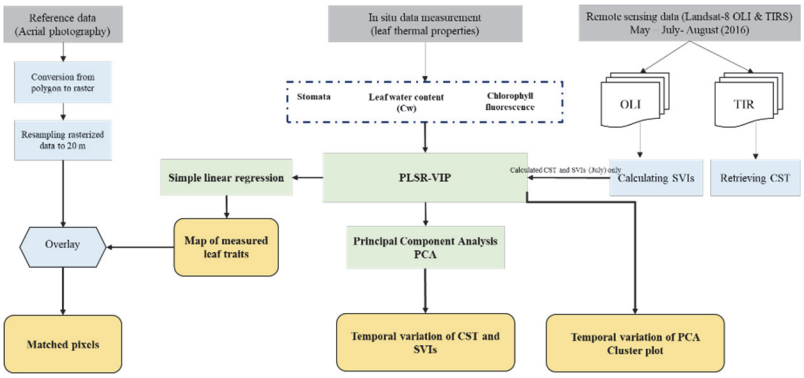

Figure 4. 3: The framework of the research methodology.

4.3 Results

4.3.1 The importance of CST versus SVIs to estimate measured leaf properties

Infestation by bark beetle caused substantial changes in all studied leaf traits during the green attack stage. The result of the Student's *t*-test demonstrated a significant difference ($p < 0.05$) between healthy and infested leaves for all the studied leaf traits (chlorophyll fluorescence, leaf water content, and stomatal conductance) (Fig. 4.4). Furthermore, as can be seen from figure 4.5, the VIP scores show that CST significantly contributes to the estimation of studied leaf traits (chlorophyll fluorescence, water content, and stomatal conductance) for both healthy and infested plots. However, among the SVIs only 5 out of 23 had a VIP score above one for both healthy and infested sample plots; these five indices are CIgreen, CVI, CI, NLI, and BGI (Fig. 4.5). The single bands of Landsat-8 showed the lowest VIP score for all measured leaf traits.

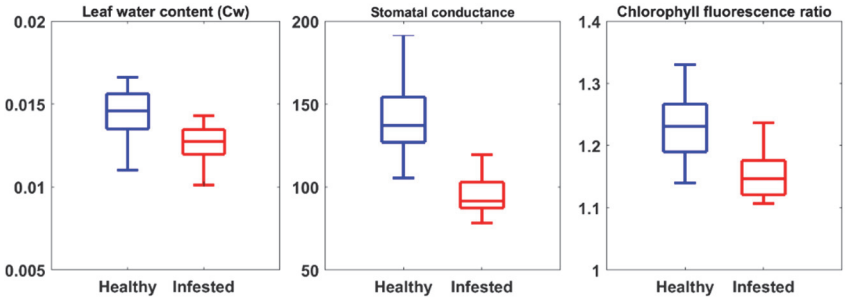

Figure 4. 4: Distribution of measured leaf traits for healthy and infested needles, in the Bavarian Forest National Park, July 2016. There is a significant difference ($p < 0.05$) in all measured leaf traits between healthy and infested samples.

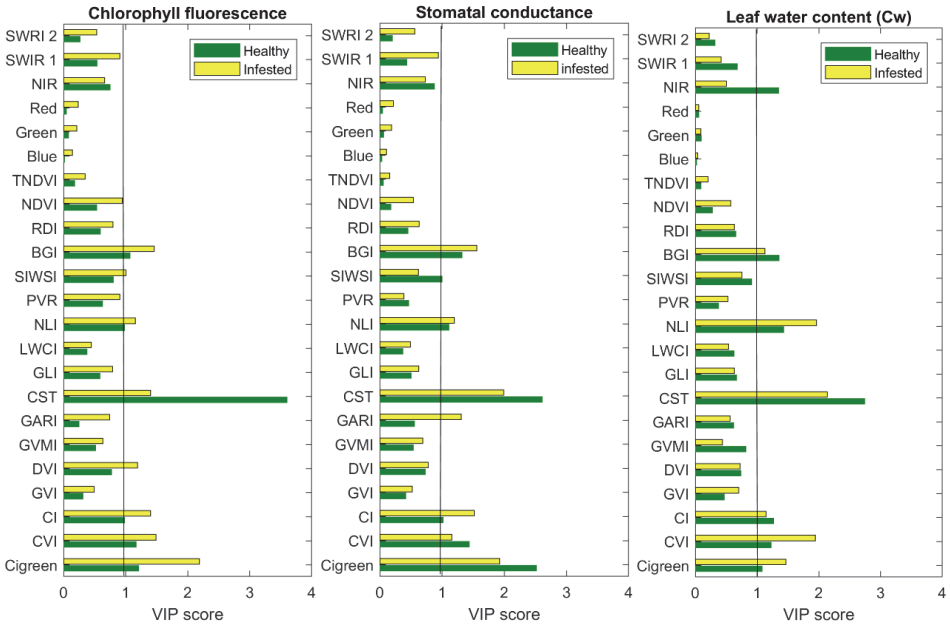

Figure 4. 5: PLSR variable importance in the projection (VIP) for predictor (CST and SVIs) and response variables (measured leaf traits) in the Bavarian Forest National Park, July 2016. (vertical black line represents VIP ≥ 1)

4.3.2 Temporal response of CST and SVIs under spruces bark beetle infestation

To assess the temporal variation of the CST and those SVIs that obtained a VIP score > 1, we studied the boxplots for all three months considered in this study. Figure 4.6 shows a comparative time-series of CST and SVIs for healthy and infested sample plots. As can be seen from this figure, the CST in infested and healthy plots differ from the SVIs by exhibiting increased temperature from the beginning of the infestation in May, whereas almost all other indices show

no differences between healthy and infested plots. Similarly, in July, when the infestation is still at its early stage (green attack), CST shows high potential for discriminating between healthy and infested sample plots. However, in August, when the infested plots entered into the advanced stage (in which the infested trees developed stress symptoms by turning their needles' colour from green to yellow to red-brown and can be detected by the human eye), CST as well as CIgreen, NLI, and BGI are significantly different ($p < 0.05$) between healthy and infested plots.

The selected SVIs, which had a VIP value > 1 (CST, CIgreen, CVI, CI, NLI, and BGI) have been used to build the PCA model. As shown in Figure 4.7, in May, when the infestation is in its early stage, there is an apparent overlap and mixed scattering between healthy and infested sample plots when SVIs were applied in the model. However, in July and August, when CST is included into the model, the majority of healthy plots tend to be on the negative side of PC1, while the infested plots are relatively scattered on the positive side of PC1. In general, we observed distinct improvement to differentiate between healthy and infested plots when both CST and SVIs were used to build the PCA model.

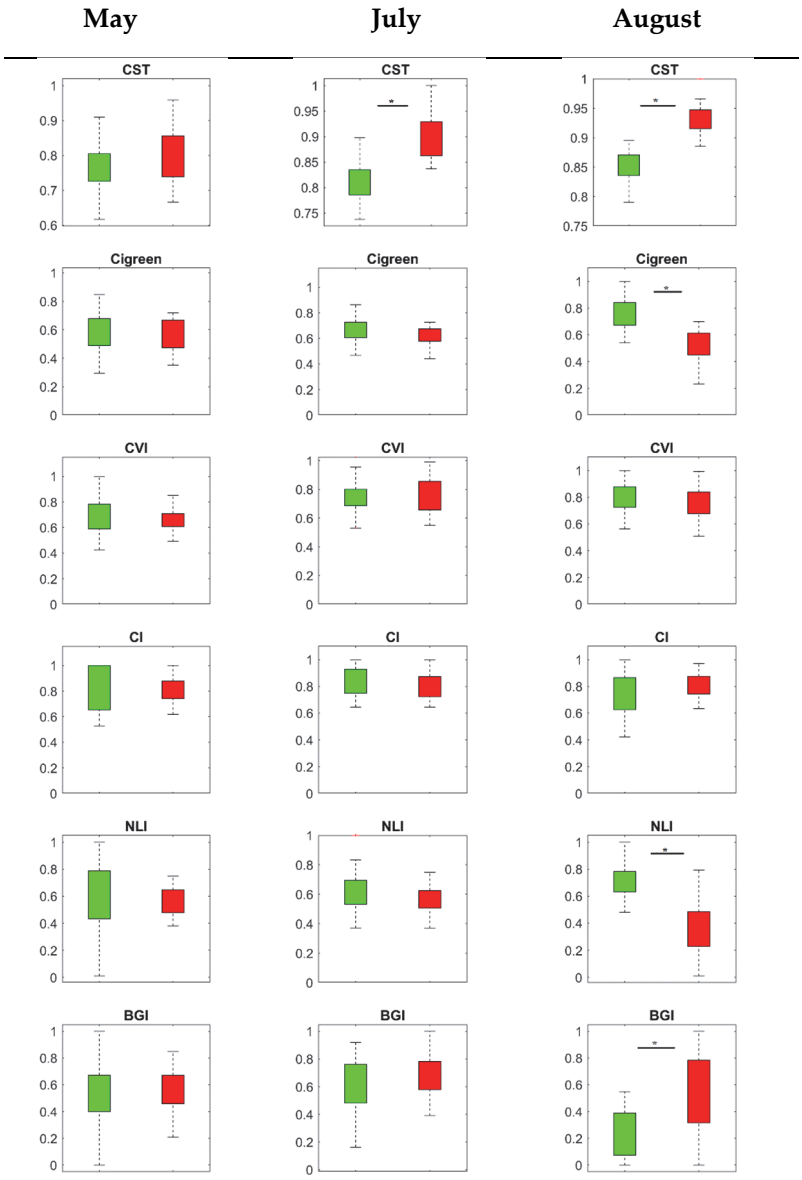

Figure 4. 6: Temporal variation of the SVIs and CST (VIP >1) for healthy and green attacked sample plots in the Bavarian Forest National Park. Blue and red boxes represent healthy and infested plots, respectively. A * indicates the significant different

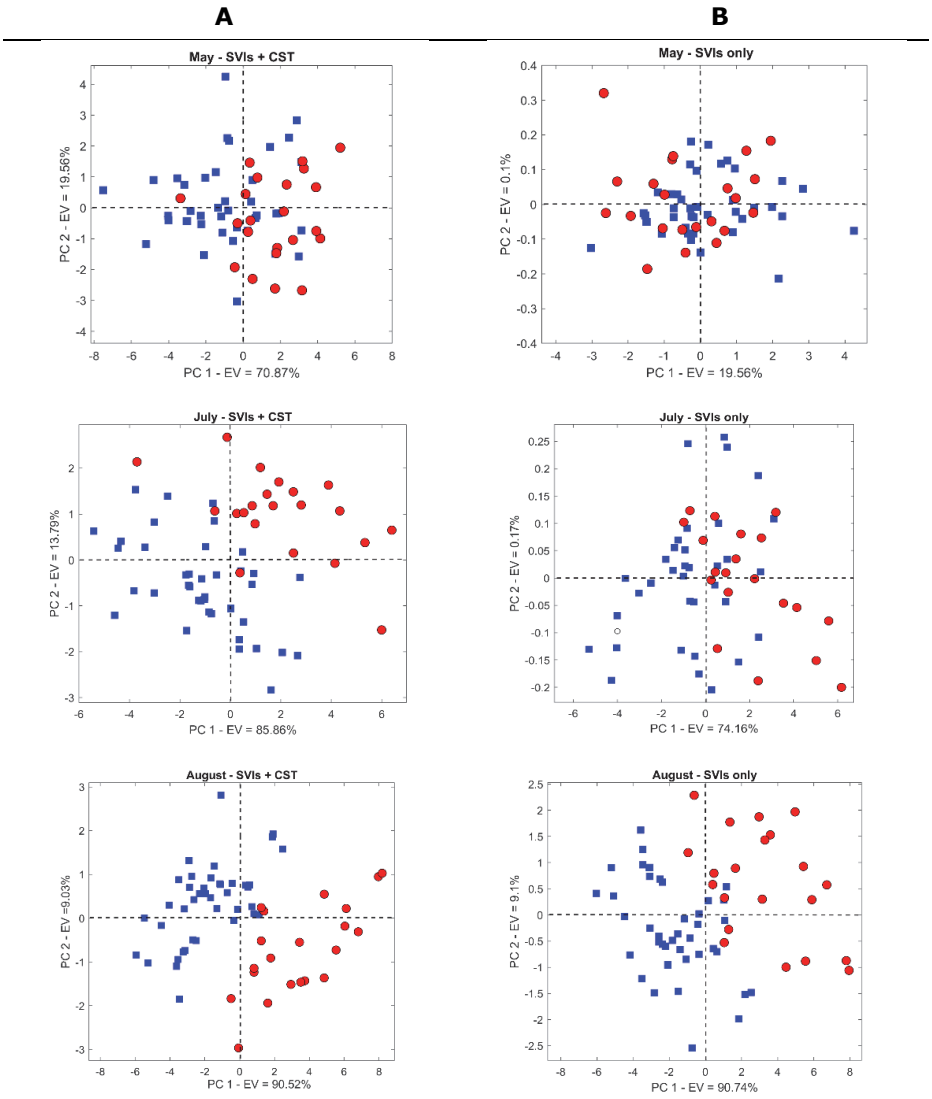

Figure 4. 7: Cluster plots based on the first two principal components (PCs), blue squares and red circles represent healthy and infested plots, respectively. (A) Cluster plots based on all spectral indices VIP >1 including CST (B) Cluster plots based all spectral indices VIP >1 excluding CST.

4.3.3 Mapping bark beetle green attack and validation

As shown in Figure 4.5, CST recorded the highest VIP score in all measured leaf traits, and therefore we considered it as the most important variable for predicting studied leaf traits. The CST was then used to estimate leaf traits (foliar stomatal conductance, chlorophyll fluorescence, and water content) and generate maps using the SLR model (Table 4.4). Following this, based on the

defined threshold value (Table 4.3), stress maps were generated using leaf traits' data. These maps were then overlaid with ground truth reference data (417 pixels) to calculate those pixels located within each stress class. Figure 4.8 and Table 5 depict those areas (pixels) that were located in each class. As can be seen from Table 5, 274 pixels out of 417 (66%) from ground truth data were located with the severely stressed class; following this, 89 (21%) pixels were located in the moderately stressed class and the remaining 54 (13%) pixels where located within the healthy class .

Table 4. 4: Regression equations between canopy surface temperature (CST) and measured leaf properties.

Equation No.	**Regression equations**
1	Leaf water content = -0.0004 CST + 0.0203
2	Stomatal conductance = -6.4377 CST + 255.66
3	Chlorophyll fluorescence = -0.0264 CST + 1.68

Table 4. 5: Assessment of the generated map using reference data obtained from Aerial photography.

Forest stress classes	**Pixels correctly matched**
Severely stressed	274
Moderately stressed	89
Healthy	54

Reference pixels (aerial photography) = 417 pixels (30m).

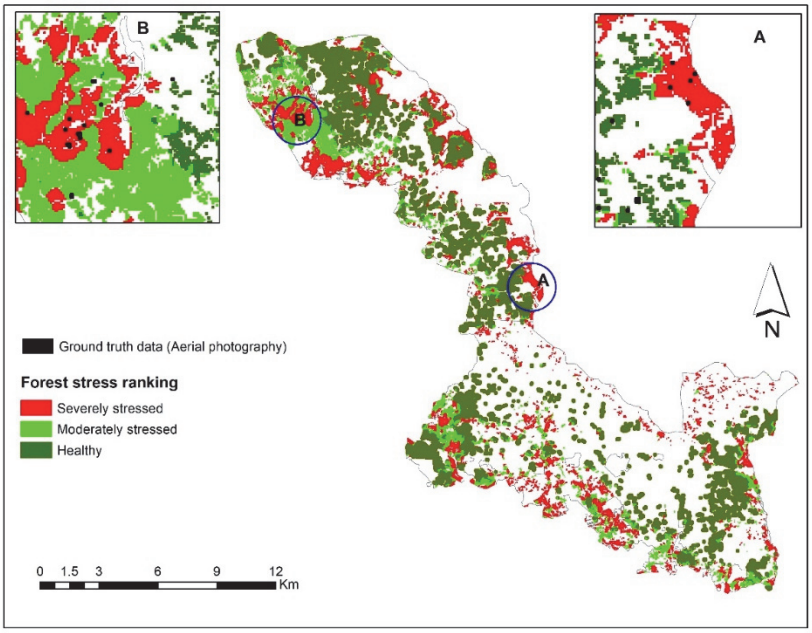

Figure 4. 8: The map showing the distribution of Norway spruce stands under different stress levels in the Bavarian Forest National Park, July 2016. The map was produced using canopy surface temperature and measured leaf traits (foliar stomatal conductance, chlorophyll fluorescence, and water content)

4.4 Discussion

In the present study, for the first time, we assessed the potential of CST and SVIs to discriminate between healthy and green-attacked trees by European spruce bark beetle (*Ips typographus*, L.). The results confirmed the superiority of CST in discriminating subtle differences between healthy and infested trees, compared to other utilised SVIs at different stages of bark beetle attack. Furthermore, all three considered leaf traits in this study exhibited significant differences ($p < 0.05$) between the two sample groups (healthy and infested), and CST was found to be an essential indicator (VIP > 1) to estimate them.

Of all 23 remote sensing variables (CST, SVIs, and single bands) used, the variable importance in projection (VIP > 1) showed that CST was by far the best at estimating studied leaf traits (Fig. 4.5). This result reaffirms findings by (Berni et al., 2009), who used TIR data obtained fixed-wing UAVs to study thermal water stress over the peach trees . Moreover, apart from the importance of CST in estimating leaf properties, we found that CST better discriminates between infested and healthy trees than other SVIs. In July and August, CST was significantly higher ($p < 0.05$) for the infested plots than for healthy ones (Fig. 4.6).. For example, in May, just at the beginning of the infestation, a slightly higher CST was observed for the infested plots, whereas

the SVIs showed no difference between the two groups. According to bark beetle phenology studies, the flight activity of bark beetles and their successful attack on living trees starts in late spring when the air temperature reaches 16.5ºC (Lobinger, 1994b; Wermelinger, 2004). The new insight offered by this result is the potential of CST to detect the subtle changes induced by bark beetles at this stage is quite important and promising. Likewise, in July, when the infestation had progressed, and the infested trees were completely stressed, CST maintained its sensitivity in differentiating between healthy and green-attacked sample plots (Fig. 4.6). It is well-known that physiological factors, such as plant water content, can control the temperature of plants through the stomatal transpiration process (Oerke et al., 2006). Therefore, the distinct variation in CST between healthy and infested plots is attributed to differences in the measured leaf traits, in particular, leaf water content. As depicted in Figure 4.4, the amount of water content was significantly lower ($p < 0.05$) in the infested plots than in the healthy ones. This may be attributed to the spores of fungi and the drilling activities of the beetle itself that affect the living cells in the phloem and xylem and, therefore, disrupt the flow of water and cause stomatal closure in infested trees (Yamaoka et al., 1990). This result further confirms our earlier finding (Abdullah et al., 2018a) showing a decrease of foliar biochemical properties (chlorophyll and nitrogen concentration) in trees infested by bark beetles (*I. typographus*, L.) at the green attack stage. Likewise, our findings are in agreement with (Cheng et al., 2010), who studied the impact of a similar species (the mountain pine beetle, *Dendroctonus* spp) on leaf water content using hyperspectral data. Infested trees tend to close their stomata to prevent further water loss and hydraulic failure (Ewers et al., 2007). This stomatal closure will temporarily offset xylem cavitation and cause damage to the photosynthetic apparatus (Chaves et al., 2003). However, this behaviour leads to other physiological changes in the infested trees, such as a decrease in the transpiration cooling process and, therefore, an increase in leaf surface temperature. Over time, this will affect the process of photosynthesis and cause a change in foliar colour (Larcher, 2003). These findings match those observed in earlier studies that the TCI index retrieved from the Landsat 7 ETM thermal band could detect areas under mountain pine beetle (*Dendroctonus* spp) green attack (Sprintsin et al., 2011).

In August, when the infestation had progressed and the subsequent degradation of the needles could be observed in the field (the infested trees developed stress symptoms by turning their needles' colour from green to yellow to red-brown), the variation of SVIs became more evident between healthy and infested plots. CST, Cigreen, NLI and BGI were shown to have the potential to detect the infested trees at that time. However, for effective management, identifying infested trees at that stage is too late, because the beetles will have already left the infested trees, and logging operations will not

have any effect on the population dynamics of the beetles at that time anymore (Fahse and Heurich, 2011; Wermelinger, 2004; Wulder et al., 2009).

In addition to the temporal variation, we also observed that CST improved discrimination between healthy and infested plots when using PCA analysis for all dates considered in this study (Fig. 4.7). In May, when the PCA model was built based on optical data only, the two groups of sample plots had mixed scattering and exhibited an apparent overlap, whereas, when CST was included into the model the healthy plots were separated from the infested ones. This indicates the increased sensitivity of Landsat-8 TIR data to changes at canopy level induced by bark beetle at a very early stage in May. One possible reason for such sensitivity of CST to spruce bark beetle infestation in May could be due to the nature of spruce bark beetle outbreaks, which generally occur over the course of several years. In other words, the healthy trees are always surrounded by other healthy trees, while, for infested trees in most cases, the infestation occurs close to the previous year's infestation (Lausch et al., 2011). Therefore, the open areas and dead trees around newly infested trees can lead to an increase in surface temperature. To confirm this, we further analysed and calculated the CST for different habitat types in the landscape. To do this, a habitat map obtained from the national park administration was used to extract the CST for each habitat type (Dupke et al., 2017). As can be observed from Figure 9, the results revealed that clear-cut areas, followed by lying dead-wood and standing dead-wood areas, had the highest CST for all three months. In contrast, mixed stands showed the lowest CST. This is supported by Peterson et al. (1986) who found that forest structure (i.e. canopy closure) is negatively correlated with simulated thermal data from the Thematic Mapper Simulator (TMS).

Similarly, Junttila et al. (2016) and Hais and Kučera (2008) have shown that higher surface temperatures were detected in dead-wood stands and clear-cut areas, respectively. Furthermore, a water body had the lowest CST, which supports the hypothesis that more moisture in healthy tree needles decreased their surface temperature. This also corresponded with our in-situ measurements that showed green-attacked trees had lower water content and more closed stomata than healthy trees (Fig. 4.4). The clear-cut area and dead-wood stands had no foliage and, thus, no leaf surface area for evapotranspiration. This resulted in higher canopy temperatures in the cleared and dead-wood stands than in intact stands.

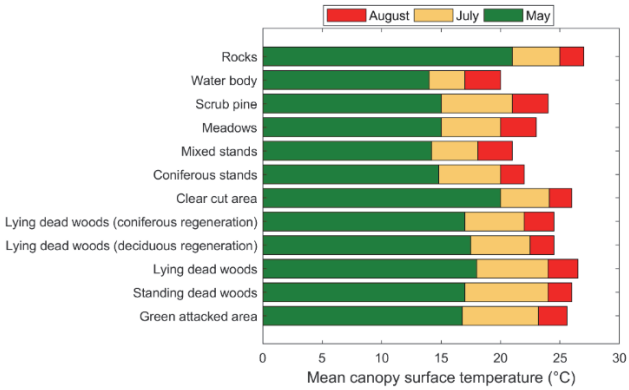

Figure 4. 9: Mean canopy surface temperature over different habitat classes in the Bavarian Forest National Park – 2016. The graph shows that standing dead-wood, lying dead-wood, clear-cut and rocky areas recorded high surface temperature comparing to other forest classes.

Moreover, an equally significant aspect of CST was found when used to estimate measured leaf traits (foliar stomatal conductance, chlorophyll fluorescence, and water content) and producing the stress map for the study area (Fig. 4.8). The stress map highlighted the sensitivity of CST for detecting canopies that are stressed by bark beetle green attack. In general, the majority (66%) of ground truth data were located within the severely stressed class — however, 13% where falsely located in the healthy class (Table 4.5). Consequently, CST derived from Landsat-8 TIR data might be used to generate hotspot maps of stressed areas within the forest that show high potential areas of bark beetle green attack. Such maps can provide valuable information to the forest management practice when they aim to control this species and preclude a mass outbreak. Furthermore, such maps can also be used to improve the bark beetle modelling community. For example, in our study and the previous studies by (Hais and Kučera, 2008) the highest temperature was observed over the dead-wood stands. Such information on the dead-wood stands combined with the less reliable information from green attacked areas can be used to improve the accuracy of predisposition models (Netherer and Nopp-Mayr, 2005)

4.5 Conclusion

The results of this study showed the potential of CST retrieved from the Landsat 8 TIR band to detect early-stage bark beetle infestation. We further found that the infestation at the green attack stage affected the leaf stomatal conductance, chlorophyll fluorescence, and water content. The CST has the highest VIP value for estimating all three leaf traits measured in this study for July. In addition, we found that CST maintained its sensitivity for monitoring and detecting bark beetle infestation before, during and after infestation. In conclusion, our key concept is that we show for the first time that satellite TIR

data has a high potential to detect bark beetle green attack and examining the link between the leaf traits and thermal remote sensing data is an important step that further improves our understanding of the relationship between Earth Observation data and plant traits for forest areas under bark beetle green attack. It is important to note that TIR images obtained from Landsat-8 are the only available satellite images that provide data at 30 m spatial resolution. However, the original data were acquired at 100 m, so the actual footprint of the pixel is larger. Therefore, further research investigating different TIR data with higher spectral and spatial resolution, such as TIR from airborne hyperspectral measurements, may improve the use of thermal imagery for bark beetle green attack detection in Norway spruce forests.

Chapter 5: Sentinel-2 accurately maps green attack stage of European spruce bark beetle (*Ips typographus*, L.) compared to Landsat-8 *

* This chapter is based on:

Abdullah, H., Darvishzadeh, R., Skidmore, A.K., and Heurich, M. Sentinel-2 accurately maps green attack stage of European spruce bark beetle (*Ips typographus*, L.) compared to Landsat-8. *Remote Sensing in Ecology and Conservation*. 2018, 1–21.

Abstract

Natural disturbances induced by insect outbreaks have increased in forest ecosystems over the past decades. To minimise economic loss and prevent a mass outbreak, early detection of bark beetle green attack – a period when trees have yet to show visual signs of infestation stress – is therefore crucial to effective and timely forest management. In this study, we evaluated the ability of spectral vegetation indices extracted from Landsat-8 and Sentinel-2 imagery to map bark beetle green attack using principal component analysis (PCA) and partial least square discriminate analysis (PLS-DA). A recent infestation map produced through visual interpretation of high-resolution aerial photographs validated the final infestation output maps. Leaf spectral measurements alongside total chlorophyll and nitrogen concentration, leaf water content, and leaf dry matter content were measured to assess the impact of bark beetle green attack on foliar properties. We observed that the majority of Spectral Vegetation Indices (SVIs) calculated from Sentinel-2, particularly red-edge dependent indices (NDRE 2 and 3) and water-related indices (SR-SWIR, NDWI, DSWI, and LWCI), were able to discriminate healthy from infested plots. In contrast, only the water-related indices (NDWI, DSWI, and RDI) from Landsat-8 were able to discriminate between healthy and infested plots efficiently. The total number of pixels identified as harbouring a green attack that matched with ground truth data (aerial photography) was higher for Sentinel-2 (67%) than for Landsat-8 (36%) SVIs, indicating the elevated sensitivity of Sentinel-2 imagery to changes induced by bark beetle green attack. We also determined that foliar chlorophyll and leaf water content were significantly higher ($p < 0.05$) in healthy trees than in green attacked trees. Our study highlights the potential of Sentinel-2 data for the early detection of bark beetle infestations and the production of reliable infestation maps at the green attack stage.

5.1 Introduction

Insect infestations, as by the European spruce bark beetle (*Ips typographus* L.), form the main disturbance events in European forests as they destroy more forested areas than all other natural disturbances together. Historically, storms and snow breakage events in Europe and North America have provided a large surplus of suitable breeding material for bark beetles, leading to outbreaks (Giunta et al., 2016; Seidl et al., 2017a). Recent outbreaks are different, however, with climate change (more drought and severe storm events) appearing to be the initiating factor (Marini et al., 2016; Netherer et al., 2015; Thom and Seidl, 2016). Increasing temperatures may result in an increased incidence of drought, possibly affecting tree health. Drought facilitates beetle outbreaks by stressing trees and increasing the frequency and severity of bark beetle outbreaks (Bentz et al., 2010; Faccoli and Bernardinelli, 2014; Filchev, 2012b; Thom and Seidl, 2016). A warmer climate may increase storm frequencies, and severity of wind throws, thus providing more breeding material for bark beetles (Marini et al., 2016). Furthermore, as the development of the bark beetle is dependent on temperature, an increase in temperature may thus lead to an increase in the beetle population size, due to their eggs hatching and developing into adults sooner (Bentz et al., 2010; Wermelinger, 2004). In recent decades, therefore, increasing disturbances due to insect outbreaks have been widely documented across different parts of the world (Lausch et al., 2013a; Seidl et al., 2014; Wulder et al., 2006a).

Timely, accurate and cost-effective information is needed to mitigate and control bark beetle outbreaks, to guide forest managers in identifying areas infested by beetles, as well as to define the timing of bark beetle control activities (Wulder et al., 2009). To obtain this information, the operation survey needs to take place at the time when the infestation at its early stage (the green attack). The green attack stage is the first interaction between the beetle and the host tree, and occurs when the host is being colonized by the bark beetle. During this stage, the infested tree is still physiologically green and very much alive, although exhibiting stress in the near infrared (invisible to the human eye) (Niemann and Visintini, 2005). Furthermore, during the green infestation, the newly hatched generation of beetles is developing within the inner bark of the infested trees. Therefore, management intervention to prevent further outbreaks may involve the removal of infested trees before the new brood emerges and migrates (Wermelinger, 2004; Wulder et al., 2009).

Traditionally, foresters perform field surveys to identify infested trees during the early green attack stage using conventional survey methods (looking for sawdust). Such surveys are very laborious and therefore make screening large areas for green attack difficult. Nowadays, remote sensing provides new opportunities to detect and map bark beetle infestation. Remotely sensed data

rely on spectral signatures from different regions in the electromagnetic spectrum. Unique spectral signatures have been linked to different functional and structural plant traits, such as pigments at 400–700 nm, leaf structure at 700-1100 nm and plant water content, nitrogen concentration, Leaf Area Index and Specific Leaf Area at 1100 to 2400 nm (Ali et al., 2016; Gitelson et al., 2002; Mahlein et al., 2013; Viña et al., 2011; Wang et al., 2015a). Stress affects plant biophysical and biochemical properties and therefore affects spectral signature. For example, chlorophyll degradation and nitrogen deficiency lead to an increase in reflectance spectra in the visible region (the red and green bands in particular). As a result, this wavelength region has been widely used as a stress indicator when utilising remote sensing data (Hendry et al., 1987). Significantly, the reflectance at the red portion of the visible region has been shown to be less sensitive to initial loss of chlorophyll content (Carter, 1993). This is due to the high spectral absorption by chlorophyll in this spectral region, which saturates the red reflectance at low chlorophyll content (Jacquemoud and Baret, 1990). In contrast, the reflectance at the green and red-edge wavelengths (centred in 550 nm and 700 nm, respectively) of the VIS region are more sensitive to changes in plant chlorophyll content (Eitel et al., 2011). Furthermore, the red-edge region has superior sensitivity when detecting changes that are induced in plants by stressors such as dehydration, disease, and insect attack, and can, therefore, improve the early detection of plant stress (Ahern, 1988b; Carter and Knapp, 2001; Carter and Miller, 1994; Eitel et al., 2011). Moreover, the NIR and SWIR regions have been used widely to assess water content and nitrogen concentration in plants (Ayala-Silva and Beyl, 2005; Carol et al., 2004; Jackson, 2004; Munoz-Huerta et al., 2013).

Several studies have utilised spectral vegetation indices (SVIs) from low-to-medium resolution satellite data to study bark beetle infestation. These studies have mainly focused on the last two infestation stages (red and grey) of attacks (Filchev, 2012b; Franklin et al., 2003; Hais et al., 2009; Havašová et al., 2015; Koch et al., 2010; Meddens et al., 2013; Wulder et al., 2006b). However, for effective and proper forest management, the detection of infestation should be early enough to allow for timely intervention to minimise the outbreak. Several studies have explored the use of commercial remote sensing data such as Worldview-2 (Filchev, 2012b; Immitzer and Atzberger, 2014), RapidEye (Marx and an der Havel, 2010b; Ortiz et al., 2013) and HyMAP airborne hyperspectral data (Lausch et al., 2013b) for the early detection of bark beetle attack, but with very limited success.

The SVIs were introduced to improve interpretation of vegetation signals when using remote-sensing data and can be used to measure vegetation status while minimising solar irradiance and soil background effects (Darvishzadeh et al., 2009; Jackson and Huete, 1991; Moulin, 1999). Additionally, the combination

of different spectral bands is closely related to biophysical and biochemical properties of foliage vigour associated with plant health and can be used to detect morphological and physiological changes caused by insect outbreaks in the forest canopy (Rullan-Silva et al., 2013). Therefore, SVIs may be expected to perform better than individual spectral bands when it comes to detecting stress induced by the bark beetle. This is especially valid when using low-to-medium resolution data that include the red-edge spectral domain (Jackson and Huete, 1991; Zhang et al., 2012). This study evaluates the ability of different SVIs from Sentinel-2 and Landsat-8 imagery to detect and help map bark beetle infestation at the green attack stage. Furthermore, we also study the impact of bark beetle green attack on foliar biochemical and biophysical properties and their spectral reflectance using foliar spectral data collected from ASD Fieldspec3.

5.2 Material and Methods

5.2.1 Study area and field data collection

The study area is the Bavarian Forest National Park, which is a 24,369 ha forest located in south-eastern Germany along the broader with the Czech Republic, between 13°12'9" E (longitude) and 49°3'19" N (latitude). This region is characterised as having a temperate climate with an annual precipitation of between 900 and 1800 mm, and a mean annual temperature of between 3.5° and 9°C (Bässler et al., 2008b). The forest is dominated by Norway spruce (*Picea abies*) (67%) and European beech (*Fagus sylvatica*) (24.5%) (Cailleret et al., 2014a). Outbreaks of the bark beetle (*Ips typographus*, L.) began in 1984 and have caused extensive disturbance to this forest. As such, the area is a suitable study site for research on bark beetle infestations and outbreaks (Heurich et al., 2010a).

During June and the beginning of July 2016, an extensive campaign was conducted to collect field measurements. The study area was divided into two different strata based on their tree condition: stands with healthy trees and stands with trees freshly infested by the bark beetle. To select the healthy stands, a stratified random sampling strategy was adopted. While, for the recently infested stands, the presence of bark beetle green attack had to be confirmed in an intensive field survey by searching for piles of dry, boring dust pushed out onto the bark surface of the tree when the beetle tunnels under the bark. According to the Bavarian Forest National Park authorities and our field survey, the infestation of bark beetles in 2016 clearly indicated outbreak conditions.

To avoid mixed reflectance from healthy and green attacked trees, only plots fully under bark beetle green attack that covered an area of 30 m × 30 m were

selected. In total, 40 and 21 plots were selected in healthy and infested stands, respectively (Fig. 5.1). The centre of each plot was measured using Differential Global Positioning System (DGPS) Leica GPS 1200 (Leica Geosystems AG, Heerbrugg, Switzerland) with an accuracy of better than 1m after post-processing. Each plot was designed as a 30 × 30 m square and within the plot stand characteristics including DBH, canopy cover, height and tree density were measured. At each plot, three to five trees were selected as representative and needle samples from each of these trees were collected separately. All the samples were taken from the trees' top layer exposed to the sunlight. A crossbow was used to shoot an arrow attached to a fishing line at a branch with sunlit leaves (Ali et al., 2016).

Leaf spectral reflectance and traits including total chlorophyll, leaf water content (Cw), leaf dry matter content (LDMC), and foliar nitrogen concentration were measured for healthy and infested samples (Table 5.1). In the field, the concentration of chlorophyll was determined using a CCM chlorophyll meter. On average ten readings were immediately taken from each fallen branch with the CCM. The needles were then removed from the fallen branches, covered with wet pulp paper and placed in a labelled plastic zip-locked bag. They were transported to the laboratory using a portable cooling box; this was done to retard possible changes in the needles' reflectance spectra and biochemical characteristics. The leaf directional hemispherical reflectance from 350 to 2500 nm was measured for the collected samples, using an ASD FieldSepc-3 Pro FR spectrometer equipped with an ASD RT3-3ZC integrating sphere (Analytical Spectral Devices, Inc., Boulder, Co, USA). Further details concerning the measurements of hemispherical needle reflectance can be found in Abdullah et al. (2018), Ali et al. (2016), Daughtry et al. (1989), and Malenovský et al. (2006). The needle samples were then dried for 72 h using an oven at 60° C, until they reached constant weight, to calculate leaf dry matter and water content (see Table 5.1). To determine foliar nitrogen, the dried needles were ground using mortar and pestle until they became a soft powder, after which they were passed through a 0.25 mm mesh screen. Subsequently, 2 mg of powdered leaves were transferred to a small aluminium capsule to measure the nitrogen content using an organic elemental analyser (FLASH 2000). The studied leaf traits (chlorophyll, water content, dry matter content, and nitrogen concentration) from the measured representative trees in each plot were then averaged to obtain the leaf traits at the plot level, hereafter referred to as plot level parameters.

Table 5. 1: The leaf traits measured for healthy and infested samples in this study. Fw, Dw and A represent fresh leaf weight (g), dry leaf weight (g), leaf dry mass per unit area (Cm), and leaf area (cm2), respectively.

Leaf traits	Equation	unit	Reference
Leaf water per mass area	(Fw-Dw)/A	Mg/cm^2	(Danson et al., 1992, Ceccato et al., 2001)
Leaf dry matter content (LDMC)	Cm / (Cm-Cw)	Mg/g	(Vile et al.,2005)
Nitrogen	----------	%	PerkinElmer 2400 CHN/O
Chlorophyll	----------	Mg/m^2	chlorophyll content meter

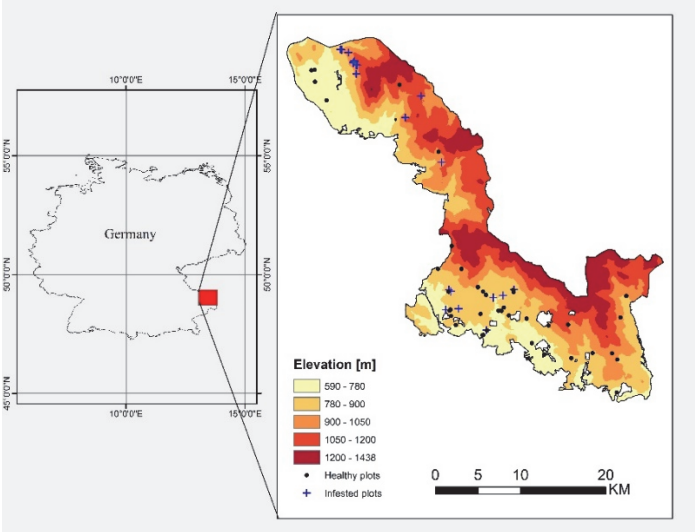

Figure 5. 1: Location of healthy and green attacked sample plots in the Bavarian Forest National Park in July 2016.

5.2.2 Satellite imagery

Open access multispectral satellite imagery from Sentinel-2 and Landsat-8 was selected for this study. To fulfil the aims of this research, cloud-free satellite data were acquired on 8 and 10 July 2016 from Sentinel-2 and Landsat-8, respectively. Landsat-8 data were obtained from USGS Global Visualization Viewer (http://glovis.usgs.gov/), and the Sentinel-2 data were obtained from the ESA Scientific Hub (https://scihub.copernicus.eu). Both images were geometrically corrected in the Universal Transform Mercator (UTM) coordinate system and matched each other with sub-pixel accuracy. Sentinel-2 delivers high spatial (10 to 20 m) and spectral (13 bands) image data. Also, it is the first freely available optical satellite providing three spectral bands in the red-edge spectral region.

To prepare the satellite images for further analysis, a series of pre-processing was applied. First, for Landsat-8, image radiometric calibration was applied to convert the pixel values to Top-of-Atmosphere (TOA) reflectance. A MODTRAN4-based atmospheric correction software package (FLAASH) developed by the Air Force Phillips Laboratory, Hanscom AFB, and Spectral Sciences, Inc. was used to convert the TOA Reflectance to surface reflectance (Adler-Golden et al., 1999) using ENVI software. For Sentinel-2, the TOA reflectance data were corrected to surface reflectance using the SEN2COR atmospheric correction software developed by ESA (http://step.esa.int/main/third-party-plugins-2/sen2cor/). Secondly, the bands with a similar spatial resolution were stacked. In general, six bands from Landsat-8 were used and stacked together, namely the bands 2,3,4,5,6 and 7, which have a 30 m spatial resolution. From the Sentinel-2, the bands 2,3,4 and 8, with a 10 m spectral resolution, were first resampled to 20 m and then stacked with bands 5,6,7,9, 12 and 13. The three bands with a 60 m spatial resolution (1,10,11) are mainly relevant for atmospheric corrections and were not used in this study. Finally, the spectral reflectance values of the sample plots were extracted from the Landsat-8 and Sentinel-2 scenes and used for further analysis. To synthesise and compare leaf reflectance data with canopy reflectance data (from Sentinel-2 and Landsat-8 data), the reflectance spectra collected from ASD FieldSepc-3 Pro FR spectrometer equipped with an ASD RT3-3ZC integrating sphere were simulated by convolving to the spectral resolution of Sentinel-2 and Landsat–8 using the linear interpolation method.

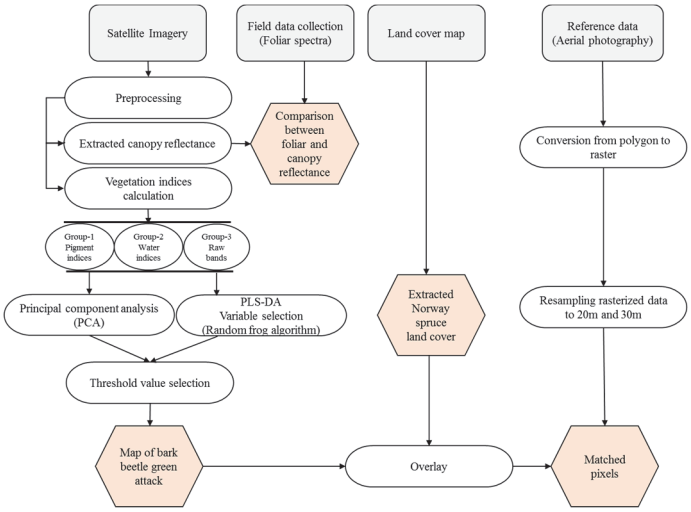

Figure 5. 2:The flow chart of the methodology used in this study

5.2.3 Spectral vegetation indices calculation

Spectral reflectance data from Sentinel-2 and Landsat-8 images were used to calculate the most widely used vegetation indices to detect changes in plant photosynthetic activity and biochemical stress, among other forms of vegetation stress (Collins and Woodcock, 1996; Eitel et al., 2006). Spectral vegetation indices include optical vegetation canopy (greenness), which is a combined property of foliar biochemical (chlorophyll, nitrogen, leaf water content) and other canopy properties (Jiang et al., 2008). To prevent using multiple copies of similar band combinations such as (red and NIR) in this study, we attempted to use statistically-independent spectral indices. In addition, we employed the raw spectral bands as independent indices and only those bands that were significantly different ($p \leq 0.5$) between healthy and infested sample plots (Table 5.2). The selected SVIs are sensitive to stress-induced variations in chlorophyll content (VIS), biomass (NIR), and water content (SWIR). Further, depending on their use, we categorised the vegetation indices into three groups: (a) chlorophyll and other pigments, (b) indices used for detection of water stress, and (c) the raw spectral bands from Sentinel-2 and Landsat-8. ENVI software was used to compute spectral vegetation indices. The equations for computing the vegetation indices are provided in (Table 5.2).

5.2.4 Statistical analysis

Three statistical analyses were employed in this study: one-way ANOVA, principal component analysis (PCA), and partial least square discriminant analysis (PLS-DA). ANOVA tests were performed to: (a) ascertain the effect of bark beetle green attack on measured leaf traits, including leaf and canopy reflectance data, and (b) to evaluate whether SVIs' between the two sample groups (healthy and infested) were significantly different. Moreover, to visually examine how well the two sample plots (healthy and infested) are separated in 2-D space based on principal component scores, the clustering method using principal component analysis is employed in this study. As such, PCA was used to evaluate the potential for different spectral vegetation indices to differentiate between healthy and infested sample plots. PCA is an unsupervised technique and remains a popular method used to reduce the dimension of multivariate data sets and to extract features (Hotelling, 1933; Pearson, 1901). The unit variance and mean centring producer were used to pre-process the data. To build the PCA model, spectral vegetation indices were treated as independent variables, and the SVIs data of all 60 sample plots (21 infested and 40 healthy plots) were analysed. PCA models were built independently for each SVIs group as follows: (a) including all SVIs (pigment, water, and raw bands); (b) including only pigment-related indices; and (c) including only water-related indices. This step is important because it allows

us to understand and identify the most effective spectral indices group for separating the healthy from the infested sample groups (Fig. 5.2).

In order to identify the key SVIs influencing the spectral separability between the healthy and infested plots, and to map bark beetle green attack, a novel method known as a Random Frog (RF) was used. The RF is a state-of-the-art variable selection algorithm, and it is a computationally efficient method using the context of the reversible jump Markov chain Monte Carlo (MCMC) technique (Green, 1995). It performs a search in the model space via both fixed-dimensional and trans-dimensional moves between different models. After a pseudo-MCMC chain is calculated, this can be used to calculate a selection probability (SP) value for each variable included in the model. The key variables can be identified regarding the ranking of all variables based on the SP value. A detailed description of the calculation of RF can be found in Yun et al. (2013). To achieve this, partial least squares-discriminant analysis (PLS-DA) was employed as a modelling method in RF (Li et al., 2012). PLS-DA is a classification technique allowing for the identification of variables that improve the separation or classification between different groups (Wold et al., 2001).

In our study, SVIs with an SP value > 0.50 were selected as an important variable to map bark beetle green attack. Following this, the selected SVIs from both satellites (Sentinel-2 and Landsat-8) were used to map bark beetle green attack. The box plot technique was used to display the distribution of SVI values for healthy and infested plots. The threshold values for green-attacked pixels were identified for each selected SVI. The criteria for selecting the threshold values were based on the area (value) of each SVI, which essentially characterised the difference (no overlap) between healthy areas and those infested by bark beetle green attack (Fig. 5.9). Consequently, a conditional decision was made using the identified threshold values from each SVI to identify those pixels in the images falling within the identified threshold range (assigned as 1) and those pixels falling outside of the threshold range (assigned as 0). For example, the following conditional decision was utilised to extract the threshold value from NDRE-2:

$$Green\ attacked\ pixels = \begin{cases} 1, & if\ 0.45 \leq NDRE2\ \leq 0.80 \\ 0, & otherwise \end{cases} \quad (5.1)$$

From the conditional statement the following threshold values are extracted: if the value of NDRE-2 is higher than 0.45 and less than 0.80, a 1 (green attack) will be assigned to that cell location on the output raster; otherwise, a 0 (false) will be assigned on the output raster. Similar conditions were applied to the other selected SVIs (Figure 8)

Finally, to generate the final infestation map, the following equation was applied to sum the infestation maps generated from each SVIs:

$$Final\ infestation\ \ map = \begin{cases} 1, & if\ \ indices\ A\ and\ B\ and\ C\ \ldots = 1 \\ 0, & otherwise \end{cases} \quad (5.2)$$

All of the above statistical analyses were carried out using MATLAB 2016b (MathWorks Inc, Natick, USA) and ArcMap (v.10.3).

5.2.5 Ancillary data and accuracy assessment

To assess how successfully the infestation maps produced in this study matched with the existing infestation areas, reference data corresponding to the locations of infested trees obtained from the Bavarian Forest National Park administration were used for validation of the output infestation maps. The flight on 11 Jun 2017 documented new dead wood (grey attack stage) from the previous year 2016, with reference data collected from airborne colour-infrared (VIS and NIR) aerial images (CIR) with 0.1 m spatial resolution. Full details about the processing and interpretation of the aerial photography in the Bavarian Forest National Park can be found (Heurich et al., 2009; Lausch et al., 2013a).

The infestation data were in the form of polygons and were rasterised twice; firstly into 20 m × 20 m grid cells to match the generated map of infestation from Sentinel-2 SVIs, and secondly into 30 m × 30 m grid cells to match the infestation map generated from Landsat-8 SVIs (Fig. 5.2). Since bark beetles only infest old and mature Norway spruce (*Picea abies* (L.) Karst), the non-spruce stands and young stands were masked using land cover data obtained from the national park administration (Dupke et al., 2017). The masked land cover was overlaid on the infestation maps generated in this study and compared with the rasterised reference data. Finally, the total number of pixels that correctly matched with the reference pixels (ground truth) were extracted and calculated (Fig. 5.2).

Table 5. 2: Spectral vegetation indices applied to leaf reflectance measurements, Sentinel-2 and Landsat-8 in the study area.

Index	Sensor		Equation	Reference
	Landsat-8	**Sentinel-2**		
(chlorophyll, pigments, greenness)				
Canopy Chlorophyll Content Index (CCCI)	×	√	$\frac{\frac{NIR - Rededge1}{NIR + Rededge1}}{\frac{NIR - Red}{NIR + Red}}$	(Barnes et al., 2000)
Chlorophyll Green (Chlgreen)	×	√	$\left(\frac{Rededge\ 3}{Green}\right)^{-1}$	(Gitelson et al., 2006)
Leaf Chlorophyll Index (LCI)	×	√	$\frac{NIR - Rededge1}{NIR + Red}$	(Pu et al., 2008)
Normalized Difference Red-Edge 2 (NDRE2)	×	√	$\frac{NIR - Rededge1}{NIR + Rededge1}$	(Haboudane et al., 2004)
Normalized Difference Red-Edge 3 (NDRE 3)	×	√	$\frac{NIR - Rededge2}{NIR + Rededge2}$	This study
Chlorophyll vegetation index (CVI)	√	√	$NIR\left(\frac{Red}{Green\text{^}2}\right)$	(Vincini et al., 2008)
Green Difference Vegetation Index (GDVI)	√	√	$\mathrm{NIR} - \mathrm{Green}$	(Tucker et al., 1979)
Green leaf index (GLI)	√	√	$\frac{2 \times (Green - Red - Blue)}{2 \times (Green + Red - Blue)}$	(Gobron et al., 2000)
Green Normalized Difference Vegetation Index (GNDVI)	√	√	$\frac{NIR - Green}{NIR + Green}$	(Fu et al., 2008)
Normalized Difference Vegetation Index (NDVI)	√	√	$\frac{NIR - Red}{NIR + Red}$	(Tucker, 1979)
Normalize Green (NG)	√	√	$\frac{Green}{(NIR + R + Green)}$	This study
Normalized Difference Green/Red Normalized green red difference index (NGRDI)	√	√	$\frac{Green - Red}{Green + Red}$	(Hunt et al., 2011)

Normalized Difference NIR/Blue Blue-normalized difference vegetation index (BNDVI)	√	√	$\frac{NIR - BLUE}{NIR + BLUE}$	(Hancock and Dougherty, 2007)
Simple Ratio Blue / Red SR-Blue/Red)	√	√	$\frac{Blue}{Red}$	This study
Chlorophyll index green (CIG)	√	√	$\left(\frac{NIR}{Green}\right) - 1$	(Gitelson et al., 2003)
Green Index (GI)	√	√	$\frac{Green}{Red}$	(Gamon and Surfus, 1999)
Plant biochemical index (PBI)	√	√	$\frac{NIR}{Green}$	This study
Coloration Index (CI)	√	√	$\frac{(RED - BLUE)}{RED}$	(Escadafal et al., 1994a)
Plant pigment ratio (PGR)	√	√	$\frac{Green - BLUE}{Green + BLUE}$	(Metternicht, 2003)
Water indices				
Disease Stress water index (DSWI)	√	√	$\frac{NIR + Green}{SWIR + Red}$	(Galvao et al., 2005)
Vegetation Moisture Index (VMI)	√	√	$\frac{(NIR + 0.1) - (SWIR + 0.02)}{(NIR + 0.1) + (SWIR + 0.02)}$	(Ceccato et al., 2002)
Leaf Water Content Index (LWCI)	√	√	$\frac{log(1 - (NIR - SWIR))}{-log(1 - (NIR - SWIR))}$	(Cohen, 1991)
Normalized Difference Infrared Index (NDWI)	√	√	$\frac{NIR - SWIR}{NIR + SWIR}$	(Hardinsky and Lemas, 1983)
Simple Ratio SWIR (SR-SWIR)	√	√	$\frac{SWIR1}{SWIR2}$	This Study
Ratio Drought Index (RDI)	√	√	$\frac{SWIR1}{NIR}$	(Pinder and McLeod, 1999)

5.3 Results

5.3.1 Impact of bark beetle green attack on measured leaf traits

The results of the ANOVA test showed significant differences ($p < 0.05$) between healthy and infested samples for all measured leaf traits in this study

except for nitrogen concentration at plot level (Fig. 5.3). At the leaf level, chlorophyll and leaf water content were significantly higher for healthy than for infested foliar. In contrast, smaller differences were observed in foliar nitrogen concentration ($p < 0.04$) between these two groups. Leaf dry matter content (LDMC) was significantly higher for the infested leaves. Similarly, at plot level, higher chlorophyll and water content was observed for the healthy plots (Fig. 5.3).

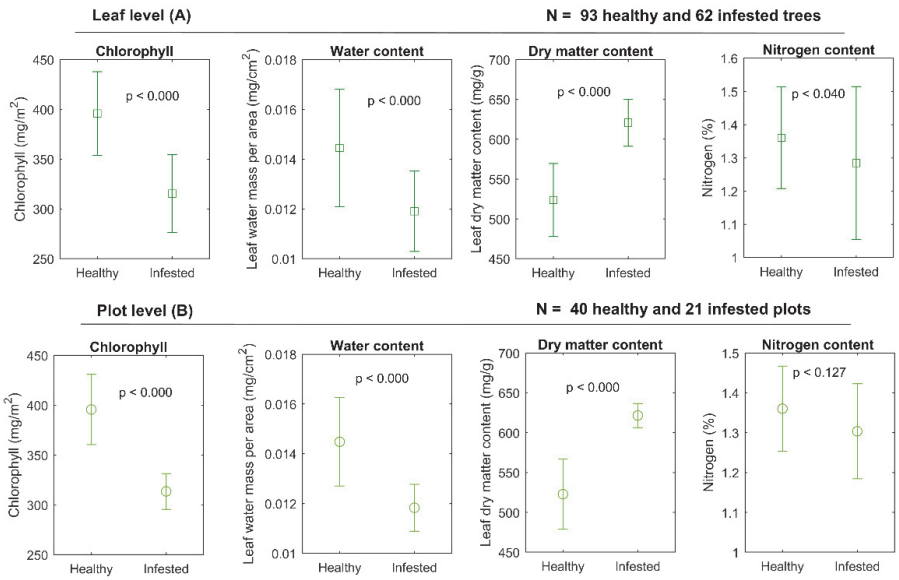

Figure 5. 3: Mean and standard deviation for measured leaf traits at both leaf (A) and plot level (B). Leaf level data is obtained from the average measurements per tree and plot level data is obtained from the average measurements of representative trees within each plot.

5.3.2 Leaf and canopy spectral variations

Figure (5.4) shows the difference between the mean reflectance of healthy and infested foliage. The difference is largest in the VIS region between 520-685 nm, the NIR (740-1130 nm) and the shortwave infrared region (1420-1850 nm and 2000-2200 nm). Similar results have been observed at canopy level for the Sentinel-2 data, particularly in the NIR and SWIR infrared regions (Fig. 5.5 A). Infested trees tend to have a higher reflectance in the VIS and SWIR regions than healthy trees. Moreover, the results of one-way ANOVA testing shows that the mean reflectance spectra of healthy and green-attacked sample plots were significantly different ($p < 0.05$) for all Sentinel-2 spectral bands at both leaf (simulated spectra) and canopy level. In contrast, for Landsat-8, no significant difference was observed at the canopy level. However, from the simulated leaf spectra of Landsat-8 spectral bands, low significance differences were observed for the red, NIR, SWIR1 and SWIR 2 bands (Table 5.3).

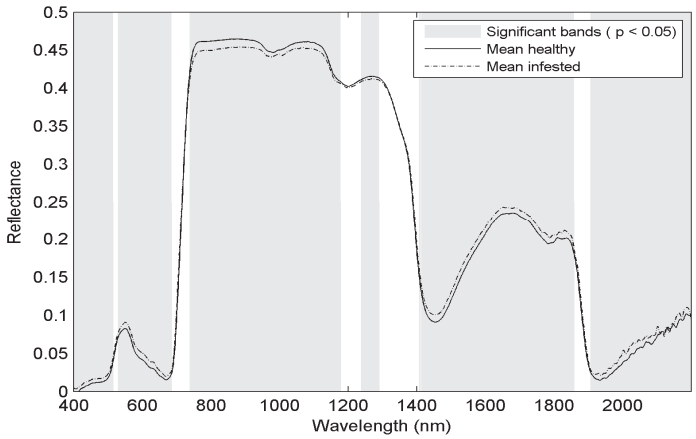

Figure 5. 4: Mean reflectance spectra of healthy and infested foliar at the green attack stage. Grey areas depict the location of wavebands displaying is a significant difference between healthy and infested spectra.

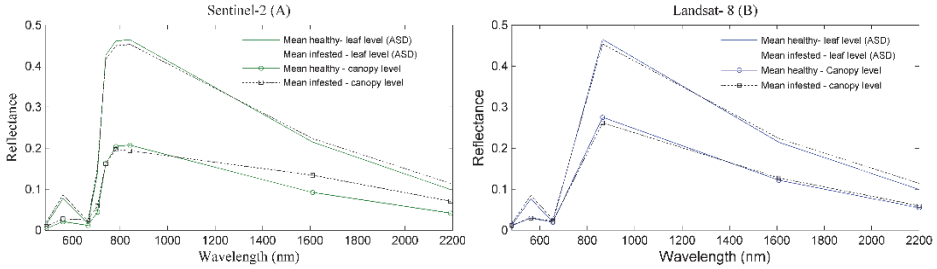

Figure 5. 5: (A) foliar and canopy reflectance using Sentinel-2 data (B) foliar and canopy reflectance using Landsat-8 data.

Table 5. 3: One-way ANOVA test between healthy and infested reflectance data at both leaf (simulated) and canopy level.

Spectral bands	Significance level (p < 0.05)			
	Landsat -8		Sentinel- 2	
	Leaf level	Canopy level	Leaf level	Canopy level
Blue	•	•	**	*
Green	•	•	**	***
Red	*	•	**	***
Red-edge1	Not available	Not available	***	***
Red-edge2	Not available	Not available	***	***
Red-edge3	Not available	Not available	**	*
NIR	*	•	**	**
NIR(a)	Not available	Not available	**	*
SWIR-1	*	•	***	***
SWIR-2	*	•	***	***

(•) Not significant, (*) Hardly significant, (**) significant, (***) Strongly significant.

5.3.3 Principal component analysis (PCA) and ANOVA test

Significant differences ($p < 0.05$), were found for all SVIs calculated from Sentinel-2 (except SR-Blue/Red, GDVI and CI) between healthy and infested trees (Fig. 5.6). Whereas, the SVIs derived from Landsat-8 were only sensitive to changes in water content (water indices) (DSWI, NDII and LWCI), and no significant differences were found for the pigment indices (Fig. 5.6). Moreover, the results of PCA revealed that the first two components (PC 1 and 2) explained more than 70% of the variance in the samples of SVIs investigated in this study. Figure 5.7 (A, B, and C) shows the clustering of two sample plots (healthy and infested) within the space of the first two principal components (PC1 and 2). As can be seen from Figure 5.7 (A), there was a slight crossover between healthy and infested sample plots when all three groups of SVIs from Sentinel-2 data were applied in the model. In contrast, the two sample plots (healthy and infested) exhibited an apparent overlap and mixed scattering for the Landsat-8 SVI groups. Furthermore, for Sentinel-2 SVIs, the majority of healthy plots tended to be on the negative side of PC1, while the infested plots were relatively scattered on the positive side of PC1 (Fig. 5.7 (B)). Notably, no obvious improvement was observed when the PCA model was built independently for each SVI group.

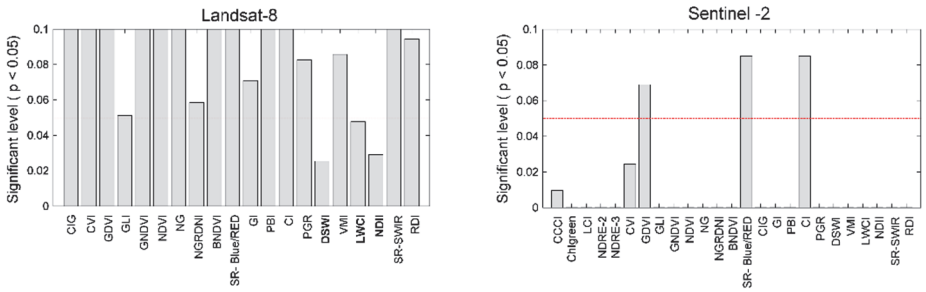

Figure 5. 6: Comparison of p-values from one-way ANOVA analysis between SVIs for healthy and infested samples (red dash line represents the significant level ($p < 0.05$)).

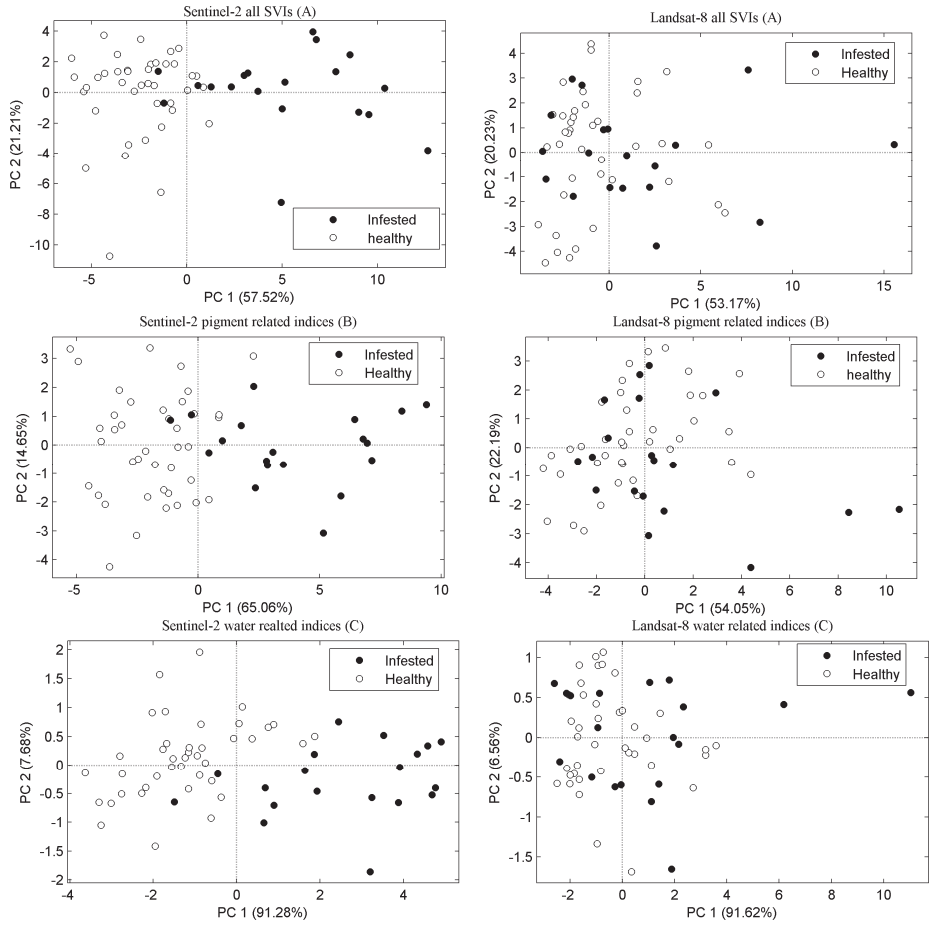

Figure 5. 7: Cluster plots based on the first two PCs: (A) Cluster plots based on all spectral indices including raw spectral bands (B) Cluster plots based on pigment indices and (C) cluster plots based on water-related indices.

5.3.4 Mapping bark beetle green attack and validation

To determine the importance of each of the SVIs when mapping bark beetle green attack, selection probability (SP) values were obtained from the RF algorithm. A total of 8 out of 24 indices shown in Figure 5.8 for Landsat-8 indicated a higher SP (> 0.5), whereas 17 of 35 SVIs were recorded with an SP value of > 0.5 for Sentinel-2 (Fig. 5.8).

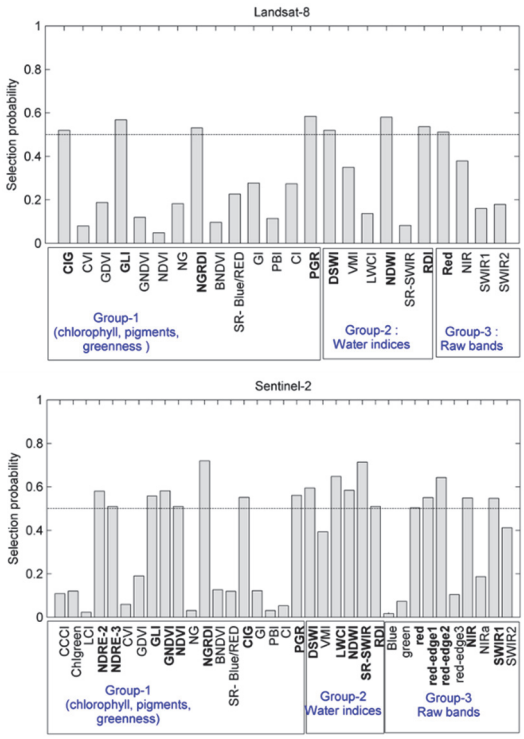

Figure 5. 8: Selection probability value of SVIs obtained from PLS-DA Random frog algorithm.

Moreover, higher variation and wider threshold values were observed between these two sample groups (healthy and infested) using the SVIs considered in this study for the Sentinel-2 data than for Landsat-8 (see Fig. 5.9). Likewise, using raw spectral bands from Sentinel-2 indicates that red, red-edge1-3, NIR and SWIR bands exhibited SP values of > 0.5. In contrast, the Landsat-8 red band had an SP value > 0.5. From Sentinel-2 data, the indices selected to generate a final infestation map included NDRE- 2, NDRE-3, GLI, GNDVI, NDVI, NGRDI, CIG, PGR, DSWI, LWCI, NDWI, SR-SWIR, RDI, red, red-edge1&2, NIR and SWIR1. However, from Landsat-8 data only CIG, GLI, NGRDI, PGR, DSWI, NDWI, DRI, and red were selected.

Based on the defined threshold value, infestation maps were generated using the Landsat-8 and Sentinel-2 SVIs data. These maps were then overlaid with ground truth reference data to calculate matched and mismatched pixels. Figure 5.10 depicts those areas (pixels) correctly matched with ground truth data (aerial photography), as well as pixels that have been falsely identified from SVIs as green attacked areas. As can be seen from Table 5.4, the number of correctly matched pixels with reference infestation data (visual interpretation of aerial photography) was higher for Sentinel-2 (67 %) than

for Landsat-8 (36 %) SVI data. Similarly, the number of falsely identified pixels (mismatched pixels) that indicated green attack using SVIs was lower for Sentinel-2 (177 pixels) than for Landsat-8 (391 pixels).

Table 5. 4: Assessment of the generated maps from Landsat-8 and Sentinel-2 SVIs using the reference data obtained from Aerial photography.

Identified pixels as green attack from (SVIs)	**Reference pixels (Aerial photography)**	**Pixels correctly matched**	**Mismatched pixels**	**Error**
Landsat-8 (612 pixels)	417 (30 m)	221 (36%)	391	64%
Sentinel-2 (539)	687 (20 m)	362 (67%)	177	33%

* The error was calculated by dividing the total number of correctly matched pixels by the total number of ground truth pixels.

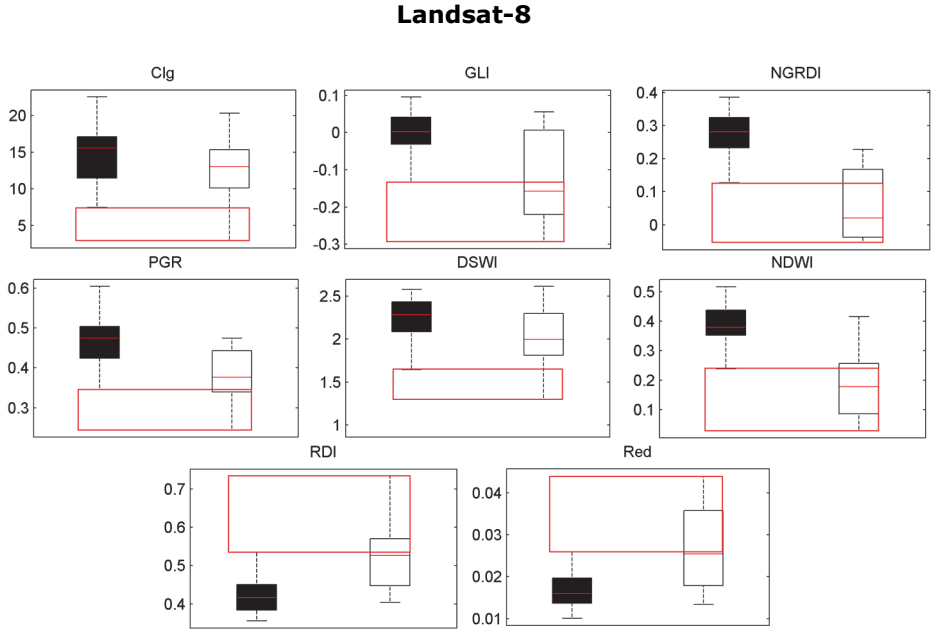

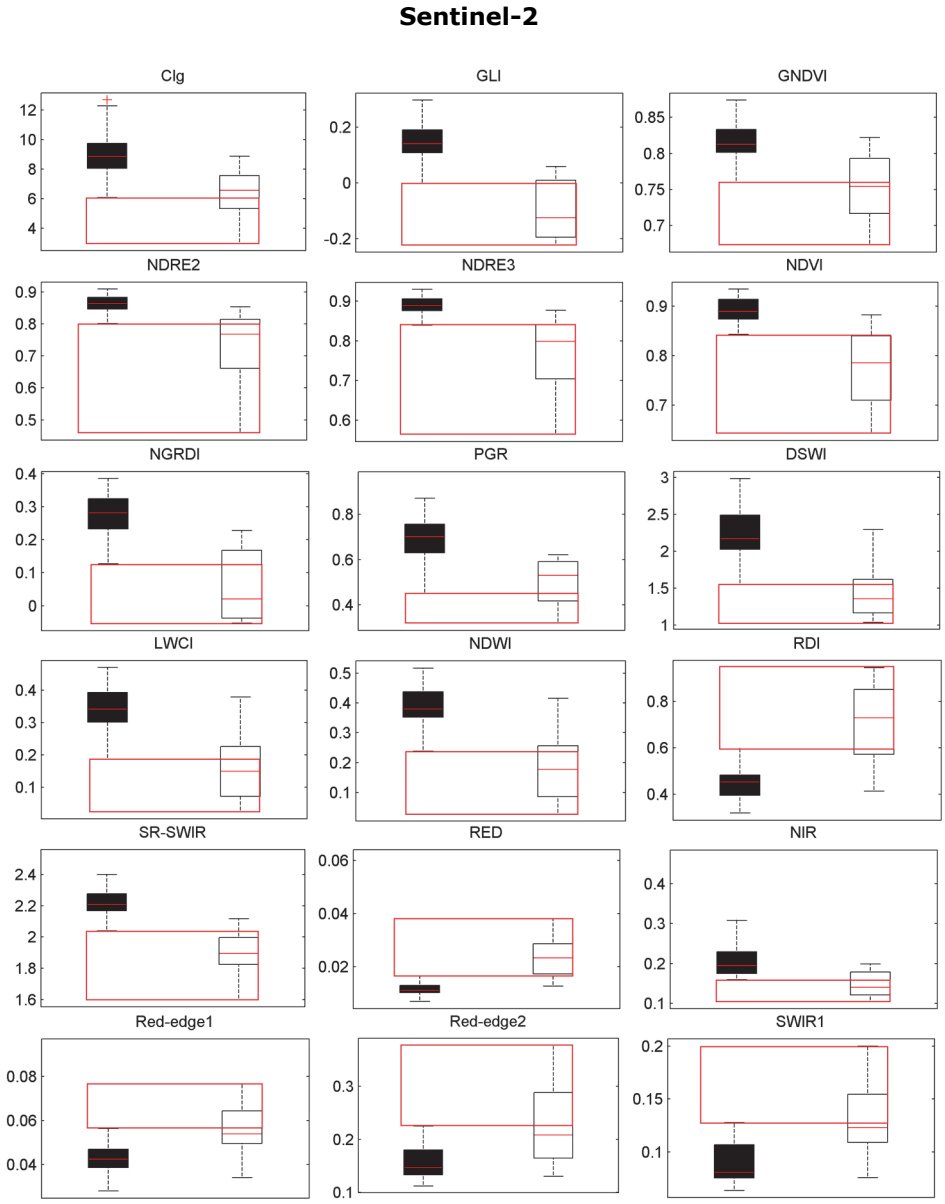

Figure 5. 9: The box plot shows the variation in SVI values calculated from Landsat-8 and Sentinel-2, between healthy and infested plots. The black and hollow boxes represent healthy and infested plots, respectively. The red box shows the selected threshold value of each SVI where there is no overlap between the two sample groups (healthy and infested)

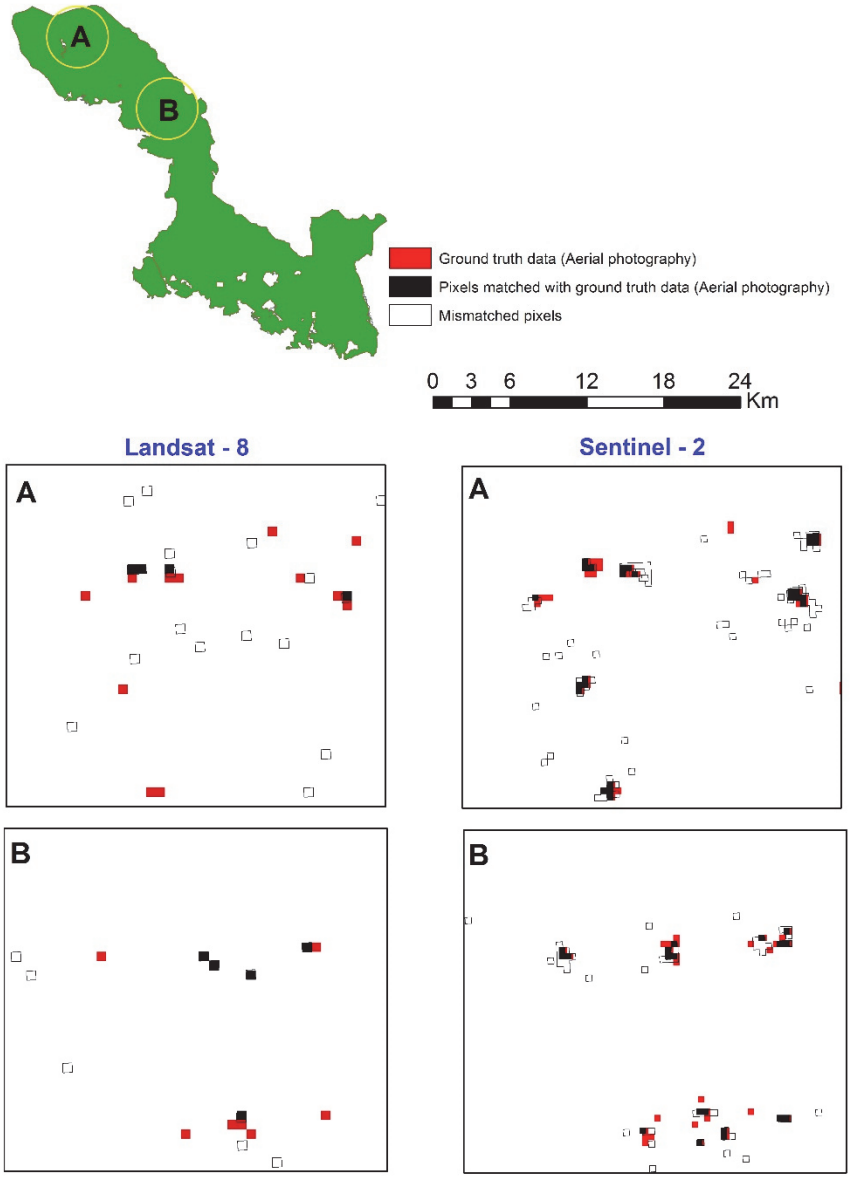

Figure 5. 10: Map showing the spruce cover under green attack stress in the Bavarian Forest National Park in July 2016 based on spectral vegetation indices from Landsat-8 and Sentinel-2 selected through the Random frog algorithm.

5.4 Discussion

Spectral vegetation indices (SVIs) calculated from Sentinel-2 have a high potential for mapping and detecting changes induced by bark beetle green attack, particularly the red-edge and water-related indices. These changes were only partly detectable by Landsat-8 due to the lower spectral and spatial

resolution of the OLI sensor. A greater number of pixels identifying green attack from Sentinel-2 SVIs matched with ground truth data (362 out of 539 pixels), whereas Landsat-8 only matched 221 pixels (out of the 612) with ground truth infestation data. Furthermore, leaf-level comparisons between healthy and green-attacked foliar samples revealed that all leaf traits considered in this study were significantly different ($p < 0.05$), particularly for chlorophyll and water content. The reduction of chlorophyll and water content in the infested trees caused changes in the foliar spectral measurements at NIR and SWIR wavelengths.

In our study, the stand characteristics between the healthy and infested plots were not significantly different (not shown). This is in line with earlier studies that found stand characteristics do not play a major role in infestation during an outbreak condition. In an epidemic level of bark beetle infestation all trees with different conditions (healthy and stressed) and different stand characteristics (large or small diameter) were under threat of this insect (Wermelinge, 2004; Lausch et al., 2011; Allain et al., 2011). However, it is important to not that in our study, DBH with the p-value of < 0.06 was narrowly exceeding the threshold of 0.05, which probably indicate that this variable may play a role in attracting the beetles. Previous findings by Hart et al. (2015) and Six and Skov (2009) indicate that DBH played a major role in the endemic level of bark beetle infestation.

A common observation in this study was that of the 19 pigment-related SVIs (group-1) calculated from Sentinel-2 imagery, eight (i.e., GLI, NDVI, GNDVI, CIG, PGR, NGRDI, and both red-edge-related indices (NDRE-2 and 3)) were most important having an SP value of < 0.5 (Fig. 5.8). When only using VNIR bands from Landsat-8, CIG, GLI, NGRDI, and PGR have the potential to differentiate between healthy and infested sample plots. The underlying reasons may relate to the existing dissimilarities in spectral and spatial resolution between these two sensors (Mandanici and Bitelli, 2016). For example, Landsat-8 has only one spectral band (30 m) in the near-infrared region, while Sentinel-2 has a series of spectral bands (20 m) in the near-infrared region (B5, B6, B7, and B8a). Furthermore, the availability of the three red-edge bands is a unique feature that distinguishes Sentinel-2 from Landsat-8. In our study, the indices developed from the red-edge bands (705–783 nm) of Sentinel-2 (NRED2 and 3) showed the highest sensitivity to bark beetle green attack, and a larger threshold was identified between healthy and infested samples for these two indices (Fig. 5.8). This result is consistent with results from previous studies (Eitel et al., 2011; Krofcheck et al., 2014; Lottering et al., 2016; Modzelewska et al., 2017), indicating that NDRE calculated from RapidEye and WorldView-2 has the capacity to detect forest stress induced by drought and insect infestation in the early phase.

Interestingly, the spectral indices using the blue band (CI, SR-BLUE/RED and BNDVI) were unable to discriminate trees stressed by bark beetle green attack for both Landsat-8 and Sentinel-2 (Fig. 5.8). This is due to the reflectance of these sensors in the blue region of the spectrum being insufficient to detect spectral variation caused by bark beetle green attack. This result confirmed earlier findings by Arellano et al. (2015), who revealed that the blue range indices calculated from Hyperion images were unable to detect forest areas polluted by hydrocarbon in the Amazon rainforest.

On the other hand, the indices calculated from a combination of SWIR and NIR or VIS bands (water-related indices) performed well for both Sentinel-2 and Landsat-8 imagery. For example, Figure 5.9 suggests that the indices DSWI, NDWI, RDI, SR-SWIR, and LWCI successfully differentiated healthy from green attacked plots using Sentinel-2. Due to the significantly lower water content and higher leaf dry matter content ($p < 0.05$) of infested samples, their spectral reflectance responded more profoundly in the SWIR region at both leaf and canopy level than the reflectance of healthy samples did (Figure 3) (Ali et al., 2016; Wang et al., 2011). This is because a reduction in leaf water content is responsible for changes in SWIR reflectance (Bowman, 1989). This is also demonstrated in Figures 5.4 and 5.5 (A and B), where distinctively higher reflectance in the SWIR region was observed for the infested samples at both leaf and canopy level. This is consistent with the study by Immitzer et al. (2016), which highlighted the importance of the SWIR in Sentinel-2 data for mapping different forest classes. Similar results have been reported for wavelengths in the NIR and SWIR regions, which are sensitive to forest disturbance caused by insect attacks. Foster et al. (2017) found that the SWIR region from hyperspectral measurements collected from ASD FieldSpec Pro was key to the detection of bark beetle (Dendroctonus rufipennis) green attack in Engelmann spruce (Picea engelmannii).

The sensitivity of SWIR bands to variation in leaf water content is due to its reflective nature, allowing it to bounce off objects while remaining invisible to the human eye. This feature of the SWIR region makes variation in leaf water content easily recognisable. Furthermore, it should be noted that not only the SWIR region is sensitive to variation in leaf water content, but that the thermal infrared region may also provide sufficient information in this regard. Landsat-8 has two spectral bands in the thermal infrared region (10.60 – 12.51 nm). Further research would, therefore, be useful to assess whether information from the thermal region can provide sufficient information for mapping bark beetle green attack.

Furthermore, the results of PCA analysis revealed that the method using different SVI groups (pigment or water-related indices) did not improve discrimination between healthy and infested sample plots when using Sentinel-

2 data (Fig. 5.7). However, with Landsat-8 data, the performance of the PCA model decreased when SVIs groups were used separately. This reduction in PCA performance was expected due to the spectral variation of infested plots not being efficiently detected by Landsat-8 images (see Fig. 5.5 (A and B)).

It should also be noted that 177 and 391 pixels indicating green attack based on Sentinel-2 and Landsat-8 data, respectively, were mismatched with the ground truth data (Table 5.4). To better understand this discrepancy, we studied the infestation data (obtained from visual interpretation of aerial photography) of the previous years, 2014 and 2015, acquired from the Bavarian Forest National Park administration. This allowed us to check whether mismatched pixels are indicating green attack corresponded with previous infestations in 2014 and 2015. To accomplish this, a similar process (as explained in Section 2.5) was applied to 2014 and 2015 infestation data and then overlaid on the mismatched pixels. As can be seen from Table 4, the results revealed that, for Sentinel-2, 12 and 57 pixels (out of the 177 mismatched pixels) matched with the infestation data of the years 2014 and 2015, respectively. While for Landsat-8 data, only 11 and 31pixels matched with infestation data for the years 2014 and 2015, respectively (Table 5.5). This highlights the sensitivity of SVIs calculated from Sentinel-2 for detecting canopies that are stressed by bark beetle green attack. It is important to note that all the pixels that were identified as a green attack, using both sensors considered in this study, were within 500 meters of the previous year's infestation when analysed using a 500-metre buffer zone around these data (not shown). Hence, we could identify the previous years' infestations, which were now at the grey attack stage.

Table 5. 5: Assessment of the mismatched pixels from Landsat-8 and Sentinel-2 SVIs using previous years' (2014 and 2015) infestation data (obtained from Aerial photography).

Mismatched pixels as green attack from (SVIs)	**Pixels correctly matched with infestation data (2014)**	**Pixels correctly matched with infestation data (2015)**
Landsat-8 (391 pixels)	11	31
Sentinel-2 (177 pixels)	12	57

5.5 Conclusion

The spectral indices derived from Sentinel-2 data performed well at detecting changes in the leaf biochemical properties (reduction in chlorophyll, increase in leaf dry matter content and decrease in water leaf water content) and their relation to canopy reflectance. The simulated Sentinel's data also showed good accordance with measured leaf reflectance using an ASD spectrometer as well as a superior response to changes in leaf biochemical properties over the whole wavelength region, as almost all utilised SVIs performed well for detecting bark

beetle green attack. Although the total number of pixels matched with ground truth data (362 pixels, 67%) obtained from the Sentinel-2 may not be high enough for operational forestry practice and management purposes, it is a promising technique for alerting to bark beetle green attacks. It can aid the detection of bark beetle infestations in a timely manner over large areas and thus form the basis for accurate and efficient bark beetle monitoring. It is possible that another type of remote sensing data with a higher resolution (such as from an Unmanned Airborne Vehicle) may provide a better result detecting bark beetle green attack. As early detection of infestations is essential for the successful control of an outbreak (Fahse and Heurich, 2011), further research applying different approaches using Sentinel-2 imagery should be undertaken with principal component analysis (PCA) and partial least square discriminate analysis (PLS-DA) from this study to check the stability and accuracy of the threshold values identified over a period of time.

Chapter 6 Synthesis: Remote sensing of European spruce (*Ips typographus*, L.) bark beetle green attack

6.1 Introduction

During the last three decades, there have been massive and increasing numbers of severe European spruce *Ips typographus*, L. bark beetle outbreaks in the coniferous forests in central Europe. These have resulted in significant ecological changes in terms of forest structure, the composition of wildlife habitats and degradation of large areas within existing forests (Christiansen and Bakke, 1988b; Fahse and Heurich, 2011; Raffa et al., 2008; Seidl et al., 2011; Seidl et al., 2014). In other words, the bark beetle count is an agent of stress and change in forest structure and function and has an effect on the ecosystem both directly and indirectly. The direct impact of the bark beetle on the ecosystem includes increasing tree mortality rates, changing forest stand density and altering the forest microclimate by reducing the forest canopy layer, which can increase the amount of sunlight to the forest floor (Beudert et al., 2015; Kurz et al., 2008; Lehnert et al., 2013; Lindenmayer and Franklin, 2002; Mikkelson et al., 2013).To control or preclude a mass outbreak and minimise the economic loss in the forest industry, early detection of a bark beetle infestation is an essential step. Detection of a bark beetle infestation at the green attack stage means locating infested trees when the beetle larvae are still confined within the tree. In this respect, remote sensing is a cost-effective and repetitive technique which is an optimal approach to monitor and assess forest stress in comparison to the more traditional (field survey) approach, which is not practical and is actually inefficient in large areas because it is significantly laborious and costly. Therefore, the current thesis has studied the utility of different types of remote sensing data obtained from a variety of sensors, including ASD FieldSpec3 and multispectral satellites (RapidEye, SPOT-5, Sentinel-2 and Landsat-8) for early detection of bark beetle infestation at both the leaf and canopy levels. Furthermore, this study provided an important opportunity to advance the understanding the impact of early bark beetle infestation on the biochemical properties of the infested trees (chlorophyll, nitrogen, chlorophyll fluoresces, leaf water content, dry matter content and stomatal conductance) (Fig. 6.1).

The results of the study have been presented and published in four scientific articles which form the main four chapters of this thesis (Chapter 2-5). While the general introduction to the bark beetle infestation, aim and objectives of the study are presented in Chapter one. In Chapter 2, foliar biochemical (chlorophyll and nitrogen concentration) and spectral reflectance properties (400–2000 nm) obtained from an ASD FieldSpec3 equipped with an integrating sphere were used to study the impact of bark beetle green attack on the needles of the infested spruce trees. Subsequently, in Chapter 3, temporal high-resolution satellite data from RapidEye and SPOT-5, parallel with field measurements of leaf properties , were used to understand and explore the dynamics of leaf traits and canopy reflectance of Norway spruce during the

early to advanced stage of bark beetle attack (green to red attack) (*Ips typographus*, L.). Leaf spectral measurements together with leaf traits (nitrogen, chlorophyll, chlorophyll fluorescence, water content and stomatal conductance) were studied from three repeated sequential measurements. In Chapter 4, the utility of thermal (TIR) and visible-short wave infrared (VIS-SWIR) data was evaluated to detect the temporal variations of the canopy due to bark beetle infestation and to study thermal sensitive foliar properties (i.e. stomatal conductance, chlorophyll fluorescence and water content). In Chapter 5, the potential of data from two freely available satellites—Sentinel-2 and Landsat-8—were compared to detect and map bark beetle infestation at the early stage with the use of field measured data (foliar reflectance and biochemical properties).

Finally, this chapter (Chapter six) synthesises the main results and provides a summary of the main findings. The chapter further discusses the practical relevance of using remote sensing data for detection of bark beetle green attack.

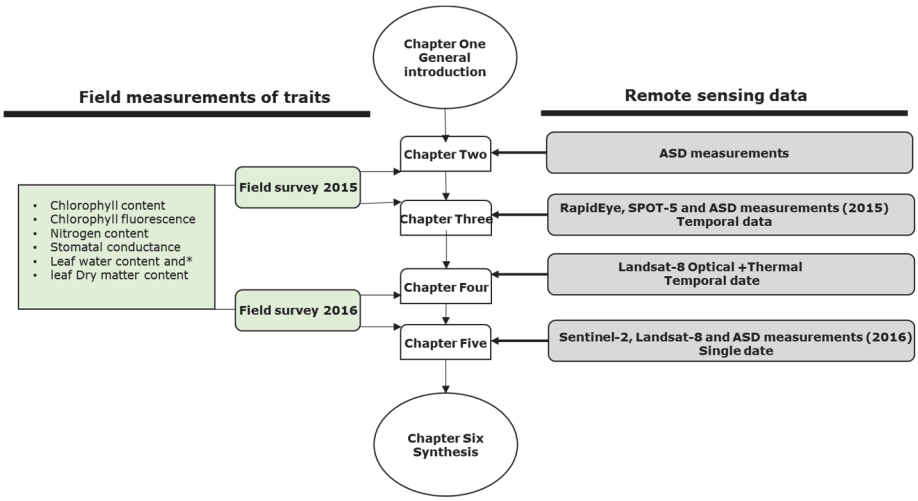

Figure 6. 1: Research framework and logical established links between chapters and utilised data.

6.2 Effects of bark beetle green attack on foliar reflectance and biochemical properties

Very few spectroscopic data are available for Norway spruce trees attacked by the European bark beetle at the leaf level, despite such data being highly beneficial for detecting pre-visual stress. Hence, we examined the potential of hyperspectral measurements (400–2,200 nm) from an ASD FieldSpec3 equipped with an integrating sphere to detect possible changes in foliar reflectance induced by bark beetle infestation.

The results of this study revealed that the mean reflectance spectra of attacked green foliage were statistically different ($p < 0.05$) compared to healthy foliage for 917 wavebands out of the 1600 wavebands considered in this study from 400–2200 nm. The findings demonstrated that the infestation of bark beetle at the green attack stage reduced the concentration of chlorophyll and nitrogen within the infested foliage. Previously, it was shown by Ahern (1988b) that the most promising spectral bands for the detection of mountain pine beetle green attack at the leaf level were located near the red edge of the spectrum. In addition, the results of variable importance in projection (VIP) obtained from partial least squares regression (PLSR) revealed that the wavelength range between 730 and 790 nm (red-edge) is the most informative spectral area affected by the European spruce bark beetle, and more pronounced in regards to chlorophyll variation between healthy and infested foliage (Fig 6.2).

Our results further demonstrated that the reflectance at NIR and SWIR regions (730–1,370 nm) was distinctively lower for the green attacked foliage than the healthy ones. This phenomenon is mostly due to the deficit in water content observed in infested trees, leading to a degeneration of the internal leaf structure at the cellular level (Slaton et al., 2001b; Zhang et al., 2012a).

The research also found that the infestation of the bark beetle at the green attack stage affected the estimation accuracy of foliar chlorophyll and nitrogen concentration using hyperspectral measurements and the accuracy decreased when the tree was infested by a bark beetle green attack. This was confirmed from the results of PLSR (Fig. 6.3). Accordingly, the study concluded that the retrieval of biochemical properties from hyperspectral measurements may be used as an indicator for efficient landscape-wide detection of a bark beetle green attack. It is, however, important to note that retrieval accuracies for the total chlorophyll and foliar nitrogen concentrations at the leaf level would probably be different from those at the canopy level because of structural and external factors, such as illumination and atmospheric conditions, that may affect the reflectance spectra at the canopy level (Ollinger, 2011; Wang, 2016).

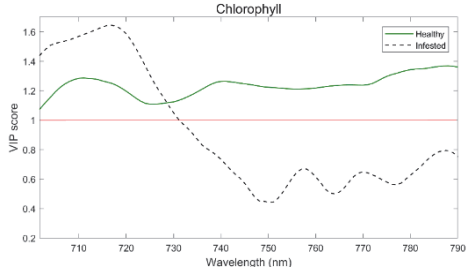

Figure 6. 2: Importance of wavelengths corresponding to the highest value of variable importance in the projection scores of partial least squares regression in healthy and infested samples.

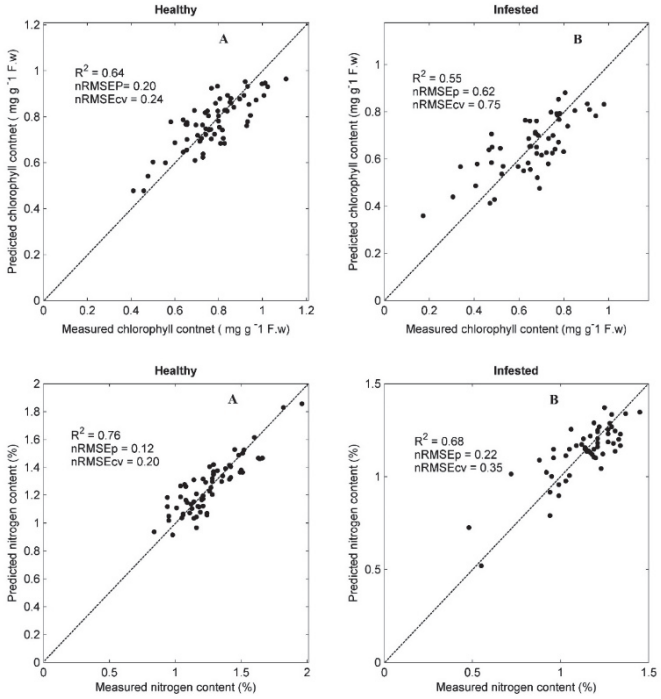

Figure 6. 3: Measured versus predicted foliar chlorophyll and nitrogen concentration for healthy (a) and infested (b) samples derived from the PLSR analysis.

6.3 Understanding dynamic changes of Norway spruce trees at both leaf and canopy level under bark beetle infestation during green to red attack stage

Continuous monitoring is essential for investigating and understanding the dynamic characteristics of leaf traits and canopy reflectance experiencing a bark beetle infestation, in order to provide possible information about changes in the infested forests at the early stage of the attack and instigate possible management interventions. Therefore, the dynamics of leaf and canopy reflectance of Norway spruce trees under bark beetle *Ips typographus*, L infestation was investigated for the first time.

Chapter 3 in this thesis discussed the potential use of two high-resolution satellites from RapidEye and SPOT-5 for the detection of a bark beetle infestation and monitoring possible changes in infested trees. *In situ* measurements of chlorophyll, chlorophyll fluoresces, nitrogen content, leaf water content and stomatal conductance were obtained for three consecutive

repeated time measurements during a field campaign in 2015, concomitant with the timing of image acquisition.

The findings showed that the variation between healthy and infested trees was increased with the progression of infestation for all studied leaf traits (particularly for stomatal conductance and chlorophyll fluorescence). Stomatal closure is the first stress-induced physiological response of infested trees in order to preserve water. These findings confirm results in section 6.4 which showed that canopy surface temperature (CST) affected by a bark beetle infestation is higher compared to the healthy situation. One observed result is an increase in leaf and canopy temperature due to a decline in transpiration cooling.

The spectral regions selected for differentiating and monitoring spectral changes induced by bark beetle infestation were the red edge and SWIR bands from RapidEye and SPOT-5, respectively. These two spectral regions outperformed other spectral regions in detecting early bark beetle infestation from June to July 2015 (Fig. 6.4). Similar results were observed at the leaf level (section 6.2), for these same two spectral regions. Furthermore, we found that the spectral vegetation indices calculated from the red edge and SWIR spectral bands, such as NDRE, DSWI, NDWI and LWCI, were the most sensitive indices that differentiated healthy from infested sites (Fig. 6.4).

This study concluded that red-edge and SWIR spectral bands of the multispectral satellites can significantly improve the monitoring and detection of forest stress under red attack, with subsequent important implications for European bark beetle management and future studies.

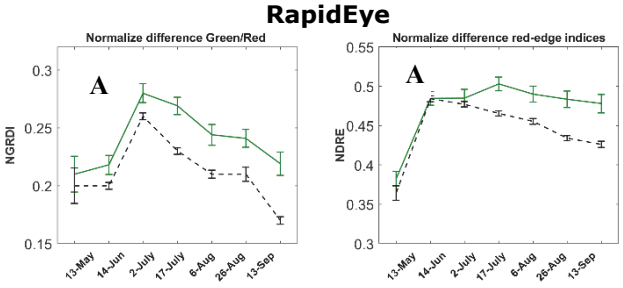

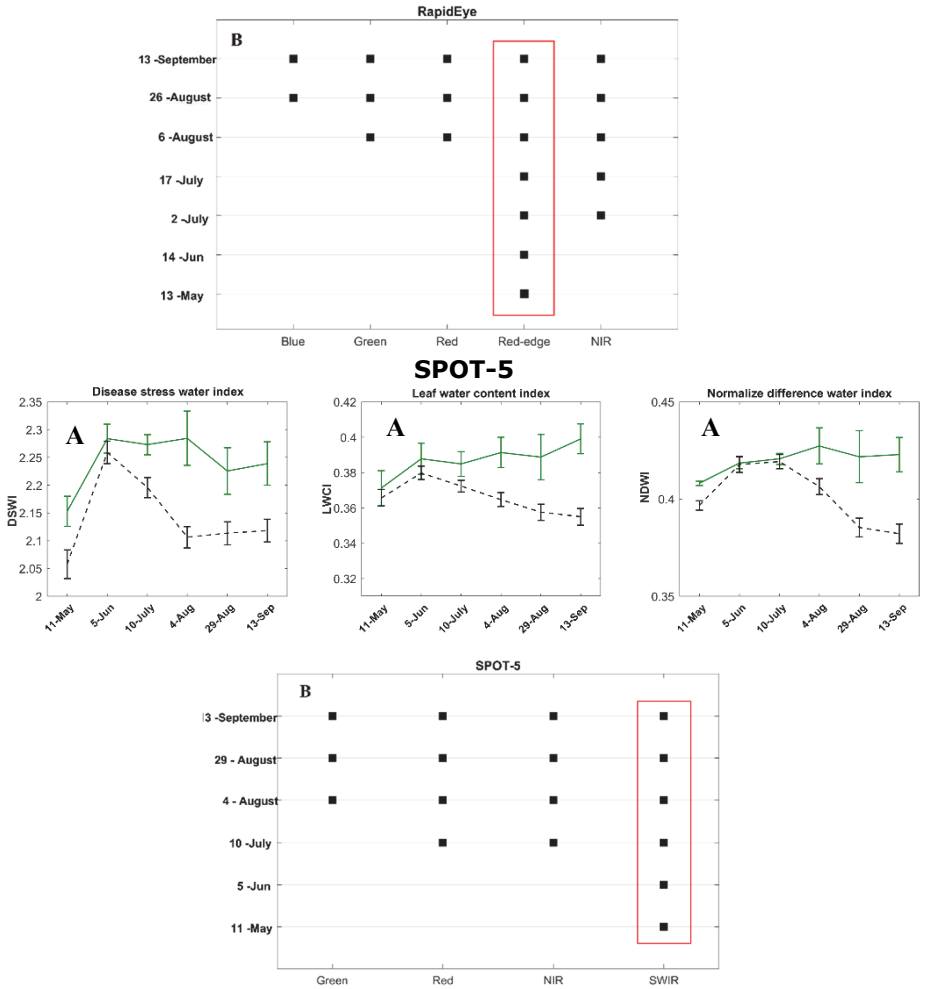

Figure 6. 4: (A) Temporal variation of studied spectral vegetation indices for healthy and infested plots in the Bavarian Forest National Park using RapidEye and SPOT-5 satellite data. Green and black lines represent healthy and infested plots, respectively; (B) Unpaired t-test of canopy reflectance between healthy and infested samples. Dark squares indicate spectral wavebands that were significantly different ($P \leq 0.05$). The red box shows the spectral region that was significantly different overall temporal data considered in this study.

6.4 Sensitivity of Landsat-8 OLI and TIRS Data to Foliar Properties of Early Stage Bark Beetle (Ips typographus, L.) Infestation

Several studies have shown that TIR data have significant potential for detecting plant diseases and pathogens at a stage before the plants exhibit visual signs (Aldea et al., 2005; Moller et al., 2007; Ni et al., 2015; Oerke et

al., 2006; Xu et al., 2006). In this respect, Chapter 3 sought to explore and compare the potential of both optical and thermal infrared (TIR) data for the detection of pre-visual symptoms induced by a bark beetle green attack. Three Landsat-8 images from May, July and August 2016 were studied, representing early, advanced, and post-infestation stages, respectively.

These results showed that CST calculated from TIR data was superior to the spectral vegetation indices obtained from optical bands for detecting subtle canopy changes due to a bark beetle infestation for the three months studied (Fig. 6.5). In addition, a strong correlation between CST with leaf water content, chlorophyll fluoresces and stomatal conductance was observed in the healthy leaves (r = –0.46, –0.55 and –0.48, respectively), whereas for the green attacked leaves, they were r = 0.05, –0.15 and –0.25, respectively (Fig. 6.6). CST was found to be an important variable for estimating measured leaf traits (VIP > 1) and improving the differentiation between healthy and green attacked sites when used with other SVIs. Accordingly, TIR may prove to be a considerably useful indicator in this context. This study concludes that the early stress induced by a bark beetle infestation is more effectively represented by data obtained from TIR compared to optical sources. This could have positive implications for future forest practice.

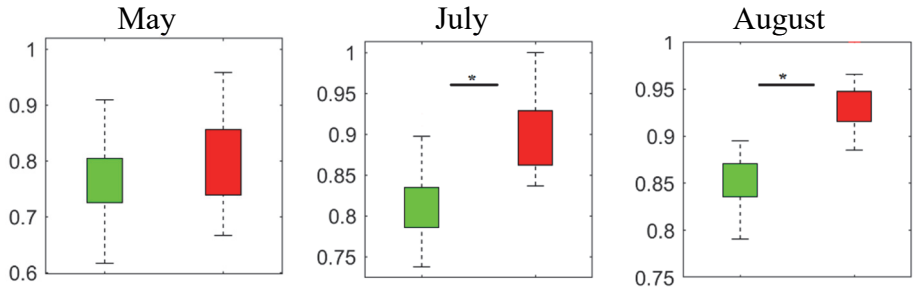

Figure 6. 5: Temporal variation of CST for healthy and green attacked sample plots in the Bavarian Forest National Park. Green and red boxes represent healthy and infested plots, respectively. A * indicates the significant difference between healthy and infested plots, respectively. A * indicates the significant difference between healthy and infested plots obtained using Student t-tests, and a blue o indicates an outlier.

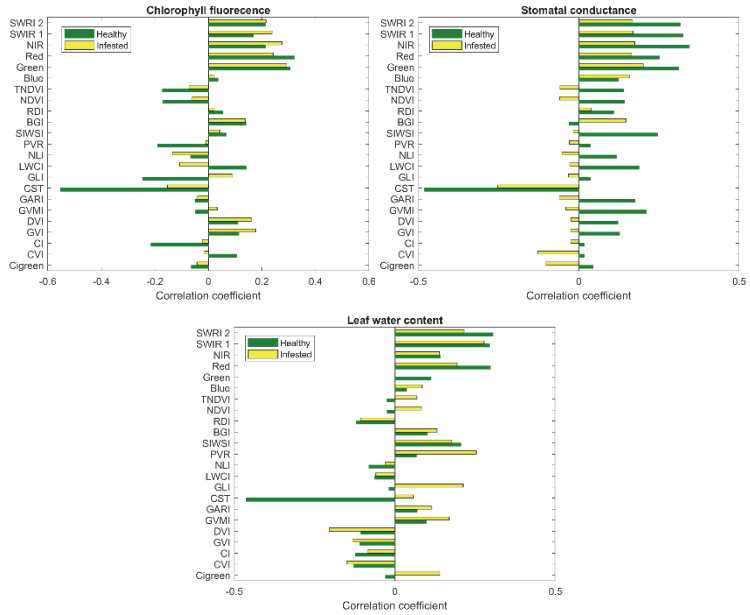

Figure 6. 6: Correlation between studied leaf traits (chlorophyll fluorescence, leaf water content, and stomatal conductance) and SVIs, in the Bavarian Forest National Park, July 2016.

6.5 Detection and mapping bark beetle green attack using spectral vegetation indices from Landsat-8 and Sentinel-2 data

Detecting and mapping *Ips typographus,* L green attack with medium resolution satellite data was addressed in Chapter 5. The potential of spectral vegetation indices from Sentinel-2 and Landsat-8 alongside field data measurements to detect a bark beetle green attack was investigated. Furthermore, the variation in reflectance spectra between healthy and infested plots was determined at the leaf and canopy level.

The research revealed that the spectral vegetation indices from Sentinel-2 satellite data have a strong potential to map and detect a bark beetle infestation at its earliest stage. Moreover, the results showed that the difference between the mean reflectance of healthy and infested foliage is most substantial in the VIS region between 520 and 685 nm, the NIR (740–1,130 nm) and the shortwave infrared region (1,420–1,850 nm and 2,000–2,200 nm). Similar results have been observed at the canopy level for the Sentinel-2 data when compared with interpolated field ASD spectrometer at the leaf level, particularly in the NIR and SWIR infrared regions, while for the Landsat-8, this variation was not detected at the canopy level (Fig. 6.7). Moreover, a good agreement exists between canopy reflectance and leaf spectra

(interpolated to Sentinel-2 spectral bands); in particular, for the red-edge and SWIR wavebands, the correlation was r = 0.50 to 0.61 ($p < 0.05$), while weaker correlations were observed between the canopy and interpolated leaf spectra for Landsat-8 image data for both healthy and infested plots (Fig. 6.7).

The spectral bands selected as the best combination of the vegetation indices for detecting and mapping bark beetle green attack were found in the red-edge and SWIR bands in Sentinel-2, including NDRE2-3, SR-SWIR, NDWI, DSWI and LWCI. This confirmed our earlier research, described in section 6.3, which studied the temporal dynamics of canopy reflectance under a bark beetle green attack and revealed that both red-edge and SIWR bands were the most informative in terms of maintaining their sensitivity for monitoring and detecting a bark beetle infestation from early to advanced stages of infestation (Fig. 6.4). An increased numbers of pixels, identified as a green attack from Sentinel-2 SVIs, were matched with ground truth data (67%), while for Landsat-8 (36%), they were matched with ground truth infestation data. This result confirmed that the spectral vegetation indices calculated from Sentinel-2 spectral bands performed better in differentiating between healthy and infested plots compared to Landsat-8 SVIs.

The study concluded that both red-edge and SIWR regions have the potential to provide valuable information about infested areas and can produce a reliable map of which areas in a forest are affected by a bark beetle green attack.

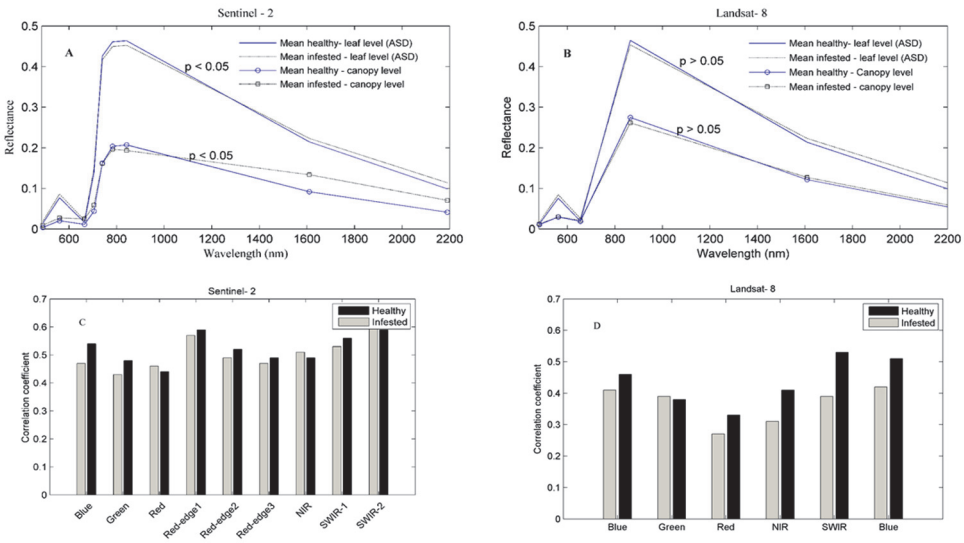

Figure 6. 7: foliar and canopy reflectance using (A) Sentinel-2 data (B) Landsat-8 data (C & D) correlation between canopy reflectance and foliar spectra (interpolated from Field ASD spectrometer to Sentinel-2 and Landsat-8 spectral bands) for both healthy and infested plots.

6.6 Practical relevance

This study contributes to applied research on the field of remote sensing of bark beetle green attack. The findings and methods applied in this work have the potential to produce useful information about bark beetle infestation at an early stage of the attack.

The results confirmed that it is possible to detect the stress induced by the bark beetle at an early stage, and prior information derived from field measurements can significantly improve this process through remote sensing data and approaches. This will facilitate regular monitoring of bark beetle infestation in conifer forests. However, the key issue is how the findings obtained by this research and reported in this thesis can be used for detecting bark beetle infestation. In other words, how, when and which spectral regions are capable of using driven information from space to detect a bark beetle green attack. We can conclude that in the remotely sensed survey of green attacked Norway spruce trees affected by the bark beetle, that high-quality observation in space, time and spectral characteristics are required, to make this survey useful in a management context, as outlined in the following points:

Spectral information: Norway spruce trees impacted by the European spruce bark beetle exhibits stress symptoms in a gradual process. Therefore, it is necessary to use remote sensors which can record and collect information over all portions of the electromagnetic spectrum (visible, near infrared-shortwave infrared and thermal infrared). At the beginning of a bark beetle infestation, the most common initial response is the closure of plant stomata to preserve water content. Therefore, it may not be possible to detect such changes and physiological stress using the visible portion (400–700 nm) of the electromagnetic spectrum. In contrast, satellites such as Landsat-8 and Sentinel-2 with the capabilities to further capture information in near, shortwave and thermal infrared regions of the electromagnetic spectrum would be more sensitive to this kind of physiological stress.

Moreover, in remote-sensing studies of bark beetle infestation, spectral characteristics is another important issue and should be considered—results from our study suggest that hyperspectral data are very important in accurately detecting forest stress induced by bark beetle green attack. Hyperspectral data can provide significant improvements in spectral information content and a closer correlation with the biochemical and physiological properties of targeted leaves or canopies when compared with data from broad-bands sensors for detecting plant stress. For example, such data are able to capitalise on both biochemical and structural properties of the target forest area and offer enhancement in detecting subtle changes in tree canopy reflectance due to physiological stress from insects or pathogens. The

hyperspectral data capturing can be performed at the early stages of bark beetle infestation, and hence improve an ability to detect the stress induced by bark beetle at its early stage. This can significantly benefit the control of massive bark beetle outbreaks and minimises economic losses compared to multispectral remote sensing, which can only detect canopy stress when infestations are at their advanced stages and are widespread.

In the optical spectral region, we identified two spectral regions—the red edge and SWIR—as being the most important spectral channels at both the leaf and canopy levels for detecting subtle changes in Norway spruce trees under a bark beetle green attack. Hence, remote sensors such as Sentinel-2, RapidEye, SPOT-5 and the HYpex camera mounted on a UVA with the capacity to collect information over these two spectral regions are providing better opportunities to detect insect-stressed forests.

Temporal information: Because Norway spruce trees infested with European spruce bark beetles do not die immediately, continuous monitoring of forests from remote sensing platforms is critically important for characterising and understanding the temporal response changes of infested trees. Multidate images, within the same months, are preferably collected when the beetles start to swarm during the European springtime. We reported in our studies that employing multi-temporal imagery from RapidEye, SPOT-5, Sentinel-2 and Landsat-8 images are providing valuable information related to the stress induced by bark beetles. We were able to identify for the first time in the European situation (and in contrast to earlier works in the United States) that mid-June to the beginning of July is an appropriate time frame for identifying early stress induced by a bark beetle infestation. It is important to note that our results at the leaf level show that the foliar properties change affectedly within 3-4 weeks from the infestation time. Therefore, it is assumed it believes that using high temporal resolution data (e.g. 3-5 day) may further improve the time frame for early detection of European spruce bark beetle.

Radiometric Resolution: One of the main issue in the study of bark beetle green attack when using remote-sensing data is the intra-class variability of the reflectance values between healthy and green attacked trees, an issue which is hampering the separability of infested and healthy classes. In this case, the radiometric resolution of remotely sensed data plays an important role. Radiometric resolution describes the actual information content in an image and offers the ability to discriminate very slight differences in energy. Therefore, the finer the radiometric resolution, the more sensitive it is to detect small differences in reflected data over different objectives on the ground. However, it is important to note that the radiometric resolution itself is insufficient for detecting such differences. For example, Sentinel-2 and Landsat-8 both have a radiometric resolution of 12-bits; however, in our study,

we showed that the potential of Sentinel-2 is higher than Landsat-8 imagery for determining subtle canopy changes induced by bark beetle due to the higher spectral and spatial resolution of Sentinel-2 data.

Spatial information: spatial resolution is a key issue in remote sensing studies of a bark beetle green attack. Different remote sensing instruments capture and collect data at different levels of scale and resolution: the higher spatial resolution may outperform lower-resolution for bark beetle green attack detection. This is especially true when they combine with high spectral and radiometric resolution data. In other words, the combination of high spectral, spatial, temporal and radiometric resolution can provide valuable information regarding bark beetle green attack detection.

Moreover, It should be noted that the importance of high spatial resolution data is increased when the bark beetle infestation occurs at an endemic level (non-outbreak). In that case, the majority of the infested trees will be within small isolated patches. Therefore, a higher spatial resolution is required because it is more appropriate for small patch detection. However, when the infestation is at an epidemic (outbreak) level, as was reported earlier in previous chapters (5), larger clusters of trees are infested; in this case, there is a possibility to detect the subtle spectral differences caused by a bark beetle green attack using moderate-resolution imagery.

6.7 The relative importance of ground-based measurements for bark beetle green attack detection

During the past decades, fundamental research has been conducted on the applicability of satellite remote sensing observations for forest parameter estimation using extensive field data measurements. The results and findings of these studies have been used in extensive calibration/validation experiments and technological innovation, to propose and develop upcoming satellite missions (i.e., Sentinels, EnMap, CHIME and HyspIRI).

In general, the purpose in ground-based measurements is to aid the calibration and interpretation of remotely sensed data. However, in the field of bark beetle infestation, ground-based measurements can provide even more contextual information to obtain high accuracy results. An on-site gathering of location and the associated characteristics of the infested tree that properly characterise states, conditions, and parameters associated with the early stage of bark beetle infestation can add value to physical imaging remote sensing observations and possibilities to interlink the canopy stress assessment with bark beetle infestation. In other words, when both *in situ* and remotely sensed data are combined in a complimentary sense, they may provide additional

information in comparison to using a single source (e.g. field data or remote sensing data alone) would be too imprecise.

As described in chapter one, the potential of remotely sensed data to provide stress signal induced by bark beetle infestation depends on the physiological response of trees and biology (lifecycle) of bark beetle. As such, in chapter two, we identified spectral wavebands that are sensitive to variation in chlorophyll and nitrogen concentration due to bark beetle green attack. Moreover, we showed that the most common initial response of bark beetle infestation is the closure of plant stomata to preserve water content. In chapter three we selected the best time frame for bark beetle green attack detection using temporal field measurements and remote sensing data. Moreover, in chapter four and five we demonstrated the potential of multispectral satellite data in detection bark beetle infestation. This information together can be used to; a) produce predictive Models to detect or assess forest health status under bark beetle infestation, and b) to propose or develop new remote sensing sensors to fulfil all requirements for bark beetle green attack detection.

6.8 Implications for commercial forestry and protected area management:

Prevention and suppression of bark beetle outbreaks comprise particularly important applied strategies in commercially managed forests (Wermelinger, 2004). However, in protected areas, management of bark beetle infestation is more complicated. Bark beetles can be viewed as natural renewal agents and therefore an essential part of ecosystems, with the integrity of their protected areas being mandated to guard against human interference. However, if left uncontrolled, bark beetles may move outside park borders, cause damage on commercial forests or private forested areas (McFarlane and Witson, 2008). Similarly, the disturbance caused by bark beetle infestation negatively impacts protected areas' visual beauty and thus potentially on the visitor experience (Müller and Job, 2009; Sheppard and Picard, 2006). Therefore, management strategies for bark beetle infestation in protected areas are always required to maintain a balance between ecological, social and economic demands.

Various bark-beetle-infestation strategies have been adopted. These approaches include salvage logging, and large-scale commercial harvesting of infested stands at the green attack stage before the new brood emerges and migrates (Wermelinger 2004; Wulder et al. 2009). Forest managers need to know the location of green attack trees in order to strategically and operationally allocate resources for mitigation and control. In this regard, our findings can provide useful information for forest management, particularly with respect to the potential of Sentinel-2 data for detecting canopy stress induced by bark beetle infestation at the green attack stage. This strategy will

reduce the various costs involved and facilitate bark beetle survey practice since the data available free of charge.

Moreover, our findings can improve bark beetle management activities by providing useful information regarding how, when and which remote-sensing data could be applied to such survey practice. For example, our findings in Chapter 3 showed that the most appropriate time for European field bark beetle management is between Jun to July (European conditions). Furthermore, the findings of our study in Chapter (2) revealed that biochemical properties (such as chlorophyll, nitrogen and water content) in infested trees are most likely affected during the green attack stage. Typically, chlorophyll, nitrogen and leaf water content have been used by an ecologist to study the interaction between the ecosystem and biological inhabitants; for example, to assess changes in plant health associated with environmental stress and disease (Roumet et al., 2006). Therefore, administrative bodies of forested areas may use such information as an indicator for the efficient landscape-wide detection of bark beetle green attack.

6.9 Future of remote-sensing platforms in monitoring bark beetle infestation: UAV and space-borne hyperspectral satellites

The traditional methods of remote-sensing data for bark beetle infestation still cannot meet the needs of forest management practice due to logistical and technological limitation factors as explained earlier in Chapter (1). As mentioned in section 6.6, in bark beetle green attack analyses, the spectral, spatial and temporal resolutions of remote-sensing platforms play a key role. In the last few decades, airborne hyperspectral sensors have been among the most important platforms providing high-spectral and -spatial resolution data. The data captured by this platform are less affected by atmospheric perturbation. However, airborne hyperspectral sensors are often relatively expensive because of their limited spatial coverage, with multiple flight lines typically being required to cover a study area. Further, a limitation such as; cloud cover and data processing is often complex and can lead to significant error. Similarly, due to technical and practical limitations such as challenging signal-to-noise ratios (SNR) in particular, as well as bottom-of-atmosphere reflectance, sensor cost, data volume and associated data processing costs and time, until now, hyperspectral satellites have been poorly represented in spaceborne missions compared to multispectral ones. Nonetheless, the future of hyperspectral remote sensing is promising, considering forthcoming launches of hyperspectral satellites. There are a number of hyperspectral satellites planned to be launched in the near and distant future. These missions will provide a better opportunity for bark beetle green attack detection (Figure 6.8).

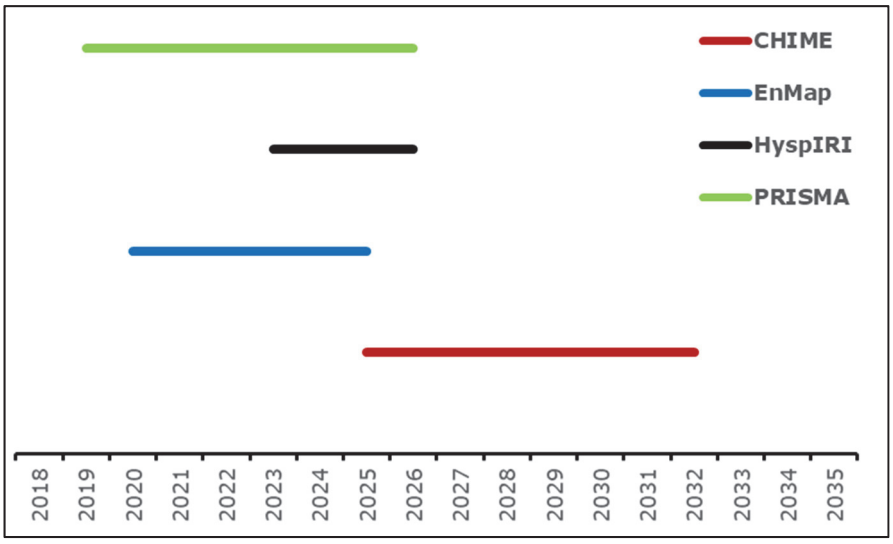

Figure 6. 8: The main planned hyperspectral sensors to be launched in the next five years.

EnMap, CHIME and HyspIRI commissioned hyperspectral sensors providing more imagery alternatives, and their newly developed image processing algorithms offering more analytical tools. Hyperspectral remote sensing is positioned to become one of the core technologies for geospatial research, exploration and monitoring of forest stress and insect infestation. For example, EnMap, CHIME and HyspIRI can all collect data over visible to shortwave infrared wavelengths (400–2,500 nm). This provision is important for the study of bark beetle infestation as we demonstrated the potential of hyperspectral measurement (400–2,500 nm) for detection of *Ips typographus*, L. green attack Chapter (2). Furthermore, the HyspIRI satellite will be the first hyperspectral sensor in space able to provide eight spectral bands in the thermal infrared region from the 3–5- and 8–12-micron regions of the spectrum. These satellites will offer a breakthrough regarding the control, prevention and mitigation of large-scale bark beetle outbreaks. Our study Chapter (4) revealed the importance of thermal bands in detecting canopy stress induced by bark beetle infestation at a very early stage. Similarly, TIR data were found to have a stronger correlation and able to better represent the stress signals from leaf thermal properties (such as leaf water content, stomatal conductance and chlorophyll fluorescence) under bark beetle infestation.

Furthermore, other remote-sensing platforms such as unmanned aerial vehicles (UAVs) as a new means of remote sensing offer significant potential concerning future remote-sensing applications in forest management. Currently, UAVs can collect data at low altitude and provide high-quality data comparable to airborne sensors. The advantages of UAV-collected data include

low cost, high accuracy abundant data, real-time capability and the ability for rapid data acquisition while transmitting image, video and orientation data in real time to ground control stations (Table.6.1).

The UAV technology has developed at a significantly rapid pace, and today, different sensors can be attached to UAVs onboard such as positioning sensors (GPS), inertial navigation sensors (INS), micro-electro-mechanical systems (MEMS), gyroscopes, accelerometers and altitude sensors (AS), all of which allow for the realization of remote sensing missions. Moreover, various sensors such as multispectral, hyperspectral, LIDAR and thermal cameras can be installed onto UAV platforms. As a result, recent data collected by UAVs are widely used for forest management practices.

The current limitation of UAVs is related to their flight time (i.e., limited battery power) and processing time of the imagery. However, there is growing interest in the forest management community in using UAVs as a promising and decision-support tool for forest disturbance studies, including bark beetle infestation management. Soon UAV can potentially fill the gap between satellite/airborne platforms with 'ground truth' data collected using ASD field spectrometers to study detection of bark beetle at the green attack stage.

Table 6. 1: Comparison between UAV and other remote-sensing platforms.

Remote sensing platforms	Swath Width	Altitude	Spatial resolution (per pixel)	Advantages	Disadvantages
Satellite	10-2800 km	600-850 km	1.2 – 1 km	-Clear and stable images -large area within each image -good historical data	-High cost for high spatial resolution images - clouds may hide ground features - fixed schedule - data may not collected at critical times
Airborne	1200-7150 m	500- 3000 m	20 – 150 cm	-Relatively flexible availability - high spatial resolution -changeable sensors	-High cost - Availability depends on weather condition
UAV	20-400 m	10 – 200 m	1-30 cm	-Relatively flexible availability - very high spatial resolution -changeable sensors - Low cost	-Unstable platform can create blurred images -May require certification to operate - Relatively limited in height above ground
Ground-based	< 5 m	< 5 m	0.1 – 1 cm	- Can be used to identify the reflectance properties of an individual leaf and plant .	-Collect the reflectance data from a single point, not creating image.

6.10 Future research Avenues

The results of this thesis outline the potential of using remotely sensed data for the detection of early-stage European spruce bark beetle infestation. In line with field data measurements and employed statistical approaches in this dissertation, further studies could be undertaken along two lines: to examine the retrieval of other foliar properties under bark beetle green attack, and the use of different remotely sensed datasets.

In this study, we revealed that the retrieval of foliar biochemical properties (chlorophyll and nitrogen concentration) from hyperspectral measurements decreases when the trees are under bark beetle infestation, and that other leaf traits (e.g. leaf water content, stomatal conductance and leaf dry matter content) is important equally in the study of bark beetle green attack. Therefore, further research could be undertaken on other vegetation traits in the future.

In Chapter 2, foliar hyperspectral measurements from ASD FieldSpec3 have been applied. However, due to the unavailability of airborne hyperspectral data (at the canopy level) when the field survey was undertaken, optical and TIR data from Sentinel-2, Landsat-8, RapidEye and SPOT-5 were used in next Chapters. Further research is critical for exploring and comparing the utility of airborne hyperspectral data in both optical and TIR domains for early detection of bark beetle green attack. Another possible extension of this study would be with respect to the use of the newly available hyperspectral camera mounted on UAV, and future planned hyperspectral satellite like EnMap, CHIME and HyspIRI these sensors able to record information for red-edge, SWIR infrared and thermal infrared region.

Bibliography

Abdullah, H., Darvishzadeh, R., Skidmore, A.K., Groen, T.A. and Heurich, M., 2018a. European spruce bark beetle (Ips typographus, L.) green attack affects foliar reflectance and biochemical properties. International Journal of Applied Earth Observation and Geoinformation, 64: 199-209.

Abdullah, H., Skidmore, A.K., Darvishzadeh, R., Heurich, M., Pettorelli, N. and Disney, M., 2018b. Sentinel-2 accurately maps green-attack stage of European spruce bark beetle (Ips typographus, L.) compared with Landsat-8. Remote Sensing in Ecology and Conservation.

Adler-Golden, S.M., Matthew, M.W., Bernstein, L.S., Levine, R.Y., Berk, A., Richtsmeier, S.C., Acharya, P.K., Anderson, G.P., Felde, J.W. and Gardner, J., 1999. Atmospheric correction for shortwave spectral imagery based on MODTRAN4, SPIE's International Symposium on Optical Science, Engineering, and Instrumentation. International Society for Optics and Photonics, pp. 61-69.

Ahern, F., 1988a. The effects of bark beetle stress on the foliar spectral reflectance of lodgepole pine. International Journal of Remote Sensing, 9(9): 1451-1468.

Ahern, F.J., 1988b. The effects of bark beetle stress on the foliar spectral reflectance of lodgepole pine. International Journal of Remote Sensing, 9(9): 1451-1468.

Aldakheel, Y. and Danson, F., 1997. Spectral reflectance of dehydrating leaves: measurements and modelling. International journal of remote sensing, 18(17): 3683-3690.

Aldea, M., Hamilton, J.G., Resti, J.P., Zangerl, A.R. and Berenbaum, M.R., 2005. Indirect effects of insect herbivory on leaf gas exchange in soybean. Plant, Cell & Environment, 28(3): 402-411.

Ali, A.M., Darvishzadeh, R., Skidmore, A.K., Duren, I.v., Heiden, U. and Heurich, M., 2016. Estimating leaf functional traits by inversion of PROSPECT: Assessing leaf dry matter content and specific leaf area in mixed mountainous forest. International Journal of Applied Earth Observation and Geoinformation, 45: 66-76.

Allain, M., Nguyen, A., Johnson, E., Williams, E., Tsai, S., Prichard, S., Freed, T. and Skiles, J., 2011. A Geospatial Assessment of Mountain Pine Beetle Infestations and Their Effect on Forest Health in Okanogan-Wenatchee National Forest. Proceedings of the American Society of Photogrammetry and Remote Sensing. Bethesda, Maryland: American Society for Photogrammetry and Remote Sensing: 20-31.

Arellano, P., Tansey, K., Balzter, H. and Boyd, D.S., 2015. Detecting the effects of hydrocarbon pollution in the Amazon forest using hyperspectral satellite images. Environ Pollut, 205: 225-39.

Atzberger, C. and Werner, W., 1998. Needle reflectance of healthy and diseased Spruce stands, 1st EARSeL workshop on imaging spectroscopy, pp. 271-283.

Ayala-Silva, T. and Beyl, C.A., 2005. Changes in spectral reflectance of wheat leaves in response to specific macronutrient deficiency. Advances in Space Research, 35(2): 305-317.

Bannari, A., Asalhi, H. and Teillet, P., 2002. Transformed difference vegetation index (TDVI) for vegetation cover mapping, Geoscience and Remote Sensing Symposium, 2002. IGARSS'02. 2002 IEEE International. IEEE, pp. 3053-3055.

Bannari, A., Morin, D., Bonn, F. and Huete, A.R., 1995. A review of vegetation indices. Remote Sensing Reviews, 13(1-2): 95-120.

Barnes, E., Clarke, T., Richards, S., Colaizzi, P., Haberland, J., Kostrzewski, M., Waller, P., Choi, C., Riley, E. and Thompson, T., 2000. Coincident detection of crop water stress, nitrogen status and canopy density using ground based multispectral data.

Bässler, C., Förster, B., Moning, C. and Müller, J., 2008a. The BIOKLIM-Project: biodiversity research between climate change and wilding in a temperate montane forest–the conceptual framework. Waldökologie, Landschaftsforschung und Naturschutz, 7: 21-33.

Bässler, C., Förster, B., Moning, C. and Müller, J., 2008b. The BIOKLIM-Project: biodiversity research between climate change and wilding in a temperate montane forest—the conceptual framework.

Bentz, B. and Endreson, D., 2003. Evaluating satellite imagery for estimating mountain pine beetle-caused lodgepole pine mortality: current status, Mountain Pine Beetle Symposium: Challenges and Solutions. Natural Resources Canada, Canadian Forest Service, Pacific Forestry Centre, Kelowna, British Columbia, pp. 154-163.

Bentz, B.J., Régnière, J., Fettig, C.J., Hansen, E.M., Hayes, J.L., Hicke, J.A., Kelsey, R.G., Negrón, J.F. and Seybold, S.J., 2010. Climate Change and Bark Beetles of the Western United States and Canada: Direct and Indirect Effects. BioScience, 60(8): 602-613.

Berni, J.A., Zarco-Tejada, P.J., González-Dugo, V. and Fereres, E., 2009. Remote sensing of thermal water stress indicators in peach, VII International Peach Symposium 962, pp. 325-331.

Beudert, B., Bässler, C., Thorn, S., Noss, R., Schröder, B., Dieffenbach-Fries, H., Foullois, N. and Müller, J., 2015. Bark Beetles Increase Biodiversity While Maintaining Drinking Water Quality. Conservation Letters, 8(4): 272-281.

Bowman, W.D., 1989. The relationship between leaf water status, gas exchange, and spectral reflectance in cotton leaves. Remote Sensing of Environment, 30(3): 249-255.

Bright, B.C., Hicke, J.A. and Meddens, A.J.H., 2013. Effects of bark beetle-caused tree mortality on biogeochemical and biogeophysical MODIS

products. Journal of Geophysical Research: Biogeosciences, 118(3): 974-982.

Buitrago Acevedo, M.F., Groen, T.A., Hecker, C.A. and Skidmore, A.K., 2017. Identifying leaf traits that signal stress in TIR spectra. ISPRS Journal of Photogrammetry and Remote Sensing, 125: 132-145.

Buitrago, M.F., Groen, T.A., Hecker, C.A. and Skidmore, A.K., 2016. Changes in thermal infrared spectra of plants caused by temperature and water stress. ISPRS Journal of Photogrammetry and Remote Sensing, 111: 22-31.

Cailleret, M., Heurich, M. and Bugmann, H., 2014a. Reduction in browsing intensity may not compensate climate change effects on tree species composition in the Bavarian Forest National Park. Forest Ecology and Management, 328: 179-192.

Cailleret, M., Heurich, M. and Bugmann, H., 2014b. Reduction in browsing intensity may not compensate climate change effects on tree species composition in the Bavarian Forest National Park. Forest Ecology and Management, 328(Supplement C): 179-192.

Campbell, P., Middleton, E., McMurtrey, J. and Chappelle, E., 2007. Assessment of vegetation stress using reflectance or fluorescence measurements. Journal of environmental quality, 36(3): 832-845.

Carlson, T.N. and Ripley, D.A., 1997. On the relation between NDVI, fractional vegetation cover, and leaf area index. Remote sensing of Environment, 62(3): 241-252.

Carol, L.J., Paul, R.W., Niels, O.M., Marvin, L.S. and Roshani, J., 2004. Estimating Water Stress in Plants Using Hyperspectral Sensing.

Carrascal, L.M., Galván, I. and Gordo, O., 2009. Partial least squares regression as an alternative to current regression methods used in ecology. Oikos, 118(5): 681-690.

Carter, G.A., 1993. Responses of leaf spectral reflectance to plant stress. American Journal of Botany: 239-243.

Carter, G.A. and Knapp, A.K., 2001. Leaf optical properties in higher plants: linking spectral characteristics to stress and chlorophyll concentration. American journal of botany, 88(4): 677-684.

Carter, G.A. and Miller, R.L., 1994. Early detection of plant stress by digital imaging within narrow stress-sensitive wavebands. Remote Sensing of Environment, 50(3): 295-302.

Carter, G.A., Seal, M.R. and Haley, T., 1998. Airborne detection of southern pine beetle damage using key spectral bands. Canadian Journal of Forest Research, 28(7): 1040-1045.

Ceccato, P., Gobron, N., Flasse, S., Pinty, B. and Tarantola, S., 2002. Designing a spectral index to estimate vegetation water content from remote sensing data: Part 1: Theoretical approach. Remote Sensing of Environment, 82(2–3): 188-197.

Chaves, M.M., Maroco, J.P. and Pereira, J.S., 2003. Understanding plant responses to drought—from genes to the whole plant. Functional plant biology, 30(3): 239-264.

Chen, G. and Meentemeyer, R., 2016. Remote Sensing of Forest Damage by Diseases and Insects, 145-162 pp.

Cheng, T., Rivard, B., Sánchez-Azofeifa, G.A., Feng, J. and Calvo-Polanco, M., 2010. Continuous wavelet analysis for the detection of green attack damage due to mountain pine beetle infestation. Remote Sensing of Environment, 114(4): 899-910.

Chinellato, F., Faccoli, M., Marini, L. and Battisti, A., 2014. Distribution of Norway spruce bark and wood-boring beetles along Alpine elevational gradients. Agricultural and Forest Entomology, 16(2): 111-118.

Chong, I.-G. and Jun, C.-H., 2005. Performance of some variable selection methods when multicollinearity is present. Chemometrics and Intelligent Laboratory Systems, 78(1-2): 103-112.

Christiansen, E. and Bakke, A., 1988a. The spruce bark beetle of Eurasia, Dynamics of forest insect populations. Springer, pp. 479-503.

Christiansen, E. and Bakke, A., 1988b. The Spruce Bark Beetle of Eurasia. In: A.A. Berryman (Editor), Dynamics of Forest Insect Populations: Patterns, Causes, Implications. Springer US, Boston, MA, pp. 479-503.

Cohen, W.B., 1991. Response of vegetation indices to changes in three measures of leaf water stress.

Collins, J.B. and Woodcock, C.E., 1996. An assessment of several linear change detection techniques for mapping forest mortality using multitemporal landsat TM data. Remote Sensing of Environment, 56(1): 66-77.

Colombo, R., Meroni, M., Marchesi, A., Busetto, L., Rossini, M., Giardino, C. and Panigada, C., 2008. Estimation of leaf and canopy water content in poplar plantations by means of hyperspectral indices and inverse modeling. Remote Sensing of Environment, 112(4): 1820-1834.

Coops, N.C., Johnson, M., Wulder, M.A. and White, J.C., 2006. Assessment of QuickBird high spatial resolution imagery to detect red attack damage due to mountain pine beetle infestation. Remote Sensing of Environment, 103(1): 67-80.

Coulson, R.N., Amman, G.D., Dahlsten, D.L., DeMars Jr, C. and Stephen, F., 1985. Forest-bark beetle interactions: bark beetle population dynamics. Integrated pest management in pine-bark beetle ecosystems. John Wiley & Sons, New York: 61-80.

Cudmore, T.J., Björklund, N., Carroll, A.L. and Lindgren, B.S., 2010. Climate change and range expansion of an aggressive bark beetle: evidence of higher beetle reproduction in naïve host tree populations. Journal of Applied Ecology, 47(5): 1036-1043.

Curran, P.J., 1989. Remote sensing of foliar chemistry. Remote sensing of Environment, 30(3): 271-278.

Curran, P.J., Dungan, J.L., Macler, B.A., Plummer, S.E. and Peterson, D.L., 1992. Reflectance spectroscopy of fresh whole leaves for the estimation of chemical concentration. Remote Sensing of Environment, 39(2): 153-166.

Darvishzadeh, R., Skidmore, A., Schlerf, M. and Atzberger, C., 2008. Inversion of a radiative transfer model for estimating vegetation LAI and chlorophyll in a heterogeneous grassland. Remote Sensing of Environment, 112(5): 2592-2604.

Daszykowski, M., Serneels, S., Kaczmarek, K., Van Espen, P., Croux, C. and Walczak, B., 2007. TOMCAT: A MATLAB toolbox for multivariate calibration techniques. Chemometrics and intelligent laboratory systems, 85(2): 269-277.

Daughtry, C., Biehl, L. and Ranson, K., 1989. A new technique to measure the spectral properties of conifer needles. Remote Sensing of Environment, 27(1): 81-91.

Demetriades-Shah, T.H., Steven, M.D. and Clark, J.A., 1990. High resolution derivative spectra in remote sensing. Remote Sensing of Environment, 33(1): 55-64.

Deshayes, M., Guyon, D., Jeanjean, H., Stach, N., Jolly, A. and Hagolle, O., 2006. The contribution of remote sensing to the assessment of drought effects in forest ecosystems. Annals of Forest Science, 63(6): 579-595.

Doughty, C.E., Field, C.B. and McMillan, A.M., 2011. Can crop albedo be increased through the modification of leaf trichomes, and could this cool regional climate? Climatic Change, 104(2): 379-387.

Dozier, J. and Warren, S.G., 1982. Effect of viewing angle on the infrared brightness temperature of snow. Water Resources Research, 18(5): 1424-1434.

Dupke, C., Bonenfant, C., Reineking, B., Hable, R., Zeppenfeld, T., Ewald, M. and Heurich, M., 2017. Habitat selection by a large herbivore at multiple spatial and temporal scales is primarily governed by food resources. Ecography, 40(8): 1014-1027.

Dye, M., Mutanga, O. and Ismail, R., 2008. Detecting the severity of woodwasp, Sirex noctilio, infestation in a pine plantation in KwaZulu-Natal, South Africa, using texture measures calculated from high spatial resolution imagery. African Entomology, 16(2): 263-275.

Egan, J.M., Jacobi, W.R., Negron, J.F., Smith, S.L. and Cluck, D.R., 2010. Forest thinning and subsequent bark beetle-caused mortality in Northeastern California. Forest Ecology and Management, 260(10): 1832-1842.

Eidmann, H., 1992. Impact of bark beetles on forests and forestry in Sweden. Journal of Applied Entomology, 114(1-5): 193-200.

Eitel, J.U., Gessler, P.E., Smith, A.M. and Robberecht, R., 2006. Suitability of existing and novel spectral indices to remotely detect water stress in Populus spp. Forest Ecology and Management, 229(1-3): 170-182.

Eitel, J.U.H., Vierling, L.A., Litvak, M.E., Long, D.S., Schulthess, U., Ager, A.A., Krofcheck, D.J. and Stoscheck, L., 2011. Broadband, red-edge information from satellites improves early stress detection in a New Mexico conifer woodland. Remote Sensing of Environment, 115(12): 3640-3646.

Escadafal, R., Belghith, A. and Ben Moussa, H., 1994a. Indices spectraux pour la dégradation des milieux naturels en Tunisie aride, 6ème Symp. Int. Mesures Physiques et Signatures en Télédétection, ISPRS-CNES, Val d'lsère, France, pp. 253–259.

Escadafal, R., Belghith, A. and Ben Moussa, H., 1994b. Indices spectraux pour la télédétection de la dégradation des milieux naturels en Tunisie aride.

Ewers, B., Mackay, D. and Samanta, S., 2007. Interannual consistency in canopy stomatal conductance control of leaf water potential across seven tree species. Tree Physiology, 27(1): 11-24.

Fabre, S., Lesaignoux, A., Olioso, A. and Briottet, X., 2011. Influence of Water Content on Spectral Reflectance of Leaves in the 3–15-$\mu\hbox {m} $ Domain. IEEE Geoscience and Remote Sensing Letters, 8(1): 143-147.

Faccoli, M. and Bernardinelli, I., 2014. Composition and Elevation of Spruce Forests Affect Susceptibility to Bark Beetle Attacks: Implications for Forest Management. Forests, 5(1): 88-102.

Fahse, L. and Heurich, M., 2011. Simulation and analysis of outbreaks of bark beetle infestations and their management at the stand level. Ecological Modelling, 222(11): 1833-1846.

Farrés, M., Platikanov, S., Tsakovski, S. and Tauler, R., 2015. Comparison of the variable importance in projection (VIP) and of the selectivity ratio (SR) methods for variable selection and interpretation. Journal of Chemometrics, 29(10): 528-536.

Fassnacht, F.E., Latifi, H., Ghosh, A., Joshi, P.K. and Koch, B., 2014. Assessing the potential of hyperspectral imagery to map bark beetle-induced tree mortality. Remote Sensing of Environment, 140: 533-548.

Fensholt, R. and Sandholt, I., 2003. Derivation of a shortwave infrared water stress index from MODIS near- and shortwave infrared data in a semiarid environment. Remote Sensing of Environment, 87(1): 111-121.

Feret, J.-B., François, C., Asner, G.P., Gitelson, A.A., Martin, R.E., Bidel, L.P.R., Ustin, S.L., le Maire, G. and Jacquemoud, S., 2008. PROSPECT-4 and 5: Advances in the leaf optical properties model separating photosynthetic pigments. Remote Sensing of Environment, 112(6): 3030-3043.

Filchev, L., 2012a. An assessment of European spruce bark beetle infestation using Worldview-2 satellite data, Proc. of European SCGIS Conf.:"Best practices: Application of GIS technologies for conservation of natural and cultural heritage sites, pp. 9-16.

Filchev, L., 2012b. An assessment of european spruce bark beetle infestation using WorldView-2 Satellite data, Proceedings of 1st European SCGIS Conference with International Participation—Best Practices: Application

of GIS Technologies for Conservation of Natural and Cultural Heritage Sites‖(SCGIS-Bulgaria, Sofia), Sofia, Bulgaria, pp. 21-23.

Foster, A.C., Walter, J.A., Shugart, H.H., Sibold, J. and Negron, J., 2017. Spectral evidence of early-stage spruce beetle infestation in Engelmann spruce. Forest Ecology and Management, 384: 347-357.

Franklin, S., Wulder, M., Skakun, R. and Carroll, A., 2003a. Mountain pine beetle red-attack forest damage classification using stratified Landsat TM data in British Columbia, Canada. Photogrammetric Engineering & Remote Sensing, 69(3): 283-288.

Franklin, S.E., Wulder, M.A., Skakun, R.S. and Carroll, A.L., 2003b. Mountain Pine Beetle Red-Attack Forest Damage Classification Using Stratified Landsat TM Data in British Columbia, Canada. Photogrammetric Engineering & Remote Sensing, 69(3): 283-288.

Fu, J., Zhou, Q., Liu, J., Liu, W., Wang, T., Zhang, Q. and Jiang, G., 2008. High levels of heavy metals in rice (Oryzasativa L.) from a typical E-waste recycling area in southeast China and its potential risk to human health. Chemosphere, 71(7): 1269-1275.

Galvao, L.S., Formaggio, A.R. and Tisot, D.A., 2005. Discrimination of sugarcane varieties in Southeastern Brazil with EO-1 Hyperion data. Remote Sensing of Environment, 94(4): 523-534.

Gamon, J. and Surfus, J., 1999. Assessing leaf pigment content and activity with a reflectometer. The New Phytologist, 143(1): 105-117.

Gartland, L.M., 2012. Heat islands: understanding and mitigating heat in urban areas. Routledge.

Geladi, P. and Kowalski, B.R., 1986. Partial least-squares regression: a tutorial. Analytica chimica acta, 185: 1-17.

Gersony, J.T., Prager, C.M., Boelman, N.T., Eitel, J.U.H., Gough, L., Greaves, H.E., Griffin, K.L., Magney, T.S., Sweet, S.K., Vierling, L.A. and Naeem, S., 2016. Scaling Thermal Properties from the Leaf to the Canopy in the Alaskan Arctic Tundra. Arctic, Antarctic, and Alpine Research, 48(4): 739-754.

Gimbarzevsky, P., Dawson, A.F. and Van Sickle, G., 1992a. Assessment of aerial photographs and multi-spectral scanner imagery for measuring mountain pine beetle damage, 333.

Gimbarzevsky, P., Dawson, A.F. and Van Sickle, G.A., 1992b. Assessment of aerial photographs and multi-spectral scanner imagery for measuring mountain pine beetle damage, 333.

Gitelson, A.A., Buschmann, C. and Lichtenthaler, H.K., 1999. The chlorophyll fluorescence ratio F 735/F 700 as an accurate measure of the chlorophyll content in plants. Remote Sensing of Environment, 69(3): 296-302.

Gitelson, A.A., Kaufman, Y.J. and Merzlyak, M.N., 1996. Use of a green channel in remote sensing of global vegetation from EOS-MODIS. Remote Sensing of Environment, 58(3): 289-298.

Gitelson, A.A., Kaufman, Y.J., Stark, R. and Rundquist, D., 2002. Novel algorithms for remote estimation of vegetation fraction. Remote sensing of Environment, 80(1): 76-87.

Gitelson, A.A., Keydan, G.P. and Merzlyak, M.N., 2006. Three-band model for noninvasive estimation of chlorophyll, carotenoids, and anthocyanin contents in higher plant leaves. Geophysical research letters, 33(11).

Gitelson, A.A., Viña, A., Arkebauer, T.J., Rundquist, D.C., Keydan, G. and Leavitt, B., 2003. Remote estimation of leaf area index and green leaf biomass in maize canopies. Geophysical Research Letters, 30(5).

Giunta, A., Jenkins, M., Hebertson, E. and Munson, A., 2016. Disturbance Agents and Their Associated Effects on the Health of Interior Douglas-Fir Forests in the Central Rocky Mountains. Forests, 7(4): 80.

Gobron, N., Pinty, B., Verstraete, M.M. and Widlowski, J.-L., 2000. Advanced vegetation indices optimized for up-coming sensors: Design, performance, and applications. IEEE Transactions on Geoscience and Remote Sensing, 38(6): 2489-2505.

Goel, N.S. and Qin, W., 1994. Influences of canopy architecture on relationships between various vegetation indices and LAI and FPAR: A computer simulation. Remote Sensing Reviews, 10(4): 309-347.

Goheen, D. and Hansen, E., 1993. Effects of pathogens and bark beetles on forests. In: T.S.G. Filip (Editor), Beetle Pathogen Interactions in Conifer Forests. Academic Press, London, pp. 175-196.

Göthlin, E., Schroeder, L.M. and Lindelöw, A., 2000. Attacks by Ips typographus and Pityogenes chalcographus on windthrown spruces (Picea abies) during the two years following a storm felling. Scandinavian Journal of Forest Research, 15(5): 542-549.

Haboudane, D., Miller, J.R., Pattey, E., Zarco-Tejada, P.J. and Strachan, I.B., 2004. Hyperspectral vegetation indices and novel algorithms for predicting green LAI of crop canopies: Modeling and validation in the context of precision agriculture. Remote sensing of environment, 90(3): 337-352.

Hais, M., Jonášová, M., Langhammer, J. and Kučera, T., 2009. Comparison of two types of forest disturbance using multitemporal Landsat TM/ETM+ imagery and field vegetation data. Remote Sensing of Environment, 113(4): 835-845.

Hais, M. and Kučera, T., 2008. Surface temperature change of spruce forest as a result of bark beetle attack: remote sensing and GIS approach. European Journal of Forest Research, 127(4): 327-336.

Hancock, D.W. and Dougherty, C.T., 2007. Relationships between blue-and red-based vegetation indices and leaf area and yield of alfalfa. Crop science, 47(6): 2547-2556.

Hardinsky, M.A. and Lemas, V., 1983. The influence of soil salinity, growth form, and leaf moisture on the spectral reflectance of Spartina

alternifolia canopies. Photogrammetric Engineering and Remote Sensing, 49: 77-83.

Hart, S.J., Veblen, T.T., Mietkiewicz, N. and Kulakowski, D., 2015. Negative feedbacks on bark beetle outbreaks: widespread and severe spruce beetle infestation restricts subsequent infestation. PLoS One, 10(5): e0127975.

Hatala, J.A., Crabtree, R.L., Halligan, K.Q. and Moorcroft, P.R., 2010. Landscape-scale patterns of forest pest and pathogen damage in the Greater Yellowstone Ecosystem. Remote Sensing of Environment, 114(2): 375-384.

Havašová, M., Bucha, T., Ferenčík, J. and Jakuš, R., 2015. Applicability of a vegetation indices-based method to map bark beetle outbreaks in the High Tatra Mountains. Annals of Forest Research, 58(2).

Heath, J., 2001a. The detection of mountain pine beetle green attacked lodgepole pine using Compact Airborne Spectrographic Imager (CASI) data, University of British Columbia.

Heath, J., 2001b. The detection of mountain pine beetle green attacked lodgepole pine using Compact Airborne Spectrographic Imager (CASI) data, University of British Columbia, Vancouver, BC, Canada, 1-72 pp.

Heinze, M. and Fiedler, H.J., 1976. Beziehungen des Chlorophyllgehaltes zu Standortsfaktoren, Ernährungszustand und Wachstum bei Koniferen. Flora, 165(3): 269-293.

Hendry, G.A., Houghton, J.D. and Brown, S.B., 1987. The degradation of chlorophyll—a biological enigma. New Phytologist, 107(2): 255-302.

Heurich, M., Beudert, B., Rall, H. and Křenová, Z., 2010a. National parks as model regions for interdisciplinary long-term ecological research: the Bavarian Forest and Šumavá National Parks underway to transboundary ecosystem research, Long-Term Ecological Research. Springer, pp. 327-344.

Heurich, M., Ochs, T., Andresen, T. and Schneider, T., 2009. Object-orientated image analysis for the semi-automatic detection of dead trees following a spruce bark beetle (Ips typographus) outbreak. European Journal of Forest Research, 129(3): 313-324.

Heurich, M., Ochs, T., Andresen, T. and Schneider, T., 2010b. Object-orientated image analysis for the semi-automatic detection of dead trees following a spruce bark beetle (Ips typographus) outbreak. European Journal of Forest Research, 129(3): 313-324.

Holm, S., 1979. A simple sequentially rejective multiple test procedure. Scandinavian journal of statistics: 65-70.

Hotelling, H., 1933. Analysis of a complex of statistical variables into principal components. Journal of educational psychology, 24(6): 417.

Hunt, E.R., Daughtry, C., Eitel, J.U. and Long, D.S., 2011. Remote sensing leaf chlorophyll content using a visible band index. Agronomy Journal, 103(4): 1090-1099.

Hunt, E.R. and Rock, B.N., 1989. Detection of changes in leaf water content using near-and middle-infrared reflectances. Remote sensing of environment, 30(1): 43-54.

Immitzer, M. and Atzberger, C., 2014. Early Detection of Bark Beetle Infestation in Norway Spruce (<I>Picea abies</I>, L.) using WorldView-2 Data
 Frühzeitige Erkennung von Borkenkä ferbefall an Fichten mittels WorldView-2 Satellitendaten. Photogrammetrie - Fernerkundung - Geoinformation, 2014(5): 351-367.

Ismail, R. and Mutanga, O., 2010. A comparison of regression tree ensembles: Predicting Sirex noctilio induced water stress in Pinus patula forests of KwaZulu-Natal, South Africa. International Journal of Applied Earth Observation and Geoinformation, 12: S45-S51.

Jackson, T., 2004. Vegetation water content mapping using Landsat data derived normalized difference water index for corn and soybeans. Remote Sensing of Environment, 92(4): 475-482.

Jacquemoud, S. and Baret, F., 1990. PROSPECT: A model of leaf optical properties spectra. Remote sensing of environment, 34(2): 75-91.

Jang, J.D., Viau, A.A. and Anctil, F., 2006. Thermal-water stress index from satellite images. International Journal of Remote Sensing, 27(8): 1619-1639.

Jensen, J.R., 2009. Remote sensing of the environment: An earth resource perspective 2/e. Pearson Education India.

Jiang, Z., Huete, A.R., Didan, K. and Miura, T., 2008. Development of a two-band enhanced vegetation index without a blue band. Remote sensing of Environment, 112(10): 3833-3845.

Jönsson, A.M., Appelberg, G., Harding, S. and Bärring, L., 2009. Spatio-temporal impact of climate change on the activity and voltinism of the spruce bark beetle, Ips typographus. Global Change Biology, 15(2): 486-499.

Junttila, S., Vastaranta, M., Hämäläinen, J., Latva-käyrä, P., Holopainen, M., Hernández Clemente, R., Hyyppä, H. and Navarro-Cerrillo, R.M., 2016. Effect of forest structure and health on the relative surface temperature captured by airborne thermal imagery – Case study in Norway Spruce-dominated stands in Southern Finland. Scandinavian Journal of Forest Research, 32(2): 154-165.

Kim, Y., Still, C.J., Hanson, C.V., Kwon, H., Greer, B.T. and Law, B.E., 2016. Canopy skin temperature variations in relation to climate, soil temperature, and carbon flux at a ponderosa pine forest in central Oregon. Agricultural and Forest Meteorology, 226-227: 161-173.

Klein, W.H., 1973. Beetle-killed pine estimates. Photogrammetric Engineering, 39(4).

Kováč, D., Navrátil, M., Malenovský, Z., Štroch, M., Špunda, V. and Urban, O., 2012. Reflectance continuum removal spectral index tracking the

xanthophyll cycle photoprotective reactions in Norway spruce needles. Functional Plant Biology, 39(12): 987.

Krofcheck, D.J., Eitel, J.U.H., Vierling, L.A., Schulthess, U., Hilton, T.M., Dettweiler-Robinson, E., Pendleton, R. and Litvak, M.E., 2014. Detecting mortality induced structural and functional changes in a piñon-juniper woodland using Landsat and RapidEye time series. Remote Sensing of Environment, 151: 102-113.

Krokene, P. and Solheim, H., 1998. Pathogenicity of four blue-stain fungi associated with aggressive and nonaggressive bark beetles. Phytopathology, 88(1): 39-44.

Kümmerlen, B., Dauwe, S., Schmundt, D. and Schurr, U., 1999. Thermography to measure water relations of plant leaves. Handbook of computer vision and applications, 3: 763-781.

Kurz, W.A., Dymond, C.C., Stinson, G., Rampley, G.J., Neilson, E.T., Carroll, A.L., Ebata, T. and Safranyik, L., 2008. Mountain pine beetle and forest carbon feedback to climate change. Nature, 452(7190): 987-90.

Larcher, W., 2003. Physiological plant ecology: ecophysiology and stress physiology of functional groups. Springer Science & Business Media.

Latifi, H., Schumann, B., Kautz, M. and Dech, S., 2014. Spatial characterization of bark beetle infestations by a multidate synergy of SPOT and Landsat imagery. Environ Monit Assess, 186(1): 441-56.

Laurent, E.J., Shi, H., Gatziolis, D., LeBouton, J.P., Walters, M.B. and Liu, J., 2005. Using the spatial and spectral precision of satellite imagery to predict wildlife occurrence patterns. Remote Sensing of Environment, 97(2): 249-262.

Lausch, A., Fahse, L. and Heurich, M., 2011. Factors affecting the spatio-temporal dispersion of Ips typographus (L.) in Bavarian Forest National Park: A long-term quantitative landscape-level analysis. Forest Ecology and Management, 261(2): 233-245.

Lausch, A., Heurich, M. and Fahse, L., 2013a. Spatio-temporal infestation patterns of Ips typographus (L.) in the Bavarian Forest National Park, Germany. Ecological Indicators, 31: 73-81.

Lausch, A., Heurich, M., Gordalla, D., Dobner, H.J., Gwillym-Margianto, S. and Salbach, C., 2013b. Forecasting potential bark beetle outbreaks based on spruce forest vitality using hyperspectral remote-sensing techniques at different scales. Forest Ecology and Management, 308: 76-89.

Lawrence, R. and Labus, M., 2003. Early detection of Douglas-fir beetle infestation with subcanopy resolution hyperspectral imagery. Western Journal of Applied Forestry, 18(3): 202-206.

Lehnert, L.W., Bässler, C., Brandl, R., Burton, P.J. and Müller, J., 2013. Conservation value of forests attacked by bark beetles: Highest number of indicator species is found in early successional stages. Journal for Nature Conservation, 21(2): 97-104.

Li, H., Xu, Q. and Liang, Y., 2014. libPLS: an integrated library for partial least squares regression and discriminant analysis. PeerJ PrePrints, 2: e190v1.

Lichtenthaler, H.K., 1987. [34] Chlorophylls and carotenoids: pigments of photosynthetic biomembranes. Methods in enzymology, 148: 350-382.

Lieutier, F., 2002. Mechanisms of resistance in conifers and bark beetle attack strategies, Mechanisms and deployment of resistance in trees to insects. Springer, pp. 31-77.

Lindenmayer, D. and Franklin, J.F., 2002. Conserving forest biodiversity: a comprehensive multiscaled approach. Island Press.

Liu, L. and Zhang, Y., 2011. Urban heat island analysis using the Landsat TM data and ASTER data: A case study in Hong Kong. Remote Sensing, 3(7): 1535-1552.

Lobinger, G., 1994a. Air temperature as a limiting factor for flight activity of two species of pine bark beetles, Ips typographus L. and Pityogenes chalcographus L.(Col., Scolytidae). Anzeiger für Schädlingskunde, Pflanzenschutz, Umweltschutz, 67(1): 14-17.

Lobinger, G., 1994b. Die Lufttemperatur als limitierender Faktor für die Schwärmaktivität zweier rindenbrütender Fichtenborkenkäferarten, Ips typographus L. undPityogenes chalcographus L.(Col., Scolytidae). Anzeiger für Schädlingskunde, 67(1): 14-17.

Lobinger, G. and Skatulla, U., 1996. Untersuchungen zum Einfluss von Sonnenlicht auf das Schwärmverhalten von Borkenkäfern. Anzeiger für Schädlingskunde, Pflanzenschutz, Umweltschutz, 69(8): 183-185.

Lottering, R., Mutanga, O. and Peerbhay, K., 2016. Detecting and mapping levels of Gonipterus scutellatus-induced vegetation defoliation and leaf area index using spatially optimized vegetation indices. Geocarto International: 1-16.

Mahlein, A.-K., Rumpf, T., Welke, P., Dehne, H.-W., Plümer, L., Steiner, U. and Oerke, E.-C., 2013. Development of spectral indices for detecting and identifying plant diseases. Remote Sensing of Environment, 128: 21-30.

Maitra, S. and Yan, J., 2008. Principle component analysis and partial least squares: Two dimension reduction techniques for regression. Applying Multivariate Statistical Models, 79: 79-90.

Malenovský, Z., Albrechtová, J., Lhotáková, Z., Zurita-Milla, R., Clevers, J., Schaepman, M. and Cudlín, P., 2006. Applicability of the PROSPECT model for Norway spruce needles. International Journal of Remote Sensing, 27(24): 5315-5340.

Mandanici, E. and Bitelli, G., 2016. Preliminary Comparison of Sentinel-2 and Landsat 8 Imagery for a Combined Use. Remote Sensing, 8(12): 1014.

Marini, L., Økland, B., Jönsson, A.M., Bentz, B., Carroll, A., Forster, B., Grégoire, J.-C., Hurling, R., Nageleisen, L.M., Netherer, S., Ravn, H.P., Weed, A. and Schroeder, M., 2016. Climate drivers of bark beetle outbreak dynamics in Norway spruce forests. Ecography: n/a-n/a.

Markham, B.L. and Barker, J.L., 1986. Landsat MSS and TM post-calibration dynamic ranges, exoatmospheric reflectances and at-satellite temperatures. EOSAT Landsat technical notes, 1(1): 3-8.

Marx, A., 2010. Detection and classification of bark beetle infestation in pure norway spruce stands with multi-temporal RapidEye imagery and data mining techniques. Photogrammetrie-Fernerkundung-Geoinformation, 2010(4): 243-252.

Marx, A. and an der Havel, B., 2010a. Erkennung von borkenkäferbefall in fichtenreinbeständen mit multi-temporalen rapideye-satellitenbildern und datamining-techniken.

Marx, A. and an der Havel, B., 2010b. Erkennung von borkenkäferbefall in fichtenreinbeständen mit multi-temporalen rapideye-satellitenbildern und datamining-techniken. Photogramm. Fernerk. Geoinf, 4: 243-252.

McFarlane, B.L. and Witson, D.O., 2008. Perceptions of ecological risk associated with mountain pine beetle (Dendroctonus ponderosae) infestations in Banff and Kootenay National Parks of Canada. Risk Analysis: An International Journal, 28(1): 203-212.

McFarlane, J., Watson, R.D., Theisen, A.F., Jackson, R.D., Ehrler, W., Pinter, P., Idso, S.B. and Reginato, R., 1980. Plant stress detection by remote measurement of fluorescence. Applied Optics, 19(19): 3287-3289.

Meddens, A.J., 2012. Mapping and detecting bark beetle-caused tree mortality in the western United States. AAT 3524572 Thesis, University of Idaho, Dissertation Abstracts International.

Meddens, A.J.H., Hicke, J.A., Vierling, L.A. and Hudak, A.T., 2013. Evaluating methods to detect bark beetle-caused tree mortality using single-date and multi-date Landsat imagery. Remote Sensing of Environment, 132: 49-58.

Mesarch, M.A., Walter-Shea, E.A., Asner, G.P., Middleton, E.M. and Chan, S.S., 1999. A revised measurement methodology for conifer needles spectral optical properties: evaluating the influence of gaps between elements. Remote Sensing of Environment, 68(2): 177-192.

Méthy, M., Olioso, A. and Trabaud, L., 1994. Chlorophyll fluorescence as a tool for management of plant resources. Remote sensing of environment, 47(1): 2-9.

Metternicht, G., 2003. Vegetation indices derived from high-resolution airborne videography for precision crop management. International Journal of Remote Sensing, 24(14): 2855-2877.

Mikkelson, K.M., Bearup, L.A., Maxwell, R.M., Stednick, J.D., McCray, J.E. and Sharp, J.O., 2013. Bark beetle infestation impacts on nutrient cycling, water quality and interdependent hydrological effects. Biogeochemistry, 115(1-3): 1-21.

Miller, Wu, J.Y., Boyer, M.G., Belanger, M. and Hare, E.W., 1991. SEASONAL PATTERNS IN LEAF REFLECTANCE RED-EDGE CHARACTERISTICS. INTERNATIONAL JOURNAL OF REMOTE SENSING, 12(7): 1509-1523.

Mirzaie, M., Darvishzadeh, R., Shakiba, A., Matkan, A.A., Atzberger, C. and Skidmore, A., 2014. Comparative analysis of different uni- and multivariate methods for estimation of vegetation water content using hyperspectral measurements. International Journal of Applied Earth Observation and Geoinformation, 26: 1-11.

Module, F., Atmospheric correction module: Quac and flaash user's guide.

Modzelewska, A., Stereńczak, K., Mierczyk, M., Maciuk, S., Bałazy, R. and Zawiła-Niedźwiecki, T., 2017. Sensitivity of vegetation indices in relation to parameters of Norway spruce stands. Folia Forestalia Polonica, 59(2).

Moller, M., Alchanatis, V., Cohen, Y., Meron, M., Tsipris, J., Naor, A., Ostrovsky, V., Sprintsin, M. and Cohen, S., 2007. Use of thermal and visible imagery for estimating crop water status of irrigated grapevine. J Exp Bot, 58(4): 827-38.

Morris, J.L., Cottrell, S., Fettig, C.J., Hansen, W.D., Sherriff, R.L., Carter, V.A., Clear, J.L., Clement, J., DeRose, R.J., Hicke, J.A., Higuera, P.E., Mattor, K.M., Seddon, A.W.R., Seppä, H.T., Stednick, J.D., Seybold, S.J. and Marini, L., 2017. Managing bark beetle impacts on ecosystems and society: priority questions to motivate future research. Journal of Applied Ecology, 54(3): 750-760.

Mullen, K.E., 2016. Early Detection of Mountain Pine Beetle Damage in Ponderosa Pine Forests of the Black Hills Using Hyperspectral and WorldView-2 Data.

Müller, J., Bußler, H., Goßner, M., Rettelbach, T. and Duelli, P., 2008. The European spruce bark beetle Ips typographus in a national park: from pest to keystone species. Biodiversity and Conservation, 17(12): 2979-3001.

Müller, J. and Bütler, R., 2010. A review of habitat thresholds for dead wood: a baseline for management recommendations in European forests. European Journal of Forest Research, 129(6): 981-992.

Müller, M. and Job, H., 2009. Managing natural disturbance in protected areas: Tourists' attitude towards the bark beetle in a German national park. Biological conservation, 142(2): 375-383.

Munoz-Huerta, R.F., Guevara-Gonzalez, R.G., Contreras-Medina, L.M., Torres-Pacheco, I., Prado-Olivarez, J. and Ocampo-Velazquez, R.V., 2013. A review of methods for sensing the nitrogen status in plants: advantages, disadvantages and recent advances. Sensors (Basel), 13(8): 10823-43.

Murtha, P. and Wiart, R., 1989. PC-based digital analysis of mountain pine beetle current-attacked and non-attacked lodgepole pine. Canadian journal of remote sensing.

Murtha, P.A., 1972a. A guide to air photo interpretation of forest damage in Canada. Publication (Canadian Forestry Service) ; no. 1292. Canadian Forestry Service, Ottawa, vi, 63 p. pp.

Murtha, P.A., 1972b. guide to air photo interpretation of forest damage in Canada.

Murtha, P.A., 1978. Remote sensing and vegetation damage: a theory for detection and assessment. Photogrammetric Engineering and Remote Sensing, 44(9).

Näsi, R., Honkavaara, E., Blomqvist, M., Lyytikäinen-Saarenmaa, P., Hakala, T., Viljanen, N., Kantola, T. and Holopainen, M., 2018. Remote sensing of bark beetle damage in urban forests at individual tree level using a novel hyperspectral camera from UAV and aircraft. Urban Forestry & Urban Greening, 30: 72-83.

Näsi, R., Honkavaara, E., Lyytikäinen-Saarenmaa, P., Blomqvist, M., Litkey, P., Hakala, T., Viljanen, N., Kantola, T., Tanhuanpää, T. and Holopainen, M., 2015. Using UAV-Based Photogrammetry and Hyperspectral Imaging for Mapping Bark Beetle Damage at Tree-Level. Remote Sensing, 7(12): 15467-15493.

Negrón, J.F., Allen, K.K., Ambourn, A., Cook, B. and Marchand, K., 2017. Large-Scale Thinnings, Ponderosa Pine, and Mountain Pine Beetle in the Black Hills, USA. Forest Science, 63(5): 529-536.

Neinavaz, E., Darvishzadeh, R., Skidmore, A.K. and Groen, T.A., 2016. Measuring the response of canopy emissivity spectra to leaf area index variation using thermal hyperspectral data. International Journal of Applied Earth Observation and Geoinformation, 53: 40-47.

Netherer, S., Matthews, B., Katzensteiner, K., Blackwell, E., Henschke, P., Hietz, P., Pennerstorfer, J., Rosner, S., Kikuta, S., Schume, H. and Schopf, A., 2015. Do water-limiting conditions predispose Norway spruce to bark beetle attack? New Phytol, 205(3): 1128-41.

Netherer, S. and Nopp-Mayr, U., 2005. Predisposition assessment systems (PAS) as supportive tools in forest management - Rating of site and stand-related hazards of bark beetle infestation in the High Tatra Mountains as an example for system application and verification, 207, 99-107 pp.

Ni, Z., Liu, Z., Huo, H., Li, Z.-L., Nerry, F., Wang, Q. and Li, X., 2015. Early Water Stress Detection Using Leaf-Level Measurements of Chlorophyll Fluorescence and Temperature Data. Remote Sensing, 7(3): 3232-3249.

Nicolaï, B.M., Beullens, K., Bobelyn, E., Peirs, A., Saeys, W., Theron, K.I. and Lammertyn, J., 2007. Nondestructive measurement of fruit and vegetable quality by means of NIR spectroscopy: A review. Postharvest Biology and Technology, 46(2): 99-118.

Niemann, K.O., Quinn, G., Stephen, R., Visintini, F. and Parton, D., 2015. Hyperspectral Remote Sensing of Mountain Pine Beetle with an Emphasis on Previsual Assessment. Canadian Journal of Remote Sensing, 41(3): 191-202.

Niemann, K.O. and Visintini, F., 2005a. Assessment of potential for remote sensing detection of bark beetle-infested areas during green attack: a literature review.

Niemann, K.O. and Visintini, F., 2005b. Assessment of potential for remote sensing detection of bark beetle-infested areas during green attack: A literature review, Natural Resources Canada, Canadian Forest Service, pp. pp. 1–14.

Nikolov, C., Konôpka, B., Kajba, M., Galko, J., Kunca, A. and Janský, L., 2014. Post-disaster Forest Management and Bark Beetle Outbreak in Tatra National Park, Slovakia. Mountain Research and Development, 34(4): 326-335.

Oerke, E., Steiner, U., Dehne, H. and Lindenthal, M., 2006. Thermal imaging of cucumber leaves affected by downy mildew and environmental conditions. Journal of experimental botany, 57(9): 2121-2132.

Öhrn, P., 2012. The spruce bark beetle Ips typographus in a changing climate.

Ollinger, S.V., 2011. Sources of variability in canopy reflectance and the convergent properties of plants. New Phytologist, 189(2): 375-394.

Ortiz, S., Breidenbach, J. and Kändler, G., 2013. Early Detection of Bark Beetle Green Attack Using TerraSAR-X and RapidEye Data. Remote Sensing, 5(4): 1912-1931.

Paine, T., Raffa, K. and Harrington, T., 1997a. Interactions among scolytid bark beetles, their associated fungi, and live host conifers. Annual review of entomology, 42(1): 179-206.

Paine, T.D., Raffa, K.F. and Harrington, T.C., 1997b. INTERACTIONS AMONG SCOLYTID BARK BEETLES, THEIR ASSOCIATED FUNGI, AND LIVE HOST CONIFERS. Annual Review of Entomology, 42(1): 179-206.

Pasztor, F., Matulla, C., Rammer, W. and Lexer, M.J., 2014. Drivers of the bark beetle disturbance regime in Alpine forests in Austria. Forest Ecology and Management, 318: 349-358.

Pearson, K., 1901. LIII. On lines and planes of closest fit to systems of points in space. The London, Edinburgh, and Dublin Philosophical Magazine and Journal of Science, 2(11): 559-572.

Peñuelas, J. and Filella, I., 1998. Visible and near-infrared reflectance techniques for diagnosing plant physiological status. Trends in plant science, 3(4): 151-156.

Peterson, D.L., Aber, J.D., Matson, P.A., Card, D.H., Swanberg, N., Wessman, C. and Spanner, M., 1988. Imaging SpectrometryRemote sensing of forest canopy and leaf biochemical contents. Remote Sensing of Environment, 24(1): 85-108.

Peterson, D.L., Westman, W.E., Stephenson, N.J., Ambrosia, V.G., Brass, J.A. and Spanner, M.A., 1986. Analysis of forest structure using Thematic Mapper simulator data. IEEE transactions on geoscience and remote sensing(1): 113-121.

Pfeifer, E.M., Hicke, J.A. and Meddens, A.J., 2011. Observations and modeling of aboveground tree carbon stocks and fluxes following a bark beetle outbreak in the western United States. Global Change Biology, 17(1): 339-350.

Pierce, L.L. and Congalton, R.G., 1988. A methodology for mapping forest latent heat flux densities using remote sensing. Remote Sensing of Environment, 24(3): 405-418.

Pierce, L.L., Running, S.W. and Riggs, G.A., 1990. Remote detection of canopy water stress in coniferous forests using the NS001 thematic mapper simulator and the thermal infrared multispectral scanner. PE&RS, Photogrammetric Engineering & Remote Sensing, 56(5): 579-586.

Pinder, J.E. and McLeod, K.W., 1999. Indications of relative drought stress in longleaf pine from Thematic Mapper data. Photogrammetric Engineering and Remote Sensing, 65: 495–501.

Porcar-Castell, A., Tyystjärvi, E., Atherton, J., van der Tol, C., Flexas, J., Pfündel, E.E., Moreno, J., Frankenberg, C. and Berry, J.A., 2014. Linking chlorophyll a fluorescence to photosynthesis for remote sensing applications: mechanisms and challenges. Journal of experimental botany, 65(15): 4065-4095.

Pu, R., Gong, P. and Yu, Q., 2008. Comparative analysis of EO-1 ALI and Hyperion, and Landsat ETM+ data for mapping forest crown closure and leaf area index. Sensors, 8(6): 3744-3766.

Qin, Z., Karnieli, A. and Berliner, P., 2001. A mono-window algorithm for retrieving land surface temperature from Landsat TM data and its application to the Israel-Egypt border region. International Journal of Remote Sensing, 22(18): 3719-3746.

Raffa, K.F., Aukema, B.H., Bentz, B.J., Carroll, A.L., Hicke, J.A., Turner, M.G. and Romme, W.H., 2008. Cross-scale drivers of natural disturbances prone to anthropogenic amplification: the dynamics of bark beetle eruptions. Bioscience, 58(6): 501-517.

Raffa, K.F., Grégoire, J.-C. and Staffan Lindgren, B., 2015. Natural History and Ecology of Bark Beetles, Bark Beetles, pp. 1-40.

Reid, R., 1961. Moisture changes in lodgepole pine before and after attack by the mountain pine beetle. The Forestry Chronicle, 37(4): 368-375.

Roberts, A., Northrup, J. and Reich, R., 2005. Mountain pine beetle detection and monitoring: replication trials for early detection, Analysis of Multi-Temporal Remote Sensing Images, 2005 International Workshop on the. IEEE, pp. 20-24.

Rohde, M., Waldmann, R. and Lunderstädt, J., 1996. Induced defence reaction in the phloem of spruce (Picea abies) and larch (Larix decidua) after attack by Ips typographus and Ips cembrae. Forest Ecology and Management, 86(1): 51-59.

Roumet, C., Fortunel, C., Kazakou, E., Garnier, E., Vile, D., Papadimitriou, M., Zarovali, M.P., Papanastasis, V.P., Skarpe, C., Rusch, G., Sternberg, M., Thébault, A., Quétier, F., Grigulis, K., Robson, M., Lavorel, S., Jouany, C., Theau, J.-P., Cruz, P., Ansquer, P., Castro, H., Freitas, H., Lepš, J., Dolezal, J., Quested, H., Eriksson, O., Golodets, C., Kigel, J., Kleyer, M., Meier, T., Lehsten, V. and Pakeman, R., 2006. Assessing the Effects of

Land-use Change on Plant Traits, Communities and Ecosystem Functioning in Grasslands: A Standardized Methodology and Lessons from an Application to 11 European SitesGarnier et al. — Methodology to Assess Effects of Land-use ChangeGarnier et al. — Methodology to Assess Effects of Land-use Change. Annals of Botany, 99(5): 967-985.

Rullan-Silva, C.D., Olthoff, A.E., Delgado de la Mata, J.A. and Pajares-Alonso, J.A., 2013. Remote Monitoring of Forest Insect Defoliation -A Review. Forest Systems, 22(3): 377.

Runesson, U.T., 1991. Considerations for early remote detection of mountain pine beetle in green-foliaged lodgepole pine, University of British Columbia.

Safranyik, L., 1974. Management of lodgepole pine to reduce losses from the mountain pine beetle.

Safranyik, L. and Carroll, A.L., 2006. The biology and epidemiology of the mountain pine beetle in lodgepole pine forests.

Safranyik, L., Carroll, A.L. and Wilson, B., 2007. The biology and epidemiology of the mountain pine beetle in lodgepole pine forests. The mountain pine beetle: a synthesis of biology, management and impacts on lodgepole pine: 3-66.

Sambaraju, K.R., Carroll, A.L., Zhu, J., Stahl, K., Moore, R.D. and Aukema, B.H., 2012. Climate change could alter the distribution of mountain pine beetle outbreaks in western Canada. Ecography, 35(3): 211-223.

Savitzky, A. and Golay, M.J., 1964. Smoothing and differentiation of data by simplified least squares procedures. Analytical chemistry, 36(8): 1627-1639.

Schelhaas, M.J., Nabuurs, G.J. and Schuck, A., 2003. Natural disturbances in the European forests in the 19th and 20th centuries. Global Change Biology, 9(11): 1620-1633.

Schmidt, K.S. and Skidmore, A.K., 2003. Spectral discrimination of vegetation types in a coastal wetland. Remote Sensing of Environment, 85(1): 92-108.

Schneider, C.A., Rasband, W.S. and Eliceiri, K.W., 2012. NIH Image to ImageJ: 25 years of image analysis. Nat Meth, 9(7): 671-675.

Schowalter, T.D., 2012. Ecology and Management of Bark Beetles (Coleoptera: Curculionidae: Scolytinae) in Southern Pine Forests. Journal of Integrated Pest Management, 3(2): 1-7.

Schulze, E.-D. and Hall, A., 1982. Stomatal responses, water loss and CO2 assimilation rates of plants in contrasting environments, Physiological plant ecology II. Springer, pp. 181-230.

Seidl, R., Rammer, W., Jäger, D. and Lexer, M.J., 2008. Impact of bark beetle (Ips typographus L.) disturbance on timber production and carbon sequestration in different management strategies under climate change. Forest Ecology and Management, 256(3): 209-220.

Seidl, R., Schelhaas, M.-J. and Lexer, M.J., 2011. Unraveling the drivers of intensifying forest disturbance regimes in Europe. Global Change Biology, 17(9): 2842-2852.

Seidl, R., Schelhaas, M.-J., Rammer, W. and Verkerk, P.J., 2014. Increasing forest disturbances in Europe and their impact on carbon storage. Nature Clim. Change, 4(9): 806-810.

Seidl, R., Thom, D., Kautz, M., Martin-Benito, D., Peltoniemi, M., Vacchiano, G., Wild, J., Ascoli, D., Petr, M., Honkaniemi, J., Lexer, M.J., Trotsiuk, V., Mairota, P., Svoboda, M., Fabrika, M., Nagel, T.A. and Reyer, C.P.O., 2017a. Forest disturbances under climate change. Nature Climate Change, 7(6): 395-402.

Seidl, R., Thom, D., Kautz, M., Martin-Benito, D., Peltoniemi, M., Vacchiano, G., Wild, J., Ascoli, D., Petr, M., Honkaniemi, J., Lexer, M.J., Trotsiuk, V., Mairota, P., Svoboda, M., Fabrika, M., Nagel, T.A. and Reyer, C.P.O., 2017b. Forest disturbances under climate change. Nat Clim Chang, 7: 395-402.

Sepulcre-Cantó, G., Zarco-Tejada, P.J., Jiménez-Muñoz, J., Sobrino, J., De Miguel, E. and Villalobos, F.J., 2006. Detection of water stress in an olive orchard with thermal remote sensing imagery. Agricultural and Forest Meteorology, 136(1-2): 31-44.

Sheppard, S. and Picard, P., 2006. Visual-quality impacts of forest pest activity at the landscape level: a synthesis of published knowledge and research needs. Landscape and Urban Planning, 77(4): 321-342.

Simard, M., Powell, E.N., Raffa, K.F. and Turner, M.G., 2012. What explains landscape patterns of tree mortality caused by bark beetle outbreaks in Greater Yellowstone? Global Ecology and Biogeography, 21(5): 556-567.

Six, D.L. and Skov, K., 2009. Response of bark beetles and their natural enemies to fire and fire surrogate treatments in mixed-conifer forests in western Montana. Forest Ecology and Management, 258(5): 761-772.

Skakun, R.S., Wulder, M.A. and Franklin, S.E., 2003. Sensitivity of the thematic mapper enhanced wetness difference index to detect mountain pine beetle red-attack damage. Remote Sensing of Environment, 86(4): 433-443.

Slaton, M.R., Hunt, E.R. and Smith, W.K., 2001a. Estimating near-infrared leaf reflectance from leaf structural characteristics. American Journal of Botany, 88(2): 278-284.

Slaton, M.R., Raymond Hunt Jr, E. and Smith, W.K., 2001b. Estimating near-infrared leaf reflectance from leaf structural characteristics. American Journal of Botany, 88(2): 278-284.

Smith, K., Steven, M. and Colls, J., 2004. Use of hyperspectral derivative ratios in the red-edge region to identify plant stress responses to gas leaks. Remote sensing of environment, 92(2): 207-217.

Snyder, W.C., Wan, Z., Zhang, Y. and Feng, Y.-Z., 1998. Classification-based emissivity for land surface temperature measurement from space. International Journal of Remote Sensing, 19(14): 2753-2774.

Sobrino, J.A., Jiménez-Muñoz, J.C., Sòria, G., Romaguera, M., Guanter, L., Moreno, J., Plaza, A. and Martínez, P., 2008. Land surface emissivity retrieval from different VNIR and TIR sensors. IEEE Transactions on Geoscience and Remote Sensing, 46(2): 316-327.

Sprintsin, M., 2011. Combining land surface temperature and shortwave infrared reflectance for early detection of mountain pine beetle infestations in western Canada. Journal of Applied Remote Sensing, 5(1).

Sprintsin, M., Chen, J.M. and Czurylowicz, P., 2011. Combining land surface temperature and shortwave infrared reflectance for early detection of mountain pine beetle infestations in western Canada. Journal of Applied Remote Sensing, 5(1): 053566-053566-13.

Stadelmann, G., Bugmann, H., Meier, F., Wermelinger, B. and Bigler, C., 2013. Effects of salvage logging and sanitation felling on bark beetle (Ips typographus L.) infestations. Forest Ecology and Management, 305: 273-281.

Stoner, W.A. and Miller, P.C., 1975. Water relations of plant species in the wet coastal tundra at Barrow, Alaska. Arctic and Alpine Research: 109-124.

Sun, Q., Tan, J. and Xu, Y., 2010. An ERDAS image processing method for retrieving LST and describing urban heat evolution: a case study in the Pearl River Delta Region in South China. Environmental Earth Sciences, 59(5): 1047-1055.

Tchakerian, M.D. and Coulson, R.N., 2011. Ecological impacts of southern pine beetle. In: Coulson, RN; Klepzig, KD 2011. Southern Pine Beetle II. Gen. Tech. Rep. SRS-140. Asheville, NC: US Department of Agriculture Forest Service, Southern Research Station. 223-234., 140: 223-234.

Tenenhaus, M., 1998. La régression PLS, edition TECHNIP. Paris.

Thom, D. and Seidl, R., 2015. Natural disturbance impacts on ecosystem services and biodiversity in temperate and boreal forests. Biological Reviews.

Thom, D. and Seidl, R., 2016. Natural disturbance impacts on ecosystem services and biodiversity in temperate and boreal forests. Biol Rev Camb Philos Soc, 91(3): 760-81.

Tucker, C.J., 1979. Red and photographic infrared linear combinations for monitoring vegetation. Remote sensing of Environment, 8(2): 127-150.

Tucker, C.J., Elgin Jr, J.H., McMurtrey Iii, J. and Fan, C., 1979. Monitoring corn and soybean crop development with hand-held radiometer spectral data. Remote Sensing of Environment, 8(3): 237-248.

Ullah, S., Skidmore, A.K., Ramoelo, A., Groen, T.A., Naeem, M. and Ali, A., 2014. Retrieval of leaf water content spanning the visible to thermal infrared spectra. ISPRS Journal of Photogrammetry and Remote Sensing, 93: 56-64.

Valor, E. and Caselles, V., 1996. Mapping land surface emissivity from NDVI: Application to European, African, and South American areas. Remote sensing of Environment, 57(3): 167-184.

Van de Griend, A. and Owe, M., 1993. On the relationship between thermal emissivity and the normalized difference vegetation index for natural surfaces. International Journal of remote sensing, 14(6): 1119-1131.

van Maarschalkerweerd, M. and Husted, S., 2015. Recent developments in fast spectroscopy for plant mineral analysis. Frontiers in plant science, 6.

Vanderhoof, M., Williams, C.A., Ghimire, B. and Rogan, J., 2013. Impact of mountain pine beetle outbreaks on forest albedo and radiative forcing, as derived from Moderate Resolution Imaging Spectroradiometer, Rocky Mountains, USA. Journal of Geophysical Research: Biogeosciences, 118(4): 1461-1471.

Verbesselt, J., Robinson, A., Stone, C. and Culvenor, D., 2009. Forecasting tree mortality using change metrics derived from MODIS satellite data. Forest Ecology and Management, 258(7): 1166-1173.

Viña, A., Gitelson, A.A., Nguy-Robertson, A.L. and Peng, Y., 2011. Comparison of different vegetation indices for the remote assessment of green leaf area index of crops. Remote Sensing of Environment, 115(12): 3468-3478.

Vincini, M., Frazzi, E. and D'Alessio, P., 2008. A broad-band leaf chlorophyll vegetation index at the canopy scale. Precision Agriculture, 9(5): 303-319.

Vlassova, L., Pérez-Cabello, F., Mimbrero, M., Llovería, R. and García-Martín, A., 2014. Analysis of the Relationship between Land Surface Temperature and Wildfire Severity in a Series of Landsat Images. Remote Sensing, 6(7): 6136-6162.

Wang, L., Qu, J.J., Hao, X. and Hunt, E.R., 2011. Estimating dry matter content from spectral reflectance for green leaves of different species. International Journal of Remote Sensing, 32(22): 7097-7109.

Wang, Z., 2016. Mapping spatial variation of Foliar Nitrogen using hyperspectral remote sensing.

Wang, Z., Skidmore, A.K., Darvishzadeh, R., Heiden, U., Heurich, M. and Wang, T., 2015a. Leaf Nitrogen Content Indirectly Estimated by Leaf Traits Derived From the PROSPECT Model. IEEE Journal of Selected Topics in Applied Earth Observations and Remote Sensing, 8(6): 3172-3182.

Wang, Z., Skidmore, A.K., Wang, T., Darvishzadeh, R. and Hearne, J., 2015b. Applicability of the PROSPECT model for estimating protein and cellulose+lignin in fresh leaves. Remote Sensing of Environment, 168: 205-218.

Waring, K.M., Reboletti, D.M., Mork, L.A., Huang, C.-H., Hofstetter, R.W., Garcia, A.M., Fulé, P.Z. and Davis, T.S., 2009. Modeling the impacts of two bark beetle species under a warming climate in the southwestern

USA: ecological and economic consequences. Environmental management, 44(4): 824-835.

Waring, R.H., 1983. Estimating forest growth and efficiency in relation to canopy leaf area. Advances in Ecological Research, 13: 327-354.

Wermelinger, B., 2004. Ecology and management of the spruce bark beetle Ips typographus—a review of recent research. Forest Ecology and Management, 202(1-3): 67-82.

Wold, S., Johansson, E. and Cocchi, M., 1993. PLS-partial least squares projections to latent structures. 3D QSAR in drug design, 1: 523-550.

Wold, S., Sjöström, M. and Eriksson, L., 2001. PLS-regression: a basic tool of chemometrics. Chemometrics and Intelligent Laboratory Systems, 58(2): 109-130.

Wood, D.L., 1982. The role of pheromones, kairomones, and allomones in the host selection and colonization behavior of bark beetles. Annual review of entomology, 27(1): 411-446.

Wulder, M.A., Dymond, C.C., White, J.C., Leckie, D.G. and Carroll, A.L., 2006a. Surveying mountain pine beetle damage of forests: A review of remote sensing opportunities. Forest Ecology and Management, 221(1): 27-41.

Wulder, M.A., White, J., Bentz, B., Alvarez, M. and Coops, N., 2006b. Estimating the probability of mountain pine beetle red-attack damage. Remote Sensing of Environment, 101(2): 150-166.

Wulder, M.A., White, J.C., Bentz, B., Alvarez, M.F. and Coops, N.C., 2006c. Estimating the probability of mountain pine beetle red-attack damage. Remote Sensing of Environment, 101(2): 150-166.

Wulder, M.A., White, J.C., Carroll, A.L. and Coops, N.C., 2009. Challenges for the operational detection of mountain pine beetle green attack with remote sensing. The Forestry Chronicle, 85(1): 32-38.

Xu, H., Zhu, S., Ying, Y. and Jiang, H., 2006. Early detection of plant disease using infrared thermal imaging, Optics East 2006. SPIE, pp. 7.

Xu, Q.-S. and Liang, Y.-Z., 2001. Monte Carlo cross validation. Chemometrics and Intelligent Laboratory Systems, 56(1): 1-11.

Yamaoka, Y., Swanson, R. and Hiratsuka, Y., 1990. Inoculation of lodgepole pine with four blue-stain fungi associated with mountain pine beetle, monitored by a heat pulse velocity (HPV) instrument. Canadian Journal of Forest Research, 20(1): 31-36.

Yoder, B.J. and Pettigrew-Crosby, R.E., 1995. Predicting nitrogen and chlorophyll content and concentrations from reflectance spectra (400–2500 nm) at leaf and canopy scales. Remote sensing of environment, 53(3): 199-211.

Zarco-Tejada, P. and Sepulcre-Cantó, G., 2007. Remote sensing of vegetation biophysical parameters for detecting stress condition and land cover changes. Estudios de la Zona no Saturada del Suelo Vol. VIII: 37-44.

Zeppenfeld, T., Svoboda, M., DeRose, R.J., Heurich, M., Müller, J., Čížková, P., Starý, M., Bače, R., Donato, D.C. and Bugmann, H., 2015. Response of

mountainPicea abiesforests to stand-replacing bark beetle outbreaks: neighbourhood effects lead to self-replacement. Journal of Applied Ecology, 52(5): 1402-1411.

Zhang, C., Chen, K., Liu, Y., Kovacs, J.M., Flores-Verdugo, F. and de Santiago, F.J.F., 2012a. Spectral response to varying levels of leaf pigments collected from a degraded mangrove forest. Journal of Applied Remote Sensing, 6(1): 063501.

Zhang, C., Liu, Y., Kovacs, J.M., Flores-Verdugo, F., de Santiago, F.F. and Chen, K., 2012b. Spectral response to varying levels of leaf pigments collected from a degraded mangrove forest. Journal of Applied Remote Sensing, 6(1): 063501-1-063501-14.

Zhang, J., Wang, Y. and Li, Y., 2006. A C++ program for retrieving land surface temperature from the data of Landsat TM/ETM+ band6. Computers & Geosciences, 32(10): 1796-1805.

Zhang, Y., Chen, J.M., Miller, J.R. and Noland, T.L., 2008. Leaf chlorophyll content retrieval from airborne hyperspectral remote sensing imagery. Remote Sensing of Environment, 112(7): 3234-3247.

Zuber, M. and Benz, G., 1992. Untersuchungen über das Schwärmverhalten von Ips typographus (L.) und Pityogenes chalcographus (L.)(Col., Scolytidae) mit den Pheromonpräparaten Pheroprax und Chalcoprax. Journal of Applied Entomology, 113(1-5): 430-436.

Summary

Forest disturbance in Europe, induced by the European spruce bark beetle *Ips typographus*, L., results in regional-scale dieback and causes major economic loss to the forest industry, particularly in Norway Spruce (*Picea abies*) forest stands. Early stress detection induced by bark beetle infestation (the so-called 'green-attack' stage — when trees are yet to show distinct symptoms observable by the human eye) is crucial and can lead to effective forest management and reduce economic losses. In this respect, remote sensing is a cost-effective and repetitive technique which offers an optimal approach for monitoring and assessing forest stress in comparison to the more traditional (field survey) approach, which is not practical and is inefficient in large areas because it is significantly laborious and costly.

The current thesis presents research regarding the potential of different types of remote sensing data obtained from a variety of sensors, including ASD FieldSpec3 and multispectral satellites (RapidEye, SPOT-5, Sentinel-2 and Landsat-8) for early detection of bark beetle infestation at both leaf and canopy levels. Moreover, the research provided an important opportunity to advance understanding regarding the impact of early bark beetle infestation on the biochemical properties of infested trees (chlorophyll, nitrogen, chlorophyll fluoresces, leaf water content, dry matter content and stomatal conductance). The leaf-level spectrometry demonstrated that a significant difference ($p < 0.05$) exists in the mean reflectance spectra between healthy and infested needle samples at the green-attack stage, with the most pronounced differences being observed in the NIR and SWIR regions. The results of our analysis demonstrated that infestation at the green-attack stage reduced the foliar biochemical concentrations (chlorophyll and nitrogen) and weakened their correlations with reflectance. The findings confirmed the importance of hyperspectral measurement as well as foliar biochemical properties (i.e. chlorophyll and nitrogen) for the detection of *Ips typographus*, L. at the green-attack stage.

Furthermore, research has moved on to the spaceborne level to evaluate the potential of different types of multispectral satellite data (RapidEye, SPOT-5, Sentinel-2 and Landsat-8) in parallel with the collection of field data (leaf traits) for early bark beetle detection. The results from analysis of different spectral vegetation indices at both leaf and canopy levels under bark beetle infestation during the green-attack stage revealed that red-edge and SWIR in the optical domain were the most important spectral regions at both leaf and canopy levels for detecting subtle changes in Norway spruce trees due to bark beetle infestation. Furthermore, from the results of temporal analysis using a time series of seven RapidEye scenes and six SPOT-5 scenes in parallel with field measurements, we identified for the first time in a European situation (in

contrast to earlier works in the US) that mid-June to the beginning of July is an appropriate time frame for detection of early stress induced by bark beetle infestation.

Our study furtherhighlighted the importance and potential of thermal infrared data from Landsat-8 for the early detection of bark beetle infestations and the production of reliable infestation maps at the green-attack stage.

In general, this study contributes to applied research in the field of remote sensing of bark beetle green attack. The findings and methods applied in this work can potentially be used to produce valuable information regarding bark beetle infestation at an early stage of the attack. Our findings can improve bark beetle management activities by providing useful information regarding how, when and which remote-sensing data could be applied to such survey practice, and therefore administrative bodies of forested areas may benefit from this information as an guidance for landscape-wide detection of bark beetle green attack.

Samenvatting

Bosverstoring in Europa, veroorzaakt door de Europese sparschorskever *Ips typographus*, L., resulteert in een terugval op regionale schaal en veroorzaakt grote economische verliezen voor de bosbouwindustrie, met name de bosgebieden met sparren (Picea abies). Vroege stressdetectie veroorzaakt door schorskever infestatie (de zogenaamde 'groene-aanval'-fase - wanneer bomen nog verschillende symptomen moeten vertonen die door het menselijk oog kunnen worden waargenomen) is cruciaal en kan leiden tot meer effectief bosbeheer alsmede het beperken van economische verliezen. In dit opzicht is teledetectie een kosteneffectieve en repetitieve techniek die een optimale aanpak biedt voor het bewaken en beoordelen van bosstress in vergelijking met de meer traditionele (veldonderzoek) benadering, wat niet praktisch is en in grote gebieden inefficiënt is, omdat het aanzienlijk arbeidsintensief en kostbaar is.

Het huidige proefschrift presenteert onderzoek naar het potentieel van verschillende soorten teledetectiegegevens die zijn verkregen door een verscheidenheid aan sensoren, waaronder ASD FieldSpec3 en multispectrale satellieten (RapidEye, SPOT-5, Sentinel-2 en Landsat-8) voor vroege detectie van schorskevers. op zowel blad- als kruinniveau. Bovendien bood het onderzoek een belangrijke mogelijkheid om begrip te kweken voor de impact van een vroege schorskevers infestatie op de biochemische eigenschappen van aangetaste bomen (chlorofyl, stikstof, chlorofylfluorescentie, bladwatergehalte, droge stofgehalte en stomatale geleiding).

Het onderzoek op bladniveau toonde aan dat er een significant verschil ($p < 0,05$) bestaat in de gemiddelde reflectantiespectra tussen gezonde en geïnfecteerde naaldmonsters in de fase van de groene aanval, waarbij de meest uitgesproken verschillen worden waargenomen in de NIR- en de SWIR-regio's. De resultaten van de studie toonden aan dat de plaag in de groene-aanvalfase de blad biochemische concentraties (chlorofyl en stikstof) verminderde en hun correlaties met de reflectie verzwakte. De bevindingen bevestigden het belang van hyperspectrale meting evenals biochemische eigenschappen van bladeren (d.w.z. chlorofyl en stikstof) voor de detectie van Ips typographus, L. in de fase van de groene aanval.

Bovendien is het onderzoek verplaatst op ruimtebereik om het potentieel van verschillende soorten multispectrale satellietgegevens (RapidEye, SPOT-5, Sentinel-2 en Landsat-8) te evalueren, parallel met de verzameling veldgegevens (bladkenmerken) voor vroege schors kever detectie. De resultaten van de analyse van verschillende spectrale vegetatie-indices op zowel blad- als kruinniveau onder schorskever infestatie tijdens het groene-aanvalstadium onthulden dat Red-Edge en SWIR in het optische domein de

belangrijkste spectrale gebieden waren op zowel blad- als kruinniveau voor detectie. subtiele veranderingen in Noorse sparren bomen als gevolg van schors keverplaag. Verder hebben we uit de resultaten van tijdanalyse met een tijdreeks van zeven RapidEye-zintuigen en zes SPOT-5-zintuigen parallel aan de verzameling in het veld, voor het eerst in een Europese situatie geïdentificeerd (in tegenstelling tot eerdere werken in de VS)) dat medio juni tot begin juli een geschikt tijdsbestek is voor detectie van vroege stress veroorzaakt door schorskevers.

Ook wezen de bevindingen van het onderzoek in hoofdstuk 4 uit naar het belang en het potentieel van thermische infraroodgegevens van Landsat-8 voor de vroege detectie van schimmelkeverbesmettingen en de productie van betrouwbare infestatiekaarten in het stadium van de groene aanval.

Over het algemeen draagt dit onderzoek bij aan toegepast onderzoek op het gebied van teledetectie van schorskevers ongevallen. De bevindingen en methoden die in dit werk worden toegepast, kunnen in een vroeg stadium van de aanval nuttige informatie opleveren over de aantasting van schorskevers. Onze bevindingen kunnen ook de beheersing van schorskevers verbeteren door nuttige informatie te verstrekken over hoe, wanneer en welke teledetectie gegevens kunnen worden toegepast op dergelijke enquêtepraktijken, en daarom kunnen bestuursorganen van beboste gebieden dergelijke informatie gebruiken als een indicator voor een efficiënte landschaps-brede detectie van de groene aanval van de schorskever.

Author's Biography

Haidi Jamal Abdullah was born on 5th January 1986 in Sulaymaniyah, Iraqi Kurdistan. He studied geography at Salahaddin University in Erbil, Iraq, and received a B.Sc. in July 2007. After graduation from 2007-2009, he was working as an assistant lecturer in the department of geography, College of Arts. In 2010 he was awarded KRG Human Capacity Development Program scholarship to pursue his master research at the department of geography, at the University of Leicester, UK. He obtained his M.Sc. in 2011 with distinction. In 2014, he was awarded another scholarship from European Commission Erasmus Mundus scholarships to pursue his doctoral research at the Faculty of Geo-information Science and Earth Observation (ITC) at the University of Twente, which resulted in this thesis.